Doctorat de l'École Normale Supérieure de Cachan

SPÉCIALITÉ : Mathématiques

THÈSE

PRÉSENTÉE PAR

François Malgouyres

POUR OBTENIR LE GRADE DE

DOCTEUR DE L'ÉCOLE NORMALE SUPÉRIEURE DE CACHAN

TITRE DE LA THÈSE :

Augmentation de résolution d'images digitales: Théorie variationnelle et applications

Soutenue le 14 Janvier 2000 devant le jury composé de :

M.	Vicent CASELLES	Rapporteur
M.	Antonin CHAMBOLLE	Examinateur
M.	Guy DEMOMENT	Rapporteur
M.	Frédéric GUICHARD	Examinateur
M.	Yves MEYER	Président
M.	Jean-Michel MOREL	Directeur
M.	Bernard ROUGÉ	Directeur
M.	Leonid RUDIN	Rapporteur

à céline

à mes parents

à mes amis

Cette thèse a successivement été effectuée au CEREMADE, à l'université Paris Dauphine (durant une année), et au CMLA, à l'ENS Cachan, qui m'ont tout deux fourni les meilleures conditions matérielles et humaines permettant la réalisation de ce travail.

Je souhaiterais d'abord remercier Yves Meyer qui m'a fait l'honneur de présider mon jury.

Messieurs Vicent Caselles, Guy Demoment et Leonid Rudin m'ont fait l'honneur d'accepter d'être les rapporteurs de ma thèse. Je veux les assurer de ma gratitude pour l'effort important qu'ils ont fourni ainsi que pour l'intérêt qu'ils ont porté à ce travail.

Jean-Michel Morel et Bernard Rougé ont codirigé cette thèse. Je tiens à leur exprimer ma gratitude, entre autre, pour leur aide, leurs encouragements, leur ouverture d'esprit, pour avoir su me faire profiter de leur expérience et de leurs connaissances et pour m'avoir fourni des sujets dont l'intérêt ne s'est jamais démenti. Je tiens particulièrement à remercier Jean-Michel Morel qui m'a donné la possibilité de faire ce travail en m'acceptant au sein de son équipe.

Je veux aussi remercier Frédéric Guichard pour avoir accepté de faire partie de mon jury. Je veux aussi le remercier pour sa collaboration à l'élaboration de la partie portant sur le suréchantillonnage.

Antonin Chambolle m'a fait l'honneur de faire partie de mon jury, je l'en remercie chaleureusement.

Je tiens à témoigner ma reconnaissance à Sylvain Durand pour sa collaboration à l'élaboration de la partie consacrée aux problèmes de déconvolution.

Je veux aussi exprimer ma gratitude aux membres des équipes image et aux doctorants, du CMLA et du CEREMADE, pour l'aide qu'ils ont pu m'apporter, ainsi que pour avoir partagé avec moi la vie de ces laboratoires, durant les trois années qui ont été nécessaires à la réalisation de cette thèse.

Je tiens enfin à remercier les ingénieurs système et personnels administratifs qui ont su simplifier un certain nombre de problèmes qui, sans eux, seraient restés insolubles.

Enfin, je remercie la DGA qui m'a permis de réaliser cette thèse par le biais d'une bourse DGA/DRET/CNRS.

Contents

Notations

- $C^k(\Omega)$: k times continuously differentiable functions from Ω to $\mathbb{R}$.
- $C_0^k(\Omega)$: k times continuously differentiable, compactly supported functions from Ω to $\mathbb{R}$.
- $|Du|(\Omega)$: total variation of a function u over the set Ω.
- $BV(\Omega)$: the set of functions of bounded variation over Ω.
- $\mathbb{T}$: the torus.
- $\mathbb{T}_N$: the torus of size N, for an integer $N > 1$.
- E^*: the dual space of E, a linear space.
- $\hat{u}$: Fourier transform, Fourier series or discrete Fourier transform of a function u.
- δ_X: Dirac delta function at the point X.
- $s * w$: convolution of s with w (the functions are periodized if necessary).
- $div(\varphi_1, \varphi_2) = \frac{\partial \varphi_1}{\partial x} + \frac{\partial \varphi_2}{\partial y}$: the divergence operator.

- $I_{\alpha,\beta}$: for given $(\alpha, \beta) \in \mathbb{R}^2$, the largest interval such that for all $\xi \in I_{\alpha,\beta}$, $-\frac{1}{2} < \alpha\xi \leq \frac{1}{2}$ and $-\frac{1}{2} < \beta\xi \leq \frac{1}{2}$.
- $\mathcal{W}_{s,u}$: the set of functions, satisfying $u_{m,n} = (s * w)(m, n)$, for given functions u and s (see Definition 6.1).
- $\mathcal{W}_{s,u}^K$: the set of band-limited functions, satisfying $u_{m,n} = (s * w)(m, n)$, for given functions u, s and an integer K which determines the band width (see (6.8)).
- $E_{K'}(w) = \frac{1}{K'^2} \sum_{m,n=0}^{K'N-1} |\nabla w(\frac{m}{K'}, \frac{n}{K'})|$: the Riemann sum approximating the total variation.

- τ_λ: soft thresholding function.
- $\tilde{\tau}_{\lambda_1,\lambda_2}$: invertible shrinkage function.

Framework and overview of the Thesis

New technology, computer vision and mathematics

The rapid evolution of computers has permitted, for about twenty years, to widely handle computer vision. Moreover, since the growth in the calculation abilities appears to be steady, we can investigate this domain with few restrictions. This has led us to the development of computer vision applications in such fields as satellite and medical imaging, video surveillance, photography and cinema. This work has benefited from these possible applications through collaborations with the CNES[1] (French spatial agency).

Another point is that the new calculation ability makes possible, for mathematicians, to perform complicated experiments. This permits to make one's intuition of a problem up with more complex objects than the traditional examples dealt with paper and pencil.

Mathematics give the concepts and formalism needed for computer vision but, also, computer vision raises new mathematical questions.

Objectives and means

One of the new questions arising in mathematics, due to the appearance of new technologies, is the way we can use images defined on discrete sets. Indeed, computers can only cope with finite data. As a consequence, images are defined on a discrete grid and their values are quantized. Therefore, the problems about the accuracy of the data and of the calculation made on these data appear naturally.

We have focused, in this work, on the notion of "image resolution" and we have examined some ideas permitting to increase it. More precisely, we have explored two ways of increasing resolution which are:

- **The oversampling**: The result is defined on a thinner grid than the original image.

[1] B. Rougé, who co-managed this thesis, works for the CNES

– **The "deblurring"**: Given a sampling grid, we try to remove blur.

These two problems are generally unsolvable, or ill posed, because of the loss of information. Our aim is therefore to take advantage of all available information. The historical framework and technique usually devoted to these problems are given by Shannon's theory and Wiener filters (see below). We will see that these topics are highly related to the spectral representation of images. As a consequence, we will look after the impact, on this way of representing images, of treatments we will apply. We have therefore analyzed how the processes we will apply act on structural objects (modeling edges) which can be represented in both space and frequency domains.

In order to study the above problems, we have mainly focused on **variational methods**. Most of the variational methods we have studied in this thesis are some "Maximum A Posteriori" methods which involve the "**total variation**". Indeed, this latter appears to be the most adapted to image restoration. We have also discussed some **linear methods** because they are easy to compute and popular (so that makes them references). At last, we study a **wavelet packet** based method which is well adapted to some deblurring cases.

Detailed plan

Part I: Preliminaries

In this part, we present the main mathematical notions and notations which are used in this thesis (the sampling process and the functional space BV). Moreover, we take advantage of the presentations of the sampling process to make some reminders on the Fourier transforms.

Then, we introduce the total variation. This latter is defined by

$$|Dw|((\mathbb{T}_N)^2) = \sup_{\varphi \in \mathcal{B}} \int_{(\mathbb{T}_N)^2} w \, div(\varphi) \, ,$$

where $\mathcal{B} = \{\varphi \in C_0^1((\mathbb{T}_N)^2)^2, \ \|\varphi\|_\infty \leq 1\}$. Note that, when w is C^1, $|Dw|((\mathbb{T}_N)^2) = \int_{(\mathbb{T}_N)^2} |\nabla w|$.

We also argue in favor of the total variation in image restoration.

Part II: Image oversampling

Chapter 3: Introduction

We detail in Chapter 1 the problematic of image oversampling. Assuming we know an image u, deduced from an unknown landscape v by

$$u_{m,n} = (s * v)(m, n) \, ,$$

where $(m,n) \in \mathbb{Z}^2$ and s is a convolution kernel (whose role is to smooth v), oversampling methods tries to recover the landscape v. Of course, such a problem is unrealistic and the real aim of such methods is to recover a "reasonable" representative of v.

We make a bibliographical analysis which shows that the most popular technique is the sinc-interpolation (see below: the description of the Chapter 5). This technique is a consequence of Shannon Theorem (see Proposition 1.1).

Chapter 4: Cylindric functions

In the rest of the part, we analyze the ability of oversampling methods to properly reconstruct edges. More precisely, we focus on the particularity of edges which is to behave locally like 1D functions. This leads us to define cylindric functions as the ones that are fully 1D. In the case of functions defined over a continuous set, for a given direction (α, β), functions cylindric along the direction (α, β) are simply defined by

$$u(x,y) = v(\alpha x + \beta y)\,,$$

for a given function v mapping $\mathbb{R}$ onto $\mathbb{R}$ and for $(x,y) \in \mathbb{R}^2$.

It appears more difficult to define such functions over $\mathbb{Z}^2$. Roughly speaking, we define them as the ones having a Fourier transform supported by the trace of a line over the (non periodized) Fourier domain (see the figure below).

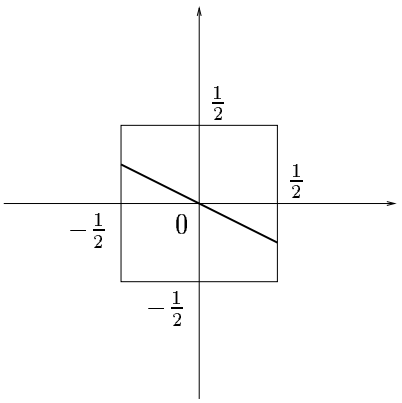

—— : spectral support of a cylindric function.

Chapter 5: Linear oversampling

Among the linear reconstructions, we can mention some classic ones

– The "duplication"

$$v(x,y) = \sum_{m,n} u_{m,n}\, 1_{]-\frac{1}{2},\frac{1}{2}]^2}(x-m, y-n)\,.$$

– The "sinc interpolation" (or "zero-padding")

$$v(x,y) = \int_{[-\frac{1}{2},\frac{1}{2}]^2} \hat{u}(\xi,\eta)\, e^{2i\pi(\xi x+\eta y)} d\xi d\eta\,.$$

– The "zero-crossing"

$$v = \sum_{m,n} u_{m,n}\, \delta_{m,n}\,,$$

where $\delta_{m,n}$ denotes the Dirac delta function at the point (m,n).

We characterize first linear and translation invariant oversamplings in terms of a convolution of the zero-crossing. Then, heuristically speaking, we show in Proposition 5.3 that such operators, as soon as they preserve cylindric functions, are a convolution of the "sinc interpolation" (defined above).

This Chapter is split into two parts depending on whether the data is assumed to have an infinite size or not. We show the link existing between the similar statements.

The conclusion of this chapter is that linear oversamplings have to cope with incompatible drawbacks. Moreover, we see that images, issued from a linear oversampling, have a predetermined regularity (which is not the one of landscapes). This has yielded us the variational approach we present in the next chapter.

Chapter 6: Variational image oversampling

In order to obtain the theoretical results stated in this chapter, we restrict ourselves to the oversampling of the N-periodic elements of $l^\infty(\mathbb{Z}^2)$ (for a positive integer N). The result is defined on the torus of size N, noted $(\mathbb{T}_N)^2$.

In order to define the variational image oversampling, we first define, for a N-periodic $u \in l^\infty(\mathbb{Z}^2)$ and a function $s \in L^2((\mathbb{T}_N)^2)$, $\mathcal{W}_{s,u}$ the set of all the functions $w \in L^2((\mathbb{T}_N)^2)$ satisfying

$$\forall (m,n) \in \{0,...,N-1\}^2,\ u_{m,n} = (s * w)(m,n)\,.$$

This set $\mathcal{W}_{s,u}$ contains all the functions which are sampled in the function u. The total variation based oversampling selects, among the elements of this set, one of those that minimizes the total variation. That is

$$Z(u) = argmin(|Dw|((\mathbb{T}_N)^2)), \text{ among } w \in \mathcal{W}_{s,u}\,. \tag{1}$$

We prove then, under weak conditions, that this problem has a solution and we state a property of "weak uniqueness".

This permits us to state, in Proposition 6.4, that **the variational oversampling preserves cylindric functions, when the convolution kernel s has a Fourier**

transform supported by $\{-\frac{1}{2}+\frac{1}{N},...,\frac{1}{2}\}^2$ (see Figure 1)[2].

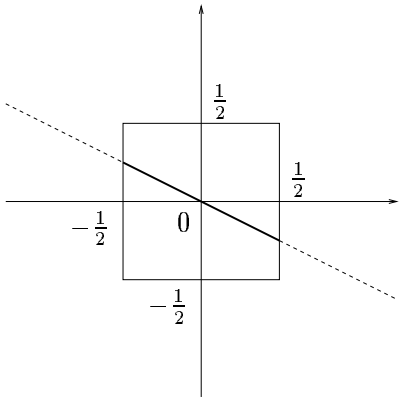

—— : represents the initial spectral support.

------ : represents the extrapolated spectral support.

Figure 1: When $\hat{s}$ is supported over $\{-\frac{1}{2}+\frac{1}{N},...,\frac{1}{2}\}^2$, the variational over-sampling preserves cylindric functions (spectral representation).

Proposition 6.4 also gives us the constraint under which all the points of the torus are enough constrained so that they do not collapse during the minimization process (on the contrary: for instance, when $\hat{s} \equiv 1$, the only constrained points are the ones of $\{0,...,N-1\}^2$ (which is of null measure in $(\mathbb{T}_N)^2$), therefore any constant function is solution of (1)). This interpretation is supported by the experiments displayed on Figure 7.8 of Chapter 7.

Having said that, we show a way to estimate a solution of (1). This estimation is done in two steps

– we prove that the solutions of the problem

$$Z(u) = argmin(|Dw|((\mathbb{T}_N)^2)), \text{ among } w \in \mathcal{W}_{s,u}^K\,, \tag{2}$$

where $\mathcal{W}_{s,u}^K$ denotes a set of band-limited elements of $\mathcal{W}_{s,u}$ (K is an integer which characterizes the band width), permits to approximate a solution of (1).

– we prove that the solutions of the problem

$$Z(u) = argmin\left(\sum_{m,n=0}^{K'N-1} |\nabla w(\frac{m}{K'},\frac{n}{K'})|\right), \text{ among } w \in \mathcal{W}_{s,u}^K\,, \tag{3}$$

for an integer $K' \geq K$, permits to approximate a solution of (2).

[2]That is to say: the high frequencies are free of any constraint and we only extrapolate $\hat{u}$ out of $\{-\frac{1}{2}+\frac{1}{N},...,\frac{1}{2}\}^2$.

In addition, we show that, when changing the minimizing functional (into the Riemann summation approximating it), we lose the ability of the oversampling to preserve cylindric functions. However, we are able to find the parameter K' (see (3)) beyond which the oversampling based on the minimization of the Riemann summation (3) preserves cylindric functions, for a given set of directions.

Then we show to evidence the link between linear oversamplings (the ones described in the preceding chapter) and variational oversamplings of the form

$$Z(u) = argmin\left(\int_{(\mathbb{T}_N)^2} |\nabla w|^2\right), \text{ among } w \in \mathcal{W}_{s,u}\,.$$

Doing this, we give the explicit result of such methods (note that we could replace the gradient ∇ by any other differential operator).

Chapter 7: Experiments

We present in this chapter some experiments which confirm the theoretical analysis described in this part. Moreover, the experiments show that the analysis made using the cylindric functions model is also relevant when edges are curved.

Part III: Image deblurring

Chapter 8: introduction

In this chapter, we detail the problematic of image deblurring. That is, let us assume we know an image u, deduced from an unknown landscape v by

$$u_{m,n} = (s * v)(m,n) + b_{m,n}\,,$$

where $(m,n) \in \mathbb{Z}^2$, s is a convolution kernel and b is a white noise. Then, deblurring methods try to recover, from u, a properly sampled version of v (that is $\tilde{v}_{m,n} = (\tilde{s} * v)(m,n)$, where $\tilde{s}$ yields a sampling operator free of aliasing, of Gibbs effect and of useless blur.)

We show that the deblurring problem is highly related to issue of denoising a "colored noise". Moreover, when $\hat{s}$ vanishes, or is small, inside $\{-\frac{1}{2}+\frac{1}{N}, ..., \frac{1}{2}\}^2$ the deblurring is an unstable problem. We also give a bibliography on that subject. We can mention the standard Wiener filter, defined by its Fourier transform

$$\frac{\hat{\Phi}\,\hat{s}^*}{\hat{\Phi}|\hat{s}|^2 + \sigma^2}\,,$$

which is the optimal (in the sense of the l^2 norm) linear deblurring, given the assumed covariance Φ of the initial landscape.

Chapter 9: Fixed chosen noise restoration (FCNR)

This method, first introduced by B. Rougé, is a wavelet-packet shrinkage method. So, we introduce wavelet-packets which, due to their ability to both concentrate information

and have a good localization in frequency domain, appear well suited to image deblurring. Taking this into account, we show that, under reasonable hypotheses, it is possible to approximate the deconvolution operator (inverting the convolution with s) by an operator which is diagonal in a wavelet-packet basis[3]. In such a case, the removal of the colored noise (issued from the deconvolution) can be achieved by an adaptative shrinkage method. This method is similar to the classic shrinkage methods of Donoho and Johnstone, except that we do not try to remove the noise but to control it. Moreover, the parameters (equivalent to the thresholds of Donoho and Johnstone) are adapted to elements of the basis (with regard to the eigenvalue of the operator associated with this element).

We show a way to avoid the choice of the best basis (we disregard here the computation complexity). Such a basis would require a good localization in space domain, to have a good decorrelation of the noise and the image, and a good localization in frequency domain, to have a good approximation of the deconvolution operator. This leads us to propose a multi-level shrinkage method which permits to cope with this duality.

Then, we are proposing a numerical scheme achieving this restoration.

Chapter 10: Variational deblurring

In order to obtain the theoretical results stated in this chapter, we restrict ourselves to the deblurring of the N-periodic elements of $l^\infty(\mathbb{Z}^2)$ (for a positive integer N). Once again, the result is defined on the torus of size N, noted $(\mathbb{T}_N)^2$. We present here a modification of the Rudin-Osher-Fatemi variational method. This modification makes possible the restoration on a grid thinner than the sampling one. The method consists in minimizing

$$E(w) = |Dw|((\mathbb{T}_N)^2) + \lambda \sum_{m,n=0}^{N-1} |(s * w)_{m,n} - u_{m,n}|^2 ,$$

among functions $w \in BV((\mathbb{T}_N)^2) \cap L^2((\mathbb{T}_N)^2)$. Similarly to Rudin-Osher-Fatemi method, this method proves to be efficient in "inverting" degradation models in which the convolution kernel s is such that $\hat{s}$ cancels inside $\{-\frac{1}{2} + \frac{1}{N}, ..., \frac{1}{2}\}^2$. Remark also that we can not expect to oversample the result very much, except if the noise is very low.

Similarly to Chapter 6, we state existence, "weak uniqueness" and consistency results. We can also state the preservation of cylindric functions. Note that, in this case, it has to be interpreted as "a necessary constraint on the interpolated points" ($\hat{s}$ must be supported by $\{-\frac{1}{2} + \frac{1}{N}, ..., \frac{1}{2}\}^2$, see the above description of the Chapter 6).

Then, we turn to the unrealistic case of spectrum interpolation. Here, we study the behavior of the minimization of the total variation if we assume the spectrum known

[3] Remark that the case of a convolution kernel s (defining the blur) having Fourier transform vanishing inside $\{-\frac{1}{2} + \frac{1}{N}, ..., \frac{1}{2}\}^2$ leaves the framework where we can approximate the deconvolution operator by an operator which is diagonal in a wavelet-packet basis.

everywhere, except over a compact set $\mathcal{K}$. More precisely, we

$$\text{minimize } |Dw|((\mathbb{T}_N)^2), \text{ with } \hat{w}_{\frac{k}{N},\frac{l}{N}} = \hat{v}_{\frac{k}{N},\frac{l}{N}} \text{ for all } (k,l) \in \mathbb{Z}^2 \setminus \mathcal{K}.$$

Despite the fact that it is unrealistic, this study provides us with instructive examples and a good intuition on the ability of the total variation to restore edges.

At last, we show how the non-differentiability of the total variation on constant zones yields the stability (and therefore the creation) of such zones. This is clearly the main drawback of the total variation since it generally leads to a loss of low contrasted textures.

We are presenting a numerical scheme achieving the variational deblurring.

Chapter 11: Numerical results and comparison

This chapter is split into two parts depending respectively on whether we are only concerned with deblurring, or if we both deblur and oversample images.

The first part is a study made in collaboration with the CNES. It shows that the FCNR, because of its ability to return results looking like natural images, is better suited, than the Rudin-Osher-Fatemi variational method, in deblurring blurs such that $\hat{s}$ does not cancel inside $\{-\frac{1}{2}+\frac{1}{N},...,\frac{1}{2}\}^2$. At the same time, because of its ability to recover lost frequencies, Rudin-Osher-Fatemi variational method is more robust. Indeed, it still works when $\hat{s}$ cancels inside $\{-\frac{1}{2}+\frac{1}{N},...,\frac{1}{2}\}^2$, which is not the case of the FCNR.

The second part presents some examples of the Rudin-Osher-Fatemi method adapted to oversampling. This shows that such methods can be interesting in cases where the noise is low. Moreover, it shows that modifying s, by letting $\hat{s} \equiv 0$ out of $\{-\frac{1}{2}+\frac{1}{N},...,\frac{1}{2}\}^2$ when it is not already the case, permits to remove this aliasing.

Industrial applications

This work has shown the ability of total variation based methods to reconstruct, in a reliable manner, some lost frequencies. This makes of these methods some powerful and inevitable tools for people who have to deal with such problems. This is why, CNES has configured for convenience of industry one of our algorithms based on Rudin-Osher-Fatemi method.

Moreover, some ideas about image oversampling, introduced in [23], have been implemented in the software "video investigator" by Cognitech and are currently being implemented by CEA-LETI for medical imaging purposes.

Part I

Preliminaries

Chapter 1

The sampling process

We present in this chapter an analysis of the sampling process. Such a presentation can be found in [24, 42]. We take advantage of this presentation to make some reminders about the Fourier transforms. These are already stated in [6, 33, 36].

The process is in general characterized by a sampling step (the distance between two adjacent samples), a convolution kernel, and the number of samples N. However, modulo a change of scale, the sampling step can be assumed equal to 1. Thus, the sampling is characterized by a convolution kernel s defined over $\mathbb{R}^2$ and the number of samples N. More precisely, given a landscape v defined over $\mathbb{R}^2$ (the landscape is identified with its projection on a plan), its sampling[1] u is defined, for $(m, n) \in \{0, ..., N-1\}^2$, by

$$u_{m,n} = (s * v)(m, n)\,, \tag{1.1}$$

where the convolution operator $*$ is defined in Appendix A (see Figure 1.1).

In order to simplify this problem, we will assume that the functions s and v are N-periodic. That amounts to neglecting some boundary effects. Therefore, s and v are assumed defined over the torus of size N, $(N\mathbb{T})^2$ (which will be denoted by $(\mathbb{T}_N)^2$).

Such a sampling process generally gives rise to numerous artifacts. For instance, Figure 1.2 presents an example of "aliasing" (the bottom image is deduced from the upper one by keeping unchanged one pixel every four; then, for the commodity of the display, we have resized the image, by duplicating every pixels). We can mainly see some hatching in the vicinity of roads while the orientation of the hatching, in the hatched zone of the initial image, has changed.

There are many other kinds of artifacts which can appear during the sampling process. They can be characterized by properties of the convolution kernel s.

[1] the acquisition process is simplified, since in general it also contains noise (at least the quantization noise).

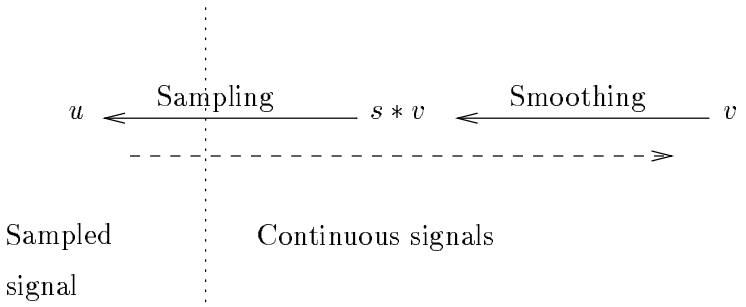

Figure 1.1: sensor model.

Most of the behaviors connected to the sampling are simply expressed using a spectral representation. This leads us to devote the rest of the chapter to the properties of the Fourier transforms which are linked to the sampling description. One can refer to the Appendix A for the definition and the first properties of the Fourier transforms and to [6, 33, 36] for wider presentations of the subject.

1.1 Poisson and Shannon

The aliasing problem, illustrated by Figure 1.2, is a direct consequence of the well known Poisson Formula [33].

Proposition 1.1 *[Poisson] Let $w \in L^1((\mathbb{T}_N)^2)$. If we assume $\sum_{k,l\in\mathbb{Z}} |\hat{w}_{\frac{k}{N},\frac{l}{N}}|$ exists, then we have*

$$\sum_{m,n=0}^{N-1} w(m,n)\, e^{-2i\pi\frac{(m\xi+n\eta)}{N}} = \sum_{k,l\in\mathbb{Z}} \hat{w}_{\frac{\xi}{N}+k,\frac{\eta}{N}+l}\,,$$

for any $(\xi,\eta) \in \{-\frac{N}{2}+1,...,\frac{N}{2}\}^2$.

Turning back to the problem sampling, we see that (1.1) can be expressed, using the Poisson formula, under the form

$$\hat{u}_{\xi,\eta} = \sum_{k,l\in\mathbb{Z}} \hat{s}_{\frac{\xi}{N}+k,\frac{\eta}{N}+l}\, \hat{v}_{\frac{\xi}{N}+k,\frac{\eta}{N}+l}\,,$$

for $(\xi,\eta) \in \{-\frac{N}{2}+1,...,\frac{N}{2}\}^2$ and denoting with $\hat{}$ either the Discrete Fourier Transform or the Fourier series (we assume here that the regularity of the convolution kernel is sufficient to ensure the existence of the sum).

This somehow explains the observations made on Figure 1.2. Indeed, the hatching on the roads are probably consequences of the copying of some frequencies. Moreover,

Figure 1.2: Up: the original image. Down: subsampling of the upper image; we did not do any previous convolution.

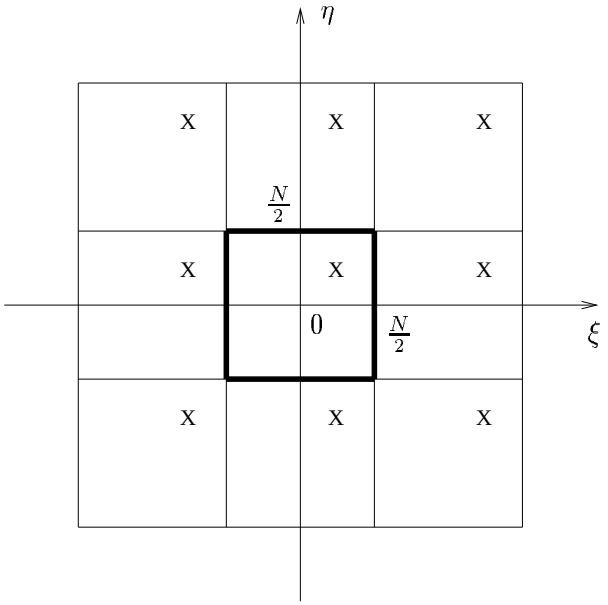

Figure 1.3: All the values of the crosses are added to the value of the cross belonging to $\{-\frac{N}{2}+1,...,\frac{N}{2}\}^2$.

we see that the hatching of the initial hatched zone was well localized in space domain while behaving locally like a pure cosine function. Therefore the Fourier transform of the mask, defining the zone of the hatching, has been centered over another (lower) frequency during the sampling process (similarly, on Figure 1.3, the frequencies in the neighbor of (for instance) the top left cross are copied in the neighbor of the cross which belongs to $\{-\frac{N}{2}+1,...,\frac{N}{2}\}^2$).

We will consider that such a behavior is unacceptable. Indeed, aliasing can appear like information. This makes images non-reliable. This leads us to look for convolution kernels $s \in L^2((\mathbb{T}_N)^2)$ satisfying

$$\hat{s}_{\frac{\xi}{N}+k,\frac{\eta}{N}+l} = 0,$$

for any $(\xi,\eta) \in \{-\frac{N}{2}+1,...,\frac{N}{2}\}^2$ and any $(k,l) \neq (0,0)$. Remark that, since we expect s to have values in $\mathbb{R}$, we must have $\hat{s}_{\frac{k}{N},\frac{k}{N}} = \overline{(\hat{s}_{-\frac{k}{N},-\frac{l}{N}})}$. So, to avoid aliasing, we must have

$$\hat{s}_{\frac{k}{N},\frac{l}{N}} = 0, \text{ for } (k,l) \notin \{-\frac{N}{2}+1,...,\frac{N}{2}-1\}^2.$$

However, this condition is seldom satisfied. For instance the Fourier series of $1_{|[-\frac{1}{2},\frac{1}{2}]^2}$ (which is often used in image sampling, since it corresponds to a simple box that would

count photons) is equal, for $(k,l) \in \mathbb{Z}^2$, to

$$\widehat{(1_{|[-\frac{1}{2},\frac{1}{2}]^2})}_{\frac{k}{N},\frac{l}{N}} = sinc(\frac{\pi k}{N}) sinc(\frac{\pi l}{N}) ,$$

where $sinc(t) = \frac{sin(t)}{t}$ for $t \neq 0$ and $sinc(0) = 1$. Remark not only that $\widehat{(1_{|[-\frac{1}{2},\frac{1}{2}]^2})}$ is not null out of $\{-\frac{1}{2} + \frac{1}{N}, ..., \frac{1}{2}\}^2$, but also that it does not cancel in the vicinity of its border (for instance $\widehat{(1_{|[-\frac{1}{2},\frac{1}{2}]^2})}_{\frac{1}{2},0} = \frac{2}{\pi}$).

Some other advantages, of having $\hat{s}_{\frac{k}{N},\frac{l}{N}} = 0$ for $(k,l) \notin \{-\frac{N}{2} + 1, ..., \frac{N}{2} - 1\}^2$, follow from the next theorem [46].

Theorem 1.1 (Shannon/Whittaker theorem) *Let $w \in L^2((\mathbb{T}_N)^2)$, such that $\hat{w}_{\frac{k}{N},\frac{l}{N}} = 0$ for $(k,l) \notin \{-\frac{N}{2} + 1, ..., \frac{N}{2} - 1\}^2$, then*

$$w(x,y) = \sum_{m,n=0}^{N-1} w(m,n)\, sinc_d(x-m) sinc_d(y-n) ,$$

for $(x,y) \in (\mathbb{T}_N)^2$ and with

$$sinc_d(t) = \begin{cases} \frac{sin\left(\pi t \frac{N-1}{N}\right)}{N\, sin\left(\frac{\pi t}{N}\right)} & , if\ t \notin N\mathbb{Z} , \\ \frac{N-1}{N} & , if\ t \in N\mathbb{Z} , \end{cases}$$

Remark that the index d, of $sinc_d$, refers to the fact that, when the Fourier transform is defined over a continuous set (the index d stands for discrete), the interpolating function is a *sinc* function[2]. When we have $\hat{s}_{\frac{k}{N},\frac{l}{N}} = 0$ for $(k,l) \notin \{-\frac{N}{2}+1, ..., \frac{N}{2}-1\}^2$, this theorem ensures that we can exactly recover $s * v$ over $(\mathbb{T}_N)^2$. Moreover, in such a case, derivatives of $s * v$ can also be deduced from u (satisfying (1.1)). This implies the reliability of the informations given by the function $s * v$ and its derivatives. This is clearly a decisive advantage, for most of the processing done on such an image.

This theorem gives the framework of most of the actual image oversampling methods. Indeed, we will see in Chapter 3 that most of them calculate, or approximate, the "sinc interpolation" defined by the theorem (even, by the way, when $s * v$ does not satisfy the hypothesis of the theorem).

We are going to see in the following that the building of such a convolution kernel s is, in practice, impossible. We will however propose a way to approximate its needed

[2]The Shannon/whittaker Theorem is more often stated for $w \in L^2(\mathbb{R}^2)$ in which case the classical *sinc* function replaces the $sinc_d$ function

properties.

1.2 Heisenberg and Gibbs

In this section, we choose the framework of functions defined over $\mathbb{R}^2$. Indeed, looking at the beginning of Chapter 1, we see that s is in fact defined over $\mathbb{R}^2$ (we did model it by an s defined over $(\mathbb{T}_N)^2$ in order to simplify the treatments at the image's boundaries).

This leads us to define the Fourier transform of a function $w \in L^1(\mathbb{R}^2)$ by[3]

$$\hat{w}(\xi,\eta) = \int_{\mathbb{R}^2} w(x,y) e^{-2i\pi(\xi x+\eta y)} dx dy\,,$$

for $(\xi,\eta) \in \mathbb{R}^2$. In such a case, the inverse Fourier Transform is defined, for $(x,y) \in \mathbb{R}^2$, by

$$w(x,y) = \int_{\mathbb{R}^2} \hat{w}(\xi,\eta)\, e^{2i\pi(\xi x+\eta y)} d\xi d\eta\,.$$

Remark that the form, adapted to this framework, of the property

$$\hat{s}_{\frac{k}{N},\frac{l}{N}} = 0, \text{ for } (k,l) \notin \{-\frac{N}{2}+1, ..., \frac{N}{2}-1\}^2\,,$$

is

$$\hat{s}(\xi,\eta) = 0, \text{ for } (\xi,\eta) \notin]-\frac{1}{2},\frac{1}{2}[^2\,.$$

The first reason that makes the building of a convolution kernel s, satisfying

$$\hat{s}(\xi,\eta) = 0, \text{ for } (\xi,\eta) \notin]-\frac{1}{2},\frac{1}{2}[^2\,,$$

impossible, is the restriction on the sensor size. Indeed, we know that

Proposition 1.2 *Let $s \in L^2(\mathbb{R}^2)$, then s and $\hat{s}$ cannot be simultaneously compactly supported.*

Indeed, in practice, the sensor which makes the convolution with s, has a finite size. Moreover, the following Heisenberg uncertainty Theorem ensures that even when we just expect s to be well localized over $]-\frac{1}{2},\frac{1}{2}[^2$, s has a limited localization in space domain.

Theorem 1.2 (Heisenberg uncertainty Theorem) *Let $s \in L^2(\mathbb{R})$ such that $x\, s(x) \in$*

[3] Remark that this definition is often extended to functions of $L^2(\mathbb{R}^2)$ (see [6]).

$L^2(\mathbb{R})$ and $\xi\,\hat{s}(\xi) \in L^2(\mathbb{R})$. Noting $\sigma_s{}^2 = \int_{\mathbb{R}} x^2 |s(x)|^2 dx$, we have

$$\sigma_s{}^2\,\sigma_{\hat{s}}{}^2 \geq \left(\frac{\int_{\mathbb{R}} |s(x)|^2 dx}{4\pi}\right)^2 .$$

This shows that, heuristically speaking, the convolution kernel s yields a "lower bounded blur". The next proposition illustrates the fact that we need more blur than this "lower bound", if we do not want the sampling of edges to oscillate.

Proposition 1.3 (Gibbs) *Let*

$$H(x) = \begin{cases} 1 & , \textit{ if } x \geq 0 \\ 0 & , \textit{ otherwise,} \end{cases}$$

and $h_K \in L^2(\mathbb{R})$ be defined, for $K > 0$, by $\widehat{h_K} = 1_{|[-K,K]}$. We have (see Figure 1.4), for $x \in \mathbb{R}$,

$$\begin{aligned} H * h_K(x) &= \frac{1}{2} + \int_0^{2\pi K x} \frac{\sin\, t}{\pi t} dt\,, \\ &= H * h_1(Kx)\,. \end{aligned}$$

The interpretation of this proposition comes from the fact that the supremum of $|H * h_K - H|$ does not depend on K (even if we have a pointwise convergence). This illustrates that the discontinuities in frequency domain yield oscillations in the vicinity of edges, in space domain.

A common way to avoid these artifacts is the use of the prolate functions, introduced in [28]. Basically, for a given open set $\Omega \subset \mathbb{R}^2$, this consists in defining a function s optimally concentrated over Ω, whose Fourier transform is supported by $]-\frac{1}{2},\frac{1}{2}[^2$. More precisely, letting

$$\mathcal{F} = \left\{ w \in L^2(\mathbb{R}^2),\ Supp(\hat{w}) \subset]-\frac{1}{2},\frac{1}{2}[^2,\ \text{and } \|w\|_2 = 1 \right\},$$

we call prolate function, the function $s \in L^2(\mathbb{R}^2)$ such that

$$s = argmax_{w \in \mathcal{F}} \int_\Omega |w|^2 .$$

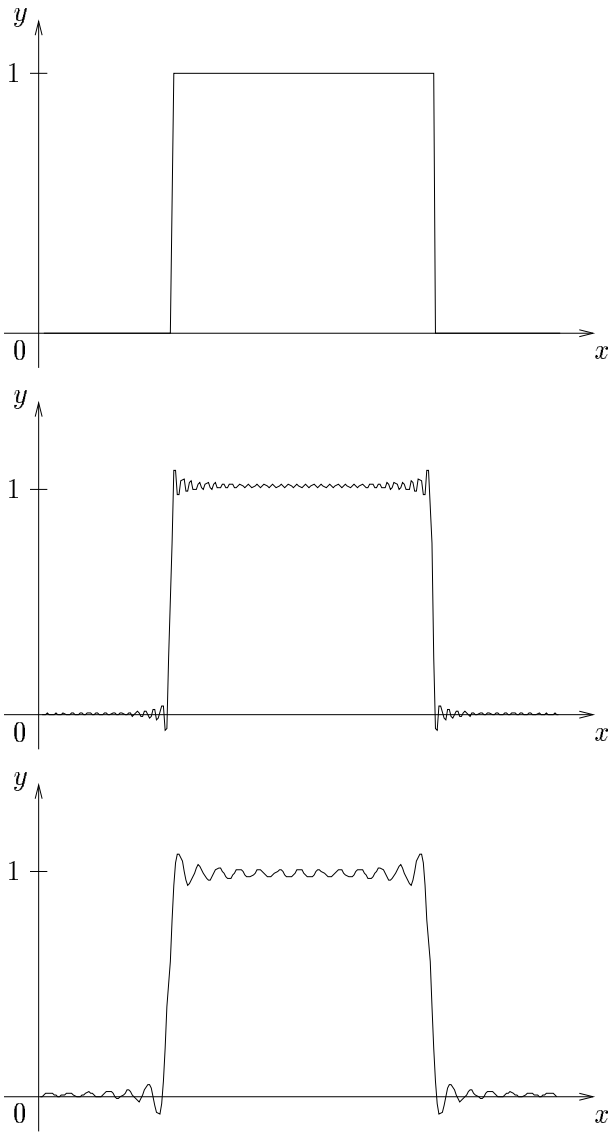

Figure 1.4: Example of Gibbs effects.
Up: initial signal; Middle-Down: Two approximations of the initial signal with a cut-off of high frequencies (the middle signal contains more frequencies than the below one).

Chapter 2

The total variation

This chapter is split into two sections respectively devoted to some reminders on the total variation and to the arguments that let us think the total variation is the most suited regularity criterion for image restoration.

2.1 Generalities on the total variation

One can refer to [3, 17, 21] for general results on total variation. Remark that the order of the following propositions has been chosen with regard to the meaning of the proposition (not with regard to their complexity). We restrict ourselves to the case of functions, having bounded variation, which are defined over the torus $(\mathbb{T}_N)^2$. Moreover, in the following $C_0^1((\mathbb{T}_N)^2)$ denotes the set of continuously differentiable, compactly supported[1] functions going from $(\mathbb{T}_N)^2$ into $\mathbb{R}$.

We define BV and the total variation by

Definition 2.1 *Let $w \in L^1((\mathbb{T}_N)^2)$, we say that w has bounded variation if and only if*

$$\sup\left\{ \int_{(\mathbb{T}_N)^2} w\, div(\varphi),\ \varphi \in C_0^1((\mathbb{T}_N)^2)^2,\ \|\varphi\|_\infty \leq 1 \right\} < \infty\,.$$

In such a case, we denote by

$$|Dw|((\mathbb{T}_N)^2) = sup\left\{ \int_{(\mathbb{T}_N)^2} w\, div(\varphi),\ \varphi \in C_0^1((\mathbb{T}_N)^2)^2,\ \|\varphi\|_\infty \leq 1 \right\},$$

the total variation of w. We note $BV((\mathbb{T}_N)^2)$ the space of functions of bounded variations. Moreover, $BV((\mathbb{T}_N)^2)$ is provided with the norm $\|\,.\,\|_{BV} = \|\,.\,\|_1 + |D\,.\,|((\mathbb{T}_N)^2)$.

[1] Remark that, since $(\mathbb{T}_N)^2$ is compact, this hypothesis is useless. We however keep it.

Remark that, for any $w \in C^1((\mathbb{T}_N)^2)$, a simple integration by parts yields

$$|Dw|((\mathbb{T}_N)^2) = \int_{(\mathbb{T}_N)^2} |\nabla w| \, .$$

Moreover, noting $C^\infty((\mathbb{T}_N)^2)$ the set of infinitely differentiable functions, we have the following approximation theorem.

Proposition 2.1 (approximation) *Let $w \in BV((\mathbb{T}_N)^2)$. Then there exists a sequence $(w_k)_{k\in\mathbb{N}}$ with $w_k \in BV((\mathbb{T}_N)^2) \cap C^\infty((\mathbb{T}_N)^2)$ such that $(w_k)_{k\in\mathbb{N}}$ converges to w in $L^1((\mathbb{T}_N)^2)$ and $\lim_{k\to\infty} \int_{(\mathbb{T}_N)^2} |\nabla w_k| = |Dw|((\mathbb{T}_N)^2)$.*

The total variation has the significant advantage over $\int_{(\mathbb{T}_N)^2} |\nabla w|$ to be lower semicontinuous.

Proposition 2.2 (lower semicontinuity) *Let $(w_k)_{k\in\mathbb{N}}$ be a sequence of functions with $w_k \in BV((\mathbb{T}_N)^2)$. Let us assume that there exists $w \in L^1((\mathbb{T}_N)^2)$ such that $(w_k)_{k\in\mathbb{N}}$ converges to w in $L^1((\mathbb{T}_N)^2)$. Then $w \in BV((\mathbb{T}_N)^2)$ and*

$$|Dw|((\mathbb{T}_N)^2) \leq \liminf_{k\to\infty} |Dw_k|((\mathbb{T}_N)^2) \, .$$

The above propositions show that BV is the "natural" space in which sequences minimizing the energy $\int_{(\mathbb{T}_N)^2} |\nabla w|$ converge. It also shows that in order to minimize the total variation we only have to consider a sequence minimizing $\int_{(\mathbb{T}_N)^2} |\nabla w|$. Let us detail a simple example which illustrates the meaning of the propositions above.

Example 2.1. For simplicity, this example deals with some functions of $BV(\mathbb{R})$ (in which case holds a definition and some properties similar to the ones stated above).

Let $v = 1_{|[-\frac{1}{2},\frac{1}{2}]}$, v is not derivable (and therefore $\int_{\mathbb{R}} |v'|$ is not defined), but it has bounded variations and we have $|D(v)|(\mathbb{R}) = 2$.

Let $h \in C_0^1(\mathbb{R})$ be such that $h(x) \geq 0$, for any $x \in \mathbb{R}$, and $\int_{\mathbb{R}} |h| = 1$. Assume moreover that h is supported by $[-\frac{1}{2}, \frac{1}{2}]$. Then, noting, for $\varepsilon \neq 0$, $h_\varepsilon(x) = \frac{1}{\varepsilon} h(\frac{x}{\varepsilon})$, we know that for any $\varepsilon \leq 1$, $h_\varepsilon * v \in C_0^1(\mathbb{R})$, and that (see Figure 2.1)

$$\int_{\mathbb{R}} |(h_\varepsilon * v)'| = |D(h_\varepsilon * v)|(\mathbb{R}) = 2 \, .$$

Moreover, we have $\lim_{\varepsilon\to 0} \|h_\varepsilon * v - v\|_1 = 0$ and of course $\lim_{\varepsilon\to 0} \int_{\mathbb{R}} |(h_\varepsilon * v)'| = |D(v)|(\mathbb{R})$, but remark that we also have (see Figure 2.1)

$$|D(h_\varepsilon * v - v)|(\mathbb{R}) = 4 \, .$$

This is why, in Proposition 2.1, we cannot state the result under the form $\lim_{k\to\infty} |D(w_k - w)|((\mathbb{T}_N)^2) = 0$.

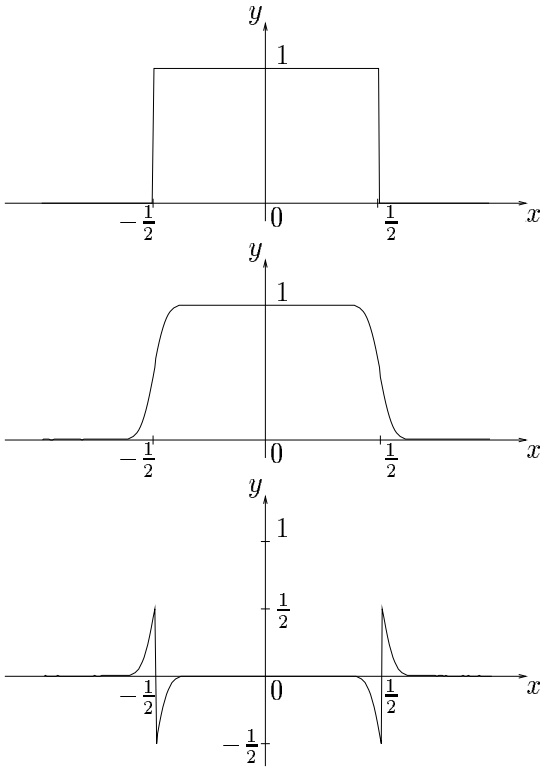

Figure 2.1: Up: the function $v = 1_{|[-\frac{1}{2},\frac{1}{2}]}$; Middle: the function $h_\varepsilon * v$, a smoothed version of v; Down: the function $h_\varepsilon * v - v$.

Remark also that if the convolution kernel h had had negative values, we would have had $\lim_{\varepsilon\to 0} \int_{\mathbb{R}} |(h_\varepsilon * v)'| > |D(v)|(\mathbb{R})$. This illustrates why we cannot expect to have the equality in Proposition 2.2.

Both following propositions will permit to prove the existence results, which we will need in Parts II and III.

Proposition 2.3 (compactness) *Let $(w_k)_{k\in\mathbb{N}}$ be a sequence of functions with $w_k \in BV((\mathbb{T}_N)^2)$ such that $|Dw_k|((\mathbb{T}_N)^2) \leq C$, for a given $C \in \mathbb{R}$. Then, there exists $w \in BV((\mathbb{T}_N)^2)$ and a sub-sequence $(w_{k_j})_{j\in\mathbb{N}}$ such that*

$$\lim_{j\to\infty} \|w_{k_j} - w\|_1 = 0$$

Proposition 2.4 (Poincaré) *There exists a constant C, such that,*

$$\forall w \in BV((\mathbb{T}_N)^2),\ \|w - \overline{w}\|_2 \leq C|Dw|((\mathbb{T}_N)^2)\,.$$

where $\overline{w} = \frac{1}{N^2}\int_{(\mathbb{T}_N)^2} w$.

2.2 Arguments in favor of the total variation

We are now going to argue for the choice of the total variation in image restoration (oversampling or deblurring) within a family of energies given by

$$E_{L,r}(w) = \int_{\mathbb{R}^2} |L(w)|^r$$

where $r \geq 1$ and L is a linear, translation invariant, isotropic and homogeneous operator (typically a differential operator of a fixed order). Homogeneous is used in the sense that there exists $ord(L) \in \mathbb{R}$, such that for any $C > 0$ and any $w \in L^1(\mathbb{R}^2)$, such that $L(w)$ exists everywhere,

$$L(w(C\,.))(x,y) = C^{ord(L)} L(w)(Cx, Cy)\,.$$

For commodity we do not distinguish yet the total variation of a function w from $\int_{\mathbb{R}^2} |\nabla w|$.

First, note that within this family, the case $r = 1$ is the most interesting, since for $r > 1$ the energy $E_{L,r}(w)$ does penalize more a point at which $|L(w)|$ is large than several points having smaller $|L(w)|$. This is simply due to the fact that $f(t) = t^r$ is strictly convex for $r > 1$ and can be regarded as a consequence of the homogeneity of $E_{L,r}(w)$ with regard to a multiplication of w by constant. We do believe such a behavior is harmful to image quality since it will split large $|L(w)|$ into several pieces without regard to their orientations (these orientations generally oscillate due to the data fidelity term (see examples of sections 6.2.1 and 6.3)). This does generally create oscillations close to points where $|L(w)|$ is large (generally edges).

Let us focus on the case where $r = 1$. If we consider an image cylindric along a direction (α, β) (which models an edge) and a dilation (or contraction) along the direction (α, β) (this modifies the edge smoothness), in such a case the homogeneity of $E_{L,1}(w)$ with regard to this dilation is $ord(L) - 1$. So, if $ord(L)$ is strictly larger than 1, $E_{L,1}(w)$ will penalize sharper edges than smooth ones (indeed, $C^{ord(L)-1}$ tends to infinity or zero with C) and similarly to previously, the minimization of $E_{L,1}(w)$ tends to create oscillations close to edges. Moreover natural images generally present sharp edges, so we cannot afford to forbid them during the restoration[2].

A simple way to sum up this is the following 1D proposition.

Proposition 2.5 *Let $w \in BV(\mathbb{R})$, and let h be an homeomorphism of $\mathbb{R}$ into $\mathbb{R}$, we have*

$$|D(w \circ h)|(\mathbb{R}) = |Dw|(\mathbb{R})\,.$$

[2]Note that this is a intuitive way to talk about Sobolev embedding Theorem which, in 1D, shows that the case $ord(L) = 1$ and $r = 1$ is the limit one beyond which the functions are smoother than continuous.

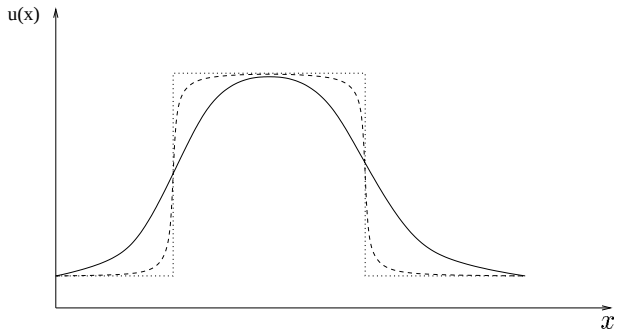

Figure 2.2: The continuous and dashed signals are deduced one from another by a change of variable, while the dot one corresponds to a limit case. The three signals have the same Total Variation.

Proof. We have, letting $\mathcal{B} = \{\varphi \in C_0^1(\mathbb{R}),\ \|\varphi\|_\infty \leq 1\}$,

$$\begin{aligned} |D(w \circ h)|(\mathbb{R}) &= \sup_{\varphi\in\mathcal{B}} \int_{\mathbb{R}} w \circ h(x)\, \varphi'(x)\, dx \\ &= \sup_{\varphi\in\mathcal{B}} \int_{\mathbb{R}} w(y)\, \varphi' \circ h^{-1}(y)\, (h^{-1})'(y)\, dy \\ &= \sup_{\varphi\in\mathcal{B}} \int_{\mathbb{R}} w(y)\, (\varphi \circ h^{-1})'(y)\, dy \\ &= \sup_{\phi\in\mathcal{B}} \int_{\mathbb{R}} w(y)\, \phi'(y)\, dy \end{aligned}$$

□

This means that the minimization of the Total Variation does no discriminations between two signals deduced one from another by a change of variable (the discrimination is done by the data fidelity term). Note that the transformation of a discontinuous function into a continuous one leaves the framework of this proposition since a continuous and a discontinuous functions are not deduced one from another by a change of variable. However, by letting the homeomorphism h tend to a function which is constant over some intervals, we observe that a discontinuous signal might have the same Total Variation as a smoothed version (see Figure 2.2).

This property is unfortunately false in 2-D. However, despite the global behavior of the Total Variation, we can consider that on the neighborhood of edges with small curvature, the 1-D behavior will dominate.

In 2-D, the Total Variation cannot only be seen as the measurement of the oscillations of an image, but also as the sum of its level lines length.

Theorem 2.1 (Coarea formula) *Let $w \in BV((\mathbb{T}_N)^2)$, we have*

$$|Du|((\mathbb{T}_N)^2) = \int_{-\infty}^{\infty} P(\mathcal{X}_\lambda w) d\lambda$$

where $\mathcal{X}_\lambda w$ denotes the level set associated to the gray level λ, and

$$P(\mathcal{X}_\lambda w) = |D(\mathcal{X}_\lambda w)|((\mathbb{T}_N)^2)$$

is its perimeter.

A proof of this theorem is, for instance, given in [21]. Remark that when the level line $\partial\mathcal{X}_\lambda w$ is Lipschitz, $P(\mathcal{X}_\lambda w)$ corresponds to the Hausdorff measure $\mathcal{H}^1$ of $\partial\mathcal{X}_\lambda w$. By minimizing the Total Variation, we tend to cancel the oscillations of the gray level (these are represented by the domain of integration) and to smooth the level lines (by minimizing their length).

There exist of course other kinds of energies. Let us cite the entropy which has already been used to restore images (see [43, 49]). The entropy is generally defined, for a positive function w, by

$$E(w) = -\int_{(\mathbb{T}_N)^2} w(x,y) log\left(\frac{w(x,y)}{\int_{(\mathbb{T}_N)^2} w}\right) dxdy\,.$$

Remark that a small change of f in a dark part of the image a-priori induces a larger change in the value of the entropy than the same change in a bright region. Therefore, we believe such an energy is not fully adapted to image restoration since it may not behave in the same way in dark and bright regions of the image.

However, most of the results we will state in the following parts are also true when the entropy is substituted to the total variation.

Part II

Image oversampling

Chapter 3

Introduction

This part deals with some oversampling methods[1]. These methods aim at recovering a function defined on an open subset Ω of $\mathbb{R}^2$ from a sampled one, defined on $\Omega \cap \mathbb{Z}^2$. This latest is assumed to be itself obtained by the composition of a convolution and a sampling applied to an unknown original function of Ω. More precisely, given Ω an open set of $\mathbb{R}^2$, we have

$$u_{m,n} = (s * v)(m, n), \tag{3.1}$$

where (m, n) belongs to $\Omega \cap \mathbb{Z}^2$, $*$ denotes the continuous convolution, s and v map $\mathbb{R}^2$ onto $\mathbb{R}$ and u maps $\Omega \cap \mathbb{Z}^2$ onto $\mathbb{R}$. Note that, in this part, we will not take into account the edge effects in the vicinity of $\partial\Omega$; we will only focus on the cases where $\Omega = \mathbb{R}^2$, or Ω is a square, identified to the torus of size N, $(N\,\mathbb{T})^2$.

Oversampling processes are generally referred to as restorations, reconstructions and interpolations. Restoration and reconstruction are commonly distinguished by the fact that they respectively aim at recovering v or $s * v$ on Ω. Moreover, they both differ from interpolation, which aims at obtaining a "nice" function w, defined on Ω, such that $w(m, n) = u_{m,n}$, for $(m, n) \in \Omega \cap \mathbb{Z}^2$. So, formally, this part is concerned both with linear reconstructions (linear is used in the sense that the reconstruction of a sum of functions is the sum of the reconstructions) and some non-linear restoration methods. However, since it is equivalent to linearly deconvolve a linear reconstruction or to directly construct a sharpest linear reconstruction, we do believe that these notions are similar (even though formally the restoration is a more general problem). Indeed, in practice, we just expect a "good" function of Ω from a sampled one.

There have been several approaches in order to solve the oversampling problem. We will distinguish two main kinds: the linear and the non-linear ones. Most of the linear methods aim at approximating the "sinc interpolation" (or "zero-padding") which consists in filling

[1] Most of the results stated in this part are covered in [31]

the lost part of the spectral domain with 0. This latest is often considered as optimal because of Shannon sampling Theorem (see [46] or Section 1.1. The shortcoming of this method is that the induced filter oscillates and is poorly localized in space domain (which yields a large algorithmic complexity for a linear interpolation). Some have reduced the algorithmic complexity (see [50]) in order to compute it, but most of the techniques propose to approximate it (see for instance [38, 48]). Here, we will mathematically formalize in Chapter 5.1 the framework of linear reconstructions and we will show that most of the usual shortcomings of such methods cannot be simultaneously avoided. More precisely, we will show that under simple hypotheses linear reconstructions are some convolutions. The properties (qualities and drawbacks) of the reconstructions can be expressed in terms of properties of a convolution kernel. We will show that the usual drawbacks correspond to incompatible properties of this convolution kernel. Consequently, it is not surprising to find numerous attempts to cope with these shortcomings as well as some articles comparing some linear reconstructions (see [30, 34]).

Non-linear methods generally take into account the local behavior of the initial function and adapt the reconstruction with regard to this behavior (see [2, 47]). This essentially allows to treat in a different manner the smooth zones and the vicinity of the edges inside the images. These reconstructions can yield good results but depend on the tool that determines the local behavior. Thus, they have several sources of shortcomings and it is therefore difficult to qualify their results. There also exist variational techniques, the aim of which is to restore images. This will be commented in a devoted section (see Section 6.3).

This part is mainly concerned with the way the oversampling methods under our scope deal with edges. More precisely, since edges arising in image processing are generally smooth (along the direction orthogonal to the one of gradient), they can be locally regarded as being 1D functions (they are almost constant along the edge direction). Therefore, we choose to model edges by what we call cylindric functions (that are those which are constant along a direction). We will see some conditions, that must satisfy the oversampling methods under our scope, in order to preserve such functions. At last, we will validate this theoretical study by some experiments (see Chapter 7).

This part is organized as follows. We first define cylindric functions. Then, in Chapter 5, we focus on linear reconstructions. We give a general property satisfied by such operators and define cylindric functions. Thereafter, we will prove that linear reconstructions that preserve cylindric images can be expressed in terms of a convolution of the "sinc interpolation". The second part of Chapter 5 is devoted to a computable definition of reconstruction (i.e. the reconstructed image is only defined on a thinner grid, and $\Omega = [0, N[)$. We state in such a case some results equivalent to the preceding ones and show that these latest are the limit cases when the initial image size grows to infinity.

In Chapter 6, we deal with variational oversampling methods, in the case where $\Omega =$

$[0, N[^2$, with $N \in \mathbb{N}$. These methods minimize a convex "energy" E among the function satisfying (3.1). Since we do believe the total variation is a good candidate to image oversampling we state our results in this particular case. Within this framework, we will show that the method is properly defined both theoretically and numerically. We then exhibit some particular total variation based oversamplings that preserve cylindric images. The end of the chapter is devoted to other variational methods. This makes a link between quadratic variational restorations and linear reconstructions.

At last, some commented experiments are displayed in Chapter 7.

Chapter 4

Cylindric functions

The idea of considering such functions appears naturally in image oversampling. Indeed, these functions can be used to model the local 1D aspect of smooth edges. Note that the loss of this 1D aspect is a common artifact of many reconstruction methods (see Chapter 7).

We are going to state different definitions of cylindric functions, depending on whether the functions are defined over $\mathbb{R}^2$ or $\mathbb{Z}^2$. As we said in the introduction, these images have the property of fluctuating only in one direction. In the case of functions of $L^\infty(\mathbb{R}^2)$, we will simply assume

Definition 4.1 *Let $u \in L^\infty(\mathbb{R}^2)$. u is called* cylindric *if and only if there exists a direction $(\alpha, \beta) \in \mathbb{R}^2 \setminus \{(0,0)\}$ and $v \in L^\infty(\mathbb{R})$ such that*

$$u(x, y) = v(\alpha x + \beta y)\,,$$

for $(x, y) \in \mathbb{R}^2$.

Such a function will be called cylindric along the direction (α, β).

Note that it is more difficult to define cylindric functions of $l^\infty(\mathbb{Z}^2)$. Indeed, remark that for any $u \in l^\infty(\mathbb{Z}^2)$ and any $(\alpha, \beta) \in \mathbb{R}^2$ such that the line $\alpha x + \beta y = 0$ has an irrational slope, there exists a function $v \in L^\infty(\mathbb{R})$, such that

$$\forall (m, n) \in \mathbb{Z}^2,\ u_{m,n} = v(\alpha m + \beta n)\,. \tag{4.1}$$

This is simply due to the fact that all the $\alpha m + \beta n$ (with m and n in $\mathbb{Z}$) are distinct in $\mathbb{R}$.

So, defining cylindric functions of $l^\infty(\mathbb{Z}^2)$ as the ones that satisfy (4.1) is not enough; we have to limit ourselves to functions v such that the sampling does not create any aliasing. More precisely, we consider that u is obtained by a sampling of the function $V(x, y) = v(\alpha x + \beta y)$, where the function V is band-limited (this permits, despite the sampling, to preserve the cylindric aspect of V).

This leads us to characterize cylindric functions over $\mathbb{Z}^2$ by their Fourier series. This latter being given as a measure supported by the segment represented on Figure 4.1.

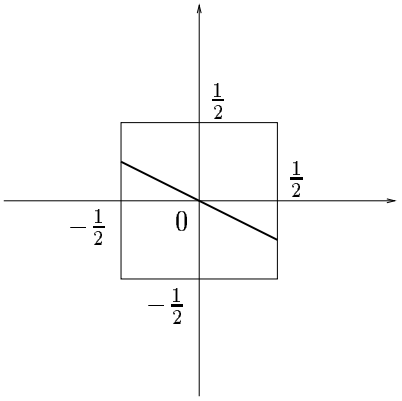

—— : spectral support of a cylindric function.

Figure 4.1: Illustration of the definition of cylindric functions.

Definition 4.2 *Let $u \in l^\infty(\mathbb{Z}^2)$. It is called* cylindric *if and only if there exists a direction $(\alpha, \beta) \in \mathbb{R}^2 \setminus \{(0,0)\}$ and $\tilde{v} \in (L^\infty(I_{\alpha,\beta}))^*$, the dual space of $L^\infty(I_{\alpha,\beta})$, such that*

$$\forall (m,n) \in \mathbb{Z}^2,\ u_{m,n} = \int_{I_{\alpha,\beta}} \tilde{v}(\xi)\, e^{2i\pi(\alpha m + \beta n)\xi} d\xi\,, \tag{4.2}$$

where $I_{\alpha,\beta}$ is the largest interval such that for all $\xi \in I_{\alpha,\beta}$, $-\frac{1}{2} < \alpha\xi \leq \frac{1}{2}$ and $-\frac{1}{2} < \beta\xi \leq \frac{1}{2}$. Such an image will be called cylindric along the direction (α, β).

Remark first that, since ,for any $(m,n) \in \mathbb{Z}^2$, $e^{2i\pi(\alpha m+\beta n)}$ belongs to $L^\infty(I_{\alpha,\beta})$, (4.2) is properly defined (even though it should have been written using a duality notation). We will abuse of the integral notation even if it is formally only valid for $\tilde{v} \in L^1(I_{\alpha,\beta})$. Moreover, note that (4.2) forces u to belong to $l^\infty(\mathbb{Z}^2)$, since

$$|u_{m,n}| \leq \|\tilde{v}\|_{\left(L^\infty(I_{\alpha,\beta})\right)^*}\,,$$

for any $(m,n) \in \mathbb{Z}^2$.

Remark also that this definition ensures that u satisfies (4.1) for the given direction (α, β) and a given function $v \in L^\infty(\mathbb{R})$.

For commodity, we do give the same name to cylindric functions of $L^\infty(\mathbb{R}^2)$ and those of $l^\infty(\mathbb{Z}^2)$. This will always be clear in context.

We will need, in the following, to restrict the set of cylindric functions (defined in Definition 4.2) of $\mathbb{Z}^2$ to the ones that are of period N (as functions of $\mathbb{Z}^2$). In such a case, taking notations of Definition 4.2, for any direction $(\alpha, \beta) \neq (0,0)$, any $(m,n) \in \mathbb{Z}^2$ and

any $(t,t') \in \mathbb{Z}^2$, we have $u_{m,n} = u_{m+tN,n+t'N}$. This yields

$$\int_{I_{\alpha,\beta}} \tilde{v}(\xi)\, e^{2i\pi(\alpha m+\beta n)\xi} d\xi = \int_{I_{\alpha,\beta}} \tilde{v}(\xi)\, e^{2i\pi(\alpha m+\beta n)\xi}\, e^{2i\pi(\alpha tN+\beta t'N)\xi} d\xi. \tag{4.3}$$

So, since for any interval $I \subset I_{\alpha,\beta}$,

$$\int_I \tilde{v}(\xi)\, e^{2i\pi(\alpha m+\beta n)\xi} d\xi\,,$$

as a function of (m,n), is also cylindric and N-periodic (its cylindric aspect is clear with regard to Definition 4.2 and the N-periodicity comes from the fact that a convolution is N-periodic as soon as one of its term is N-periodic), we have, for $\tilde{v}(\xi)d\xi$ almost every ξ and any $(t,t') \in \mathbb{Z}^2$,

$$e^{2i\pi\alpha N} = 1, \text{ and } e^{2i\pi\beta N\xi} = 1\,.$$

Thus, for $\tilde{v}(\xi)d\xi$ almost every ξ,

$$\alpha N\xi \in \mathbb{Z}, \text{ and } \beta N\xi \in \mathbb{Z}\,.$$

Therefore, (α,β) must be chosen such that the line $\alpha x + \beta y = 0$ has a rational slope and $\tilde{v}$ must be a sum of Dirac masses. More precisely we have

$$\forall (m,n) \in \mathbb{Z}^2,\ u_{m,n} = \sum_{\xi \in \tilde{I}_{\alpha,\beta}} \tilde{v}(\xi) e^{2i\pi(\alpha m+\beta n)\xi}\,, \tag{4.4}$$

where $\tilde{I}_{\alpha,\beta}$ is a discrete set such that for all $\xi \in \tilde{I}_{\alpha,\beta}$, there exists $(k,l) \in \mathbb{Z}^2$ such that $\alpha N\xi = k$ and $\beta N\xi = l$ with $-\frac{1}{2} \le \alpha\xi \le \frac{1}{2}$ and $-\frac{1}{2} \le \beta\xi \le \frac{1}{2}$. Note that, in such a case, the summation in (4.4) can be done over $(k,l) \in \{-N/2+1, ..., N/2\}^2$ satisfying $\beta k - \alpha l = 0$. This means that the DFT of u is supported by the trace of the line $\beta x - \alpha y = 0$ on the grid $\{(\frac{k}{N}, \frac{l}{N}),\ -N/2+1 \le k,l \le N/2\}$. This justifies the definition of N-periodic cylindric functions.

Lemma and Definition 4.1 *Let $N \in \mathbb{N}$ and let $u \in l^\infty(\mathbb{Z}^2)$ be periodic of period N and $(\alpha,\beta) \in \mathbb{Z}^2 \setminus \{(0,0)\}$. We say u is cylindric along the direction (α,β) if and only if its discrete Fourier transform is supported by*

$$\left\{ (k,l) \in \{-\frac{N}{2}+1, ..., \frac{N}{2}\}^2,\ \beta k - \alpha l = 0 \right\}\,.$$

Once again, we give the same name to cylindric functions whether it is periodic or not. This will always be clear in context.

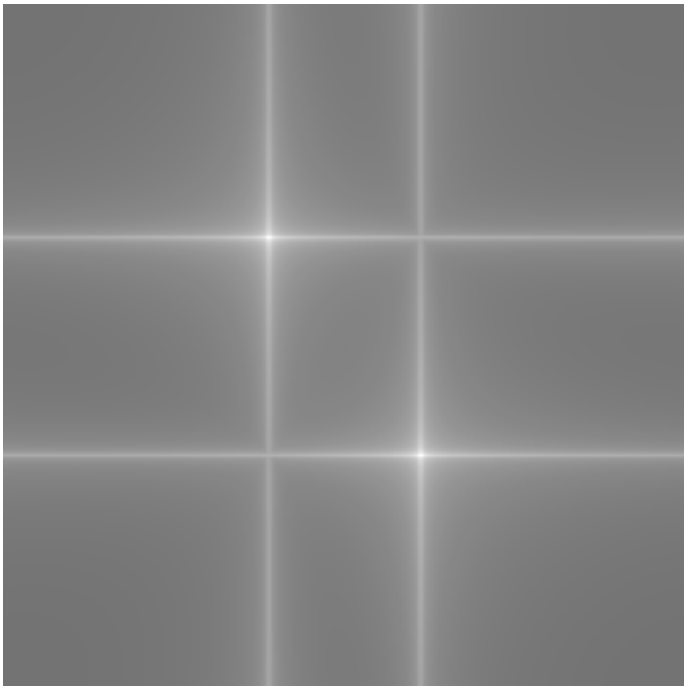

Figure 4.2: Fourier transform of the sampled version of $sin(0.7x + y)$ (this latter is not N periodic, with N the image size).

Remark. The Figure 4.2 represents the discrete Fourier transform of a function u which is the restriction on $\{0, ..., N-1\}^2$ of a function v of $l^\infty(\mathbb{Z}^2)$, cylindric but not N-periodic.

Let us go further to details. Let $(\alpha, \beta) \in \mathbb{R}^2 \setminus \{(0,0)\}$ and $u \in l^\infty(\mathbb{Z}^2)$ be periodic of period N. Let us assume there exists $\tilde{v} \in (L^\infty(I_{\alpha,\beta}))^*$ satisfying, for $(m,n) \in \{0, ..., N-1\}^2$,

$$u_{m,n} = \int_{I_{\alpha,\beta}} \tilde{v}(\xi)\, e^{2i\pi(\alpha m + \beta n)\xi} d\xi.$$

Note that we do not assume that (4.3) holds. Then, the discrete Fourier transform of u is

$$\hat{u}_{k,l} = \int_{I_{\alpha,\beta}} \tilde{v}(\xi) \sum_{m,n=0}^{N-1} e^{-2i\pi m(\frac{k}{N} - \alpha\xi)} e^{-2i\pi n(\frac{l}{N} - \beta\xi)} d\xi\,,$$

for $(k,l) \in \{-\frac{N}{2} + 1, ..., \frac{N}{2}\}^2$.

For instance, in a case where u is N-periodic, the arguments given before Definition 4.1, yields

$$\hat{u}_{k,l} = \tilde{v}(\xi)\,,$$

for ξ such that $\alpha\xi = \frac{k}{N}$ and $\beta\xi = \frac{l}{N}$.

On the other hand if, for instance, $\tilde{v} = \delta_{\xi_0}$ with ξ_0 such that $\alpha N\xi_0 \notin \mathbb{Z}$ and $\beta N\xi_0 \notin \mathbb{Z}$, we have, for $(k,l) \in \{-\frac{N}{2}+1, ..., \frac{N}{2}\}^2$,

$$\hat{u}_{k,l} = f(\frac{k}{N} - \alpha\xi_0)\, f(\frac{l}{N} - \beta\xi_0)\,,$$

with

$$f(t) = \frac{sin(\pi N\, t)}{sin(\pi\, t)}\, e^{-i\pi(N-1)\, t}\,.$$

This is precisely the case illustrated on Figure 4.2.

Chapter 5

Linear oversampling

This chapter is devoted to translation invariant and linear oversampling. Formally, we have to talk about reconstructions, since we do not take into account the convolution involved in the degradation model. The main interest of such reconstructions holds in the fact that they generally have a small computational complexity.

We first expose, both in a theoretical and a practical framework, that, under reasonable hypotheses, linear reconstructions are some convolutions. We show, then, how to choose the convolution kernel in order to preserve cylindric images. This characterization shows to advantage some contradictions in the needed behavior of the reconstructions.

5.1 Linear oversampling and cylindric functions

Let us introduce the framework and some notations that will be used all along the section. We focus on the reconstruction of functions of $l^\infty(\mathbb{Z}^2)$ such that the reconstructed images do belong to $L^\infty(\mathbb{R}^2)$. To do so, we need to use the Fourier transform and Fourier series of functions of respectively $L^1(\mathbb{R}^2)$ and $L^1(\mathbb{Z}^2)$. This latter is defined, in a way similar to Appendix A, by

$$\hat{h}(\xi,\eta) = \int_{\mathbb{R}^2} h(x,y) e^{-2i\pi(\xi x+\eta y)} dxdy\,,$$

for $(\xi,\eta) \in \mathbb{R}^2$. Similarly, we also define the Fourier series of a function $h \in l^1(\mathbb{Z}^2)$ by

$$\hat{h}(\xi,\eta) = \sum_{(m,n)\in\mathbb{Z}^2} h_{m,n} e^{-2i\pi(\xi m+\eta n)}\,,$$

for $(\xi,\eta) \in]-\frac{1}{2},\frac{1}{2}]^2$. One can refer to [6, 32, 36] for general properties of the Fourier transforms.

Moreover, we define the following generic linear interpolations of a signal $u \in l^2(\mathbb{Z}^2)$

– The "duplication"

$$v(x,y) = \sum_{m,n} u_{m,n}\, 1_{]-\frac{1}{2},\frac{1}{2}]^2}(x-m, y-n)\,.$$

– The "zero-padding" (or "sinc interpolation")

$$v(x,y) = \int_{[-\frac{1}{2},\frac{1}{2}]^2} \hat{u}(\xi,\eta)\, e^{2i\pi(\xi x+\eta y)} d\xi d\eta\,.$$

– The "zero-crossing"

$$v = \sum_{m,n} u_{m,n}\, \delta_{m,n}\,,$$

where $\delta_{m,n}$ denotes the Dirac delta function at the point (m,n). Note that the zero-crossing is not really a reconstruction since its result v is not a function but a measure.

Let us first give some simple definitions and classical facts.

Definition 5.1 *Let Z be a linear operator continuous from $l^\infty(\mathbb{Z}^2)$ into $L^\infty(\mathbb{R}^2)$. Z is called* translation invariant *if for any $u \in l^\infty(\mathbb{Z}^2)$, any $(m,n) \in \mathbb{Z}^2$ and any $(x,y) \in \mathbb{R}^2$,*

$$Z(T_{m,n}(u))(x,y) = Z(u)(x-m, y-n)\,,$$

where $T_{m,n}$ denotes the translation by (m,n) of a function of $l^\infty(\mathbb{Z}^2)$ ($T_{m,n}(u)(k,l) = u(k-m, l-n)$).

We also define a weak notion of locality by

Definition 5.2 *Let Z be a linear operator continuous from $l^\infty(\mathbb{Z}^2)$ into $L^\infty(\mathbb{R}^2)$. Z is called* local *if for any $u \in l^\infty(\mathbb{Z}^2)$ and any $(x,y) \in \mathbb{R}^2$, $\lim_{N\to\infty} Z(u_{|\{-N,\dots,N\}^2})(x,y)$ exists and*

$$Z(u)(x,y) = \lim_{N\to\infty} Z(u_{|\{-N,\dots,N\}^2})(x,y)\,,$$

where $u_{|\{-N,\dots,N\}^2}$ denotes the restriction of u to $\{-N,\dots,N\}^2$.

This notion discards linear operators that would not only depend on the local behavior of the function but also on its global one. For instance, Hahn-Banach theorem [51] permits to extend to $l^\infty(\mathbb{Z}^2)$ an operator, defined over $\mathcal{V} = \{u \in l^\infty(\mathbb{Z}^2),\ lim_{|(m,n)|\to\infty} u_{m,n} \text{ exists}\}$, of the kind

$$u \to Z(u)(x,y) = \lim_{|(m,n)|\to\infty} u_{m,n}\,.$$

Such an operator is linear, translation invariant, continuous from $l^\infty(\mathbb{Z}^2)$ into $L^\infty(\mathbb{R}^2)$ but does not reconstruct images in an interesting manner since, on the considered subspace $\mathcal{V}$ the result is constant on $\mathbb{R}^2$. The above notion of locality ruled such operators out of our framework.

Linear operators that are both translation invariant and local can easily be characterized in terms of a convolution. More precisely, we have

Proposition 5.1 *Let Z be a linear, local and translation invariant operator continuous from $l^\infty(\mathbb{Z}^2)$ into $L^\infty(\mathbb{R}^2)$. Then there exists a unique convolution kernel $h \in L^1(\mathbb{R}^2)$ and $C > 0$, such that*

$$\forall (x,y) \in \mathbb{R}^2, \quad \sum_{(m,n)\in\mathbb{Z}^2} |h(x-m, y-n)| < C \tag{5.1}$$

and

$$\forall u \in l^\infty(\mathbb{Z}^2),\ \forall (x,y) \in \mathbb{R}^2,\ Z(u)(x,y) = \sum_{(m,n)\in\mathbb{Z}^2} u_{m,n}\, h\,(x-m, y-n)\ .$$

The converse statement is also true.

Note that this result is close to classic ones (see [33]).

Proof Let Z satisfy the hypotheses of the above proposition and

$$l_0^\infty(\mathbb{Z}^2) = \{u \in l^\infty(\mathbb{Z}^2),\ u_{m,n} = 0 \text{ except for a finite number of } (m,n) \in \mathbb{Z}^2\}\,.$$

For any $u \in l_0^\infty(\mathbb{Z}^2)$ we will note $u = \sum_{m,n} u_{m,n}\delta^{m,n}$. The operator Z also maps $l_0^\infty(\mathbb{Z}^2)$ into $L^\infty(\mathbb{R}^2)$ and since Z is linear, we have, for $u \in l_0^\infty(\mathbb{Z}^2)$,

$$Z(u)(x,y) = \sum_{m,n} u_{m,n} Z(\delta^{m,n})(x,y),$$

for any $(x,y) \in \mathbb{R}^2$. Moreover, since Z is translation invariant, we have

$$Z(u)(x,y) = \sum_{m,n} u_{m,n} Z(\delta^{0,0})(x-m, y-n)\,.$$

Letting $h = Z(\delta^{0,0})$ and using the continuity assumption of the operator, we can show that h satisfies (5.1) (by taking $u^N = sign(h(x-m, y-n))_{|\{-N,\dots,N\}^2}$ and letting N grow to infinity), and therefore belongs to $L^1(\mathbb{R}^2)$. Moreover, for any $u \in l^\infty(\mathbb{Z}^2)$ and any

$(x, y) \in \mathbb{R}^2$,

$$\begin{aligned} Z(u)(x,y) &= \lim_{N\to\infty} Z(u_{|\{-N,\ldots,N\}^2})(x,y) \\ &= \sum_{(m,n)\in\mathbb{Z}^2} u_{m,n}\, h\,(x-m, y-n) \end{aligned}$$

since Z is local and the sum converges absolutely.

The proofs of the uniqueness of h and of the converse statement are obvious (note that the locality assumption on Z is somehow translated in the fact that h satisfies (5.1)). □

The operators described by this proposition are therefore some convolutions of the zero-crossing interpolation with a convolution kernel h. We will therefore describe local and translation invariant linear reconstructions by this convolution kernel.

Note also that (5.1) implies that h belongs to $L^1(\mathbb{R}^2)$ (so the assertion $h \in L^1(\mathbb{R}^2)$ has no consequences on the above proposition). Moreover, since $h \in L^1(\mathbb{R}^2)$, its Fourier transform exists and is a continuous function belonging to $L^\infty(\mathbb{R}^2)$. That is a point that will often be used in the rest of the section.

In the following, we will focus on a particular set of linear, local and translation invariant operators, continuous from $l^\infty(\mathbb{Z}^2)$ to $L^\infty(\mathbb{R}^2)$, that are the regular ones. Let us define this notion

Definition 5.3 *Let Z be such as in Proposition 5.1. Z is called* regular *if there exists $C \in \mathbb{R}$, such that the kernel h defining Z satisfies*

$$\forall (\xi,\eta) \in \mathbb{R}^2,\ \sum_{(k,l)\in\mathbb{Z}^2} |\hat{h}(\xi+k, \eta+l)| < C\,. \tag{5.2}$$

This notion is clearly a notion of regularity. Indeed, functions satisfying (5.2) are continuous. Moreover, functions whose third derivatives are in $L^1(\mathbb{R}^2)$ satisfy (5.2).

Under this assumption of regularity, the Poisson formula holds, in other words

Lemma 5.1 (Poisson) *Let $h \in L^1(\mathbb{R}^2)$ satisfying (5.1) and (5.2), then h also satisfies*

$$\forall (\xi,\eta) \in \mathbb{R}^2,\ \sum_{(m,n)\in\mathbb{Z}^2} h(m,n) e^{-2i\pi(\xi m+\eta n)} = \sum_{(k,l)\in\mathbb{Z}^2} \hat{h}(\xi+k, \eta+l)\,. \tag{5.3}$$

This result is classic (see [12, 32]) and expresses the Fourier transform (the left-hand side term of (5.3)) of a sampling of a function according to the Fourier transform of the function.

Let us now state our definition of linear zooms.

Definition 5.4 *Let Z be a linear, local, translation invariant and regular operator continuous from $l^\infty(\mathbb{Z}^2)$ into $L^\infty(\mathbb{R}^2)$. Z is called* linear zoom *if Z transforms an image constant along an axis direction into an image constant along the same axis direction.*

This definition of a linear zoom simply expresses the need of satisfying some basic properties such as a weak notion of locality, translation invariance (doing linear reconstruction, there are no reasons to *a priori* deal in different ways with the different parts of the initial image), regularity of the result, continuity (which leads to the stability of the zoom) and also to impose them to restore correctly horizontal and vertical structures. Note also that this latter, in the case of signals, would be that the reconstruction of a constant signal is constant. Moreover, in such a case, we could have stated a proposition similar to Proposition 5.2.

We are now going to characterize these objects using h (the kernel that defines Z).

Proposition 5.2 *Let Z be a linear, local, translation invariant and regular operator continuous from $l^\infty(\mathbb{Z}^2)$ into $L^\infty(\mathbb{R}^2)$. Let h be the convolution kernel defining Z. Z is a linear zoom if and only if*

$$\forall k \in \mathbb{Z} \setminus \{0\},\ \forall \xi \in \mathbb{R},\ \hat{h}(k,\xi) = \hat{h}(\xi,k) = 0\,. \tag{5.4}$$

Proof The proof is similar to the one of Proposition 5.3 (to follow). □

Note that, this heuristically means that there exists h such that

$$\forall u \in l^\infty(\mathbb{Z}^2),\ Z(u) = h * u^d\,,$$

where u^d denotes the duplication interpolation of the image u (see Section 5.2). Indeed, the Fourier transform of $1_{]-\frac{1}{2},\frac{1}{2}]^2}$ satisfies (5.4) and only vanishes on $\{(\xi,\eta) \in \mathbb{R}^2,\ \xi \in \mathbb{Z} \text{ or } \eta \in \mathbb{Z}\}$.

Let us now develop this point. We could expect linear zooms to preserve cylindric images whatever the direction is. Note, once again, that the idea of being interested in the preservation of cylindric images is driven by the observation that a classical artifact in image reconstruction is the creation of hatched edges.

Proposition 5.3 *Let Z be a linear zoom and let h be the convolution kernel that defines Z. Assume that for any direction $(\alpha,\beta) \in \mathbb{R}^2 \setminus \{(0,0)\}$ and any image u cylindric along the direction (α,β), $Z(u)$ is also cylindric along the direction (α,β). Then*

$$\forall (\xi,\eta) \in \mathbb{R}^2,\ \textit{such that } |\xi| > \frac{1}{2} \textit{ or } |\eta| > \frac{1}{2},\ \hat{h}(\xi,\eta) = 0\,. \tag{5.5}$$

Conversely, any linear, local and translation invariant operator continuous from $l^\infty(\mathbb{Z}^2)$ into $L^\infty(\mathbb{R}^2)$ associated with a kernel h satisfying (5.5) is a linear zoom and preserves cylindric images along any direction.

Note that, heuristically, this proposition means that linear zooms preserving cylindric images can be expressed in terms of a convolution of the "sinc interpolation". We cannot give the proposition in this form since the "sinc interpolation" is not continuous from $l^\infty(\mathbb{Z}^2)$ into $L^\infty(\mathbb{R}^2)$.

Note also that, since Definition 4.2 is relatively restrictive, the "sinc interpolation", defined in the introduction, gives an exact reconstruction for cylindric images (see [46]). We know, in other respects, that it yields oscillatory results (since the convolution kernel associated with the "sinc interpolation" oscillates). This latter behavior is not taken into account by the analysis of cylindric functions and therefore by this proposition.

Proof Let $(\alpha, \beta) \in \mathbb{R}^2 \setminus \{(0,0)\}$ and $u \in l^\infty(\mathbb{Z}^2)$ a cylindric function along the direction (α, β). We know that there exists $\tilde{v} \in (L^\infty(I_{\alpha,\beta}))^*$ linked with u by (4.2) and that there exists $h \in L^1(\mathbb{R}^2)$ such that

$$Z(u)(x,y) = \sum_{(m,n)\in\mathbb{Z}^2} h(x-m, y-n)\, u_{m,n}\,.$$

Using (4.2), we get

$$Z(u)(x,y) = \sum_{(m,n)\in\mathbb{Z}^2} h(x-m, y-n) \int_{I_{\alpha,\beta}} \tilde{v}(\xi) e^{2i\pi(\alpha m+\beta n)\xi} d\xi\,. \tag{5.6}$$

Remark that, since h satisfies (5.1), for any $(x,y) \in \mathbb{R}^2$ and any $K > 0$, both following sums exist and

$$\left| \sum_{|m| \text{ or } |n|\geq K} h(x-m, y-n) e^{2i\pi(\alpha m+\beta n)\xi} \right| \leq \sum_{|m| \text{ or } |n|\geq K} |h(x-m, y-n)|\,,$$

where the left-hand term does not depend on ξ and converges to 0 when K grows to infinity. Therefore, since $\tilde{v}$ is continuous over $L^\infty(I_{\alpha,\beta})$, (5.6) can be written,

$$Z(u)(x,y) = \int_{I_{\alpha,\beta}} \tilde{v}(\xi) \sum_{(m,n)\in\mathbb{Z}^2} h(x-m, y-n) e^{2i\pi(\alpha m+\beta n)\xi} d\xi\,.$$

Then, if we write $h_{x,y}(x', y') = h(x+x', y+y')$, we have

$$Z(u)(x,y) = \int_{I_{\alpha,\beta}} \tilde{v}(\xi) \sum_{(m,n)\in\mathbb{Z}^2} h_{x,y}(m,n) e^{-2i\pi(\alpha m+\beta n)\xi} d\xi\,.$$

Using Poisson formula (5.3), we get

$$Z(u)(x,y) = \int_{I_{\alpha,\beta}} \tilde{v}(\xi) \sum_{(k,l)\in\mathbb{Z}^2} \widehat{h_{x,y}}(\alpha\xi + k, \beta\xi + l) d\xi \,. \tag{5.7}$$

This formula expresses the fact that the spectrum of $Z(u)$ is the spectrum of u, periodized and weighted by h (see Figure 5.1).

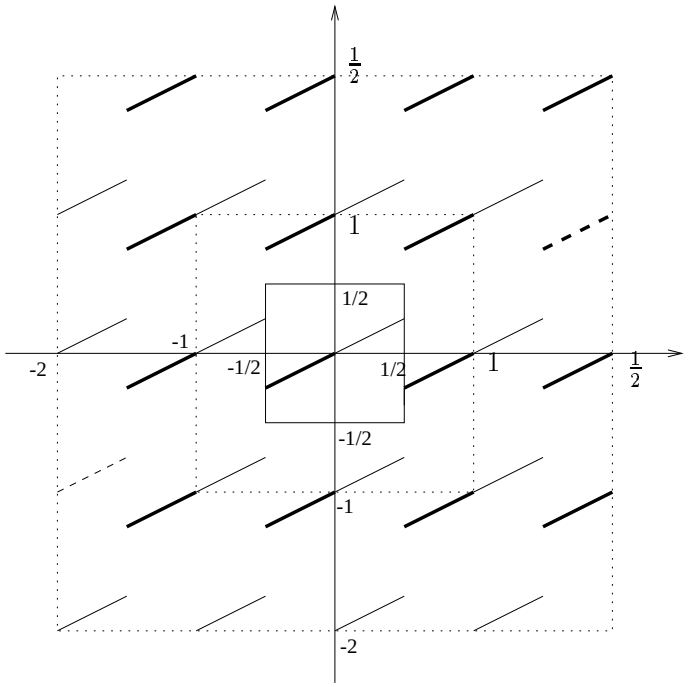

Figure 5.1: The spectrum of a linear zoom is a weighted periodization of the initial image spectrum. This figure represents the support of a linear zoom of an image cylindric along the direction $(2,1)$ (the dashed segment are also in the direction $(2,1)$).

Expressing the fact that $Z(u)$ is cylindric along the direction (α,β), we know that

$$\forall t \in \mathbb{R},\ Z(u)(x,y) - Z(u)(x-\beta t, y+\alpha t) = 0 \,,$$

which, using (5.7), gives

$$\forall t \in \mathbb{R},\ \int_{I_{\alpha,\beta}} \tilde{v}(\xi) \sum_{(k,l)\in\mathbb{Z}^2} \widehat{h_{x,y}}(\alpha\xi + k, \beta\xi + l) \left[1 - e^{-2i\pi(\beta k - \alpha l)t}\right] = 0 \,.$$

Since this equality holds for any $\tilde{v} \in (L^\infty(I_{\alpha,\beta}))^*$, we finally have for any $t \in \mathbb{R}$

$$\sum_{(k,l)\in\mathbb{Z}^2} \widehat{h_{x,y}}(\alpha\xi+k,\beta\xi+l)e^{-2i\pi(\beta k-\alpha l)t} = \sum_{(k,l)\in\mathbb{Z}^2} \widehat{h_{x,y}}(\alpha\xi+k,\beta\xi+l)\,.$$

The conclusion follows from the following lemma

Lemma 5.2 *For any pair $(\alpha,\beta)\in\mathbb{R}^2$ such that the line defined by $\alpha x+\beta y=0$ has an irrational slope and for any $(a_{k,l})_{k,l}\in l^1(\mathbb{Z}^2)$,*

$$\forall t\in\mathbb{R},\ \sum_{(k,l)\in\mathbb{Z}^2} a_{k,l}e^{-2i\pi(\beta k-\alpha l)t}=0\ \Rightarrow\ \forall(k,l)\in\mathbb{Z}^2,\ a_{k,l}=0\,. \tag{5.8}$$

Note that for any $(a_{k,l})_{k,l}\in l^1(\mathbb{Z}^2)$, $\sum_{(k,l)\in\mathbb{Z}^2} a_{k,l}e^{-2i\pi(\beta k-\alpha l)t}$ is in $L^\infty(\mathbb{R})$ and so it has a computable Fourier transform in the sense of tempered distributions. Therefore, the left-hand part of (5.8) yields

$$\sum_{(k,l)\in\mathbb{Z}^2} a_{k,l}\,\delta_{(\beta k-\alpha l)}=0\,.$$

Since the $(\beta k-\alpha l)$ are all distinct, this implies

$$\forall(k,l)\in\mathbb{Z}^2,\ a_{k,l}=0\,.$$

□

Turning back to the proof of Proposition 5.3, we finally find that if Z preserves cylindric functions along any direction, $\hat{h}(\xi,\eta)=0$ for any $(\xi,\eta)\in\mathcal{C}$ with

$$\mathcal{C}=\bigcup_{(k,l)\neq(0,0)}\mathcal{C}_{k,l}$$

and

$$\begin{aligned}\mathcal{C}_{k,l} \;=\; \{(\alpha\xi+k,\beta\xi+l),\ (\alpha,\beta)\in\mathbb{R}^2\setminus\{(0,0)\},&\text{ such that the line}\\ -\beta y+\alpha x=0&\text{ has an irrational slope and }\xi\in I_{\alpha,\beta}\}\,.\end{aligned}$$

It is easy to check that $\mathcal{C}_{k,l}$ is dense in $]k-\frac{1}{2},k+\frac{1}{2}]\times]l-\frac{1}{2},l+\frac{1}{2}]$, so that $\mathcal{C}$ is dense in $\mathbb{R}^2\setminus]-\frac{1}{2},\frac{1}{2}[^2$. The result follows from the fact that (5.1) imposes $\hat{h}$ to be continuous. The converse statement directly follows from (5.7). Indeed, when h satisfies (5.5), a calculation similar to one yielding (5.7), guarantees that the linear zooms defined by h preserves cylindric functions. □

Remark that in the previous proof, we could have avoided the use of (α, β) such that $\alpha x + \beta y = 0$ has an irrational slope. Indeed, going a little bit further to the analysis (see Figure 5.1), we could have got

$$\begin{aligned} \mathcal{C}_{k,l} &= \{(\alpha\xi + k, \beta\xi + l),\ (\alpha, \beta) \in \mathbb{R}^2 \setminus \{(0,0)\}, \\ &\qquad \text{such that } -\beta k + \alpha l \neq 0, \text{ and } \xi \in I_{\alpha,\beta}\}\ . \end{aligned}$$

Note that even the restriction of this $\mathcal{C}_{k,l}$ to the pairs (α, β), such that $\alpha x + \beta y = 0$ has a rational slope, is dense in $[k - \frac{1}{2}, k + \frac{1}{2}] \times [l - \frac{1}{2}, l + \frac{1}{2}]$.

At this point, in order to determine an h yielding good results, the most important remaining problem is the locality of h (otherwise, we shall have blurred and/or oscillating results and large computation cost). Note that, since $\hat{h}$ is compactly supported, we can neither expect h to be well located nor to yield sharp results. We can of course use prolate functions (see [28] or Chapter 1), which are a way to deal with Heisenberg uncertainty principle (see [33]). Unfortunately, such functions define reconstruction which lead to blurred results (see Chapter 7).

Now, this analysis shows us that linear reconstructions cannot yield fully satisfactory results, in the sense that they cannot completely avoid all the artifacts mentioned above. This is simply due to the fact that the removal of these artifacts leads us to ask contradictory properties from the kernel h. Therefore, if one still wants to reconstruct images linearly, one has to balance with all these shortcomings with regard to the expected properties the reconstructed images shall satisfy.

5.2 Numerical zooming and cylindric functions

In this section, we focus on a very practical aspect of the reconstruction that is the numerical zooming (i.e. the case where both the image and its oversampled version are of finite size). Therefore, taking notations of (3.1), we let $\Omega = [0, N[^2$, and we assume the initial data to be periodic. Moreover, since the result has to be estimated and run on a computer, we will assume the resolution to be enhanced by a factor $K > 1$ (K is called the level of zoom) and the result to be given as a function of $\{0, ..., KN - 1\}^2$.

In this section, elements of $\mathbb{R}^{N^2}$ describe discrete images of size $N \times N$, and have two subscripts.

Let us state some results similar to the one of Section 5.1, but adapted to this framework.

Definition 5.5 *Let $N > 0$ and $K > 1$ be some integers and let Z be a linear operator from $\mathbb{R}^{N^2}$ into $\mathbb{R}^{(KN)^2}$. Z is said to be* translation invariant *if for any $u \in \mathbb{R}^{N^2}$ and any*

$(m,n) \in \{0,...N-1\}^2$

$$Z(T_{m,n}(u)) = T'_{Km,Kn}(Z(u))\,,$$

where $T_{m,n}$ and $T'_{Km,Kn}$ denote indices translations of respectively (m,n) and (Km,Kn) in respectively $\mathbb{R}^{N^2}$ and $\mathbb{R}^{(KN)^2}$.

Proposition 5.4 *Let $N > 0$ and $K > 1$ be some integers and let Z be a translation invariant linear operator from $\mathbb{R}^{N^2}$ into $\mathbb{R}^{(KN)^2}$. Then, there exists a unique $h \in \mathbb{R}^{(KN)^2}$, such that*

$$\forall u \in \mathbb{R}^{N^2},\ \forall (m,n) \in \{0,...,KN-1\}^2,\ Z(u)_{m,n} = (h * u^0)_{m,n}\,, \tag{5.9}$$

where u^0 denotes the zero crossing of u and is characterized by

$${u^0}_{m,n} = \begin{cases} u_{m',n'} & , \text{ if } m = Km' \text{ and } n = Kn' \\ 0 & , \text{ otherwise.} \end{cases} \tag{5.10}$$

h is called the convolution kernel associated with Z.

Conversely, any operator of the form $h * u^0$, with u^0 defined above, is linear and translation invariant.

This proposition is analogous to Proposition 5.1. Note that, unlike in Proposition 5.1, we do have locality and regularity hypotheses neither on Z nor on h.

Proof For any $(m,n) \in \{0,...,N-1\}^2$, we note $e^{m,n} \in \mathbb{R}^{N^2}$ the discrete image equal to 0 everywhere, except for the subscript (m,n), where $e^{m,n}$ has value 1. Let $u \in \mathbb{R}^{N^2}$ and $(m,n) \in \{0,...,N-1\}^2$, we have

$$u_{m,n} = \sum_{m',n'=0}^{N-1} u_{m',n'}\ e^{m',n'}_{m,n}\,.$$

Therefore, since Z is linear and translation invariant, we have

$$\begin{aligned} Z(u)_{m,n} &= \sum_{m',n'=0}^{N-1} u_{m',n'}\, Z(e^{m',n'})_{m,n} = \sum_{m',n'=0}^{N-1} u_{m',n'}\, Z(T_{m',n'}(e^{0,0}))_{m,n}\,, \\ &= \sum_{m',n'=0}^{N-1} u_{m',n'}\, T_{Km',Kn'}(Z(e^{0,0}))_{m,n} = \sum_{m',n'=0}^{N-1} u_{m',n'}\, Z(e^{0,0})_{m-Km',n-Kn'}\,. \end{aligned}$$

So, setting $h = Z(e^{0,0})$, we have (5.9). The uniqueness and the converse statement are obvious. □

This proposition shows that linear and translation invariant numerical zooms are some convolutions of the zero-crossing (see (5.10)). So, similarly to the preceding section, the difference between linear reconstructions holds in the convolution kernel h.

Let us express (5.9) in the frequency domain. It is easy to check that, for any $u \in \mathbb{R}^{N^2}$ and any $(\xi, \eta) \in \{-\frac{KN}{2}+1, ..., \frac{KN}{2}\}^2$,

$$\widehat{u^0}_{\xi,\eta} = \hat{u}_{\xi[N],\eta[N]}$$

where $\xi[N]$ denotes the unique integer of $\{-\frac{N}{2}+1, ..., \frac{N}{2}\}$ such that there exists $q \in \mathbb{Z}$, satisfying $\xi = qN + \xi[N]$.

Therefore, we see that for any linear operator Z satisfying the hypotheses of the proposition, there exists a signal $h \in \mathbb{R}^{(KN)^2}$, such that for any discrete image $u \in \mathbb{R}^{N^2}$ and any $(\xi, \eta) \in \{-\frac{KN}{2}+1, ..., \frac{KN}{2}\}^2$, we have

$$\widehat{Z(u)}_{\xi,\eta} = \hat{h}_{\xi,\eta} \hat{u}_{\xi[N],\eta[N]} .$$

For instance, if we note $h^d \in \mathbb{R}^{(KN)^2}$ the convolution kernel associated with the duplication reconstruction (which is of course linear and translation invariant), we have for $(\xi, \eta) \in \{-\frac{KN}{2}+1, ..., \frac{KN}{2}\}^2$

$$\widehat{h^d}_{\xi,\eta} = \widehat{h^{d1}}_{\xi} \, \widehat{h^{d1}}_{\eta} , \tag{5.11}$$

with

$$\widehat{h^{d1}}_{\xi} = \begin{cases} \frac{e^{-2i\pi\frac{\xi[N]}{N}}-1}{e^{-2i\pi\frac{\xi}{KN}}-1} & \text{if } \xi \neq 0 , \\ \\ K & \text{if } \xi = 0 . \end{cases}$$

Once again, similarly to Proposition 5.2, we can state

Proposition 5.5 *Let $N > 0$ and $K > 1$ be some integers and let Z be a translation invariant linear operator from $\mathbb{R}^{N^2}$ into $\mathbb{R}^{(KN)^2}$. Then, Z preserves images cylindric*[1] *along the axis directions if and only if there exists $h \in \mathbb{R}^{(KN)^2}$ such that*

$$\forall u \in \mathbb{R}^{N^2}, \; Z(u) = h * u^d ,$$

where u^d denotes the duplication of the image u.

[1] *The definition of cylindric elements in $\mathbb{R}^{N^2}$ (respectively $\mathbb{R}^{(KN)^2}$) comes from the identification of $\mathbb{R}^{N^2}$ (respectively $\mathbb{R}^{(KN)^2}$) to N-periodic (respectively KN-periodic) elements of $l^\infty(\mathbb{Z}^2)$.*

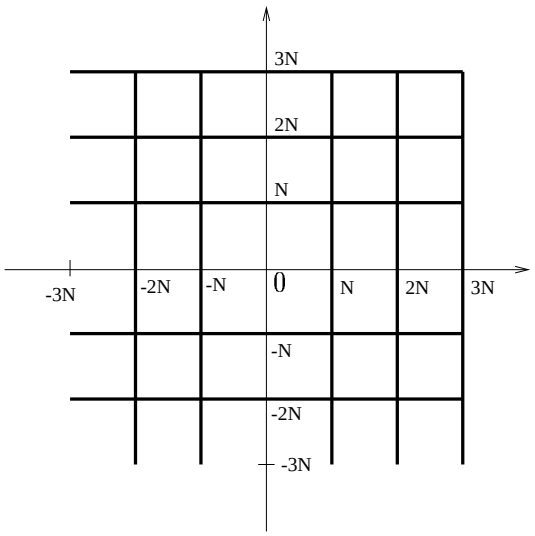

Figure 5.2: The thick lines represent $\mathcal{Z}$ in the case $K = 6$.

Proof Let $u \in \mathbb{R}^{N^2}$, and $v \in \mathbb{R}^N$, such that for any $(m,n) \in \{0,...,N\}^2$, $u_{m,n} = v_m$. We know that there exists $h' \in \mathbb{R}^{(KN)^2}$ and $V \in \mathbb{R}^{KN}$, such that for any $(m,n) \in \{0,...,KN\}^2$

$$(Z(u))_{m,n} = (h' * u^0)_{m,n} = V_m \, .$$

So, looking at the Discrete Fourier Transform of $Z(u)$, we observe that for any $(\xi,\eta) \in \{-\frac{KN}{2}+1,...,\frac{KN}{2}\}^2$, $\widehat{h'}_{\xi,\eta}\hat{u}_{\xi[N],\eta[N]}$ must be supported by $\{-\frac{KN}{2}+1,...,\frac{KN}{2}\} \times \{0\}$.

Doing the same reasoning with images cylindric along the other axis direction, we finally find that

$$\forall (\xi,\eta) \in \mathcal{Z}, \ \widehat{h'}_{\xi,\eta} = 0 \, ,$$

with (see Figure 5.2)

$$\mathcal{Z} = \left\{ (\xi,\eta) \in \left(\{-\frac{KN}{2}+1,...,\frac{KN}{2}\} \setminus \{0\} \right)^2 , \ \xi[N] = 0 \text{ or } \eta[N] = 0 \right\} .$$

We conclude the proof with the remark that if $(\xi,\eta) \in \mathcal{Z}$, $\widehat{h^d}_{\xi,\eta} = 0$ (see (5.11)).
The converse statement is obvious. □

Note that, in the above proposition, the lack of uniqueness comes from the fact that

the linear operator Z does not depend on $\hat{h}_{\xi,\eta}$ for $(\xi,\eta) \in \{-\frac{KN}{2}+1,...,\frac{KN}{2}\}^2 \setminus \mathcal{Z}$.

Let us now state a statement equivalent to proposition 5.3 in the case of numerical zooms.

Proposition 5.6 *Let $N > 0$ and $K > 1$ be some integers and let Z be a translation invariant linear operator from $\mathbb{R}^{N^2}$ into $\mathbb{R}^{(KN)^2}$. Assume that for any direction $(\alpha,\beta) \in \mathbb{R}^2 \setminus \{(0,0)\}$ and any image u cylindric along the direction (α,β), $Z(u)$ is also cylindric along the direction (α,β). Then, there exists $h \in \mathbb{R}^{(KN)^2}$ such that*

$$\forall u \in \mathbb{R}^{N^2},\ Z(u) = h * u^c\,,$$

where u^c denotes the numerical zoom associated with the kernel h^c defined by $\widehat{h^c} = 1_{|\mathcal{C}^{K,N}}$, with

$$\mathcal{C}^{K,N} = \left\{(\xi,\eta) \in \{-\frac{KN}{2}+1,...,\frac{KN}{2}\}^2,\ (\xi[N],\eta[N]) \neq (0,0) \text{ and } \xi\,.(\eta[N]) = \eta\,.(\xi[N])\right\} \cup \{(0,0)\}\,.$$

Conversely, any operator of the form $Z(u) = h * u^c$ with $h \in \mathbb{R}^{(KN)^2}$ is linear, translation invariant and preserves cylindric images along any direction.

Proof The proof is analog to the one of the proposition 5.5. □

Remark that $\mathcal{C}^{K,N}$ is simply the set of all the pairs of frequencies (ξ,η) for which $(\xi[N],\eta[N])$ (the frequency on which it aliases) is not $(0,0)$ and belongs to the trace of the line passing by $(0,0)$ and (ξ,η) (see Figure 5.3).

Note that $\mathcal{C}^{K,N}$ can also be described by taking as a point of departure a low frequency (see Figure 5.3). With that in mind, we define, for any pair $(\xi,\eta) \in \mathbb{Z}^2 \setminus \{(0,0)\}$, (ξ',η') the "irreducible" representative of the direction (ξ,η) by

$$(\xi',\eta') = \begin{cases} (1,0) & \text{, if } \eta = 0\,, \\ (0,1) & \text{, if } \xi = 0\,, \\ sign(\xi)\,\frac{(\xi,\eta)}{gcd(|\xi|,|\eta|)} & \text{, if } \xi \neq 0 \text{ and } \eta \neq 0\,, \end{cases}$$

where $sign(x)$ is the sign of x and $gcd(m,n)$ denotes the greatest common divisor of the integers m and n.

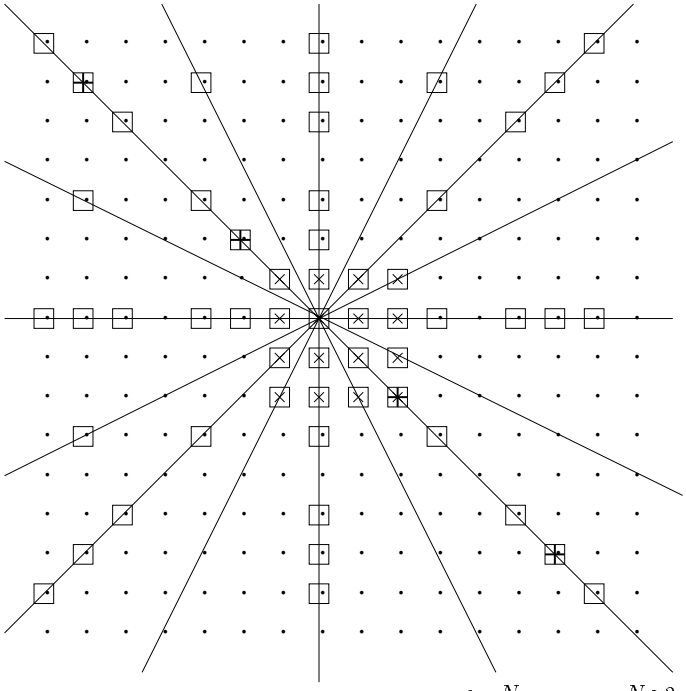

$\times$: represents a frequency of $\{-\frac{N}{2}+1, ..., \frac{N}{2}\}^2$.
$\cdot$: represents a frequency of $\{-\frac{KN}{2}+1, ..., \frac{KN}{2}\}^2$.
$\square$: represents an element of $\mathcal{C}^{4,4}$.
$\boxplus$: represents an element of $\mathcal{C}^{4,4}$ on which $\hat{u}_{2,2}$ is copied.

Figure 5.3: Example of a set $\mathcal{C}^{K,N}$, in the case where $K = 4$ and $N = 4$. The lines all cross at the origin of the frequency domain.

Taking these notations, we have

$$\mathcal{C}^{K,N} = \left\{ (\xi + kN\xi', \eta + kN\eta') \in \{-\frac{KN}{2}+1, ..., \frac{KN}{2}\}^2, \text{ with } (\xi,\eta) \in \{-\frac{N}{2}+1, ..., \frac{N}{2}\}^2 \setminus \{(0,0)\} \text{ and } k \in \mathbb{Z} \right\}. \quad (5.12)$$

Contrary to what happens in Proposition 5.3, there can remain non null frequencies out of $\{-\frac{N}{2}+1, ..., \frac{N}{2}\}^2$. This is basically due to the fact that, in the case numerical zoom, the trace of the line on the discrete grid is not of null measure. However, the following proposition shows that the cancellation of the high frequencies is a limit case of the above proposition when N tends to infinity.

Proposition 5.7 *Let $K > 1$ be an integer, we have*

$$\frac{1}{N^2}\sum_{(\xi,\eta)\in\mathcal{C}^{K,N}}\delta_{\frac{\xi}{N},\frac{\eta}{N}} \quad \xrightarrow[N\to\infty]{\mathcal{S}'(\mathbb{R}^2)} \quad 1_{|[-\frac{1}{2},\frac{1}{2}]^2}\,,$$

where $\delta_{x,y}$ denotes the Dirac delta function at the point (x,y). Moreover, this convergence is uniform in K.

Generalities on $\mathcal{S}'(\mathbb{R}^2)$ and $\mathcal{S}(\mathbb{R}^2)$ are available in [6]. The main reasons that make of $\mathcal{S}'(\mathbb{R}^2)$ the natural space for this convergence is that $\mathcal{S}'(\mathbb{R}^2)$ contains Dirac delta function as well as continuous functions and that the Fourier transform defines a continuous isomorphism from $\mathcal{S}'(\mathbb{R}^2)$ onto itself.

In fact, the convergence occurs in a sense weaker than $\mathcal{S}'(\mathbb{R}^2)$. Indeed, we could have stated

$$\forall\varphi\in C_0^0(\mathbb{R}^2),\ \lim_{N\to\infty}\frac{1}{N^2}\sum_{(\xi,\eta)\in\mathcal{C}^{K,N}}\varphi(\frac{\xi}{N},\frac{\eta}{N})=\int_{[-\frac{1}{2},\frac{1}{2}]^2}\varphi\,,$$

where $C_0^0(\mathbb{R}^2)$ denotes the set of continuous and compactly supported functions of $\mathbb{R}^2$.

Proof Let K be a positive integer, we split $\mathcal{C}^{K,N}$ into the two disjoint sets

$$\mathcal{C}^{K,N}=\left\{-\frac{N}{2}+1,...,\frac{N}{2}\right\}^2\cup\mathcal{R}^{K,N}\,.$$

The Riemann summation Theorem ensures that

$$\tfrac{1}{N^2}\textstyle\sum_{(\xi,\eta)\in\{-\frac{N}{2}+1,...,\frac{N}{2}\}^2}\delta_{\frac{\xi}{N},\frac{\eta}{N}} \quad \xrightarrow[N\to\infty]{\mathcal{S}'(\mathbb{R}^2)} \quad 1_{|[-\frac{1}{2},\frac{1}{2}]^2}\,,$$

so we only have to prove that

$$S^{K,N}=\tfrac{1}{N^2}\textstyle\sum_{(\xi,\eta)\in\mathcal{R}^{K,N}}\delta_{\frac{\xi}{N},\frac{\eta}{N}} \quad \xrightarrow[N\to\infty]{\mathcal{S}'(\mathbb{R}^2)} \quad 0\,.$$

Let $\varphi\in\mathcal{S}(\mathbb{R}^2)$, we have

$$\begin{aligned}|\langle S^{K,N},\varphi\rangle| &= \frac{1}{N^2}\left|\sum_{(\xi,\eta)\in\mathcal{R}^{K,N}}\varphi(\frac{\xi}{N},\frac{\eta}{N})\right| \\ &\le \frac{1}{N^2}\sum_{(\xi,\eta)\in\mathcal{R}^{\infty,N}}\left|\varphi(\frac{\xi}{N},\frac{\eta}{N})\right|\,,\end{aligned}$$

where, $\mathcal{R}^{\infty,N}$ follows from (5.12) and is given by

$$\mathcal{R}^{\infty,N} = \Big\{ (\xi + kN\xi', \eta + kN\eta') \in \mathbb{Z}^2, \text{ with } (\xi,\eta) \in \{-\frac{N}{2}+1, ..., \frac{N}{2}\}^2 \setminus \{(0,0)\} \text{ and } k \neq 0 \Big\} .$$

Moreover, there exists C such that, for any $(x,y) \in \mathbb{R}^2$,

$$|\varphi(x,y)| \leq \frac{C}{sup(|x|,|y|)^2} ,$$

so we have

$$\begin{aligned} |\langle S^{K,N}, \varphi \rangle| &\leq \frac{1}{N^2} \sum_{(\xi,\eta) \in \left\{-\frac{N}{2}+1,...,\frac{N}{2}\right\}^2 \setminus \{(0,0)\}} \sum_{k \neq 0} \frac{CN^2}{sup(|\xi + kN\xi'|, |\eta + kN\eta'|)^2} \\ &\leq \frac{1}{N^2} \sum_{(\xi,\eta) \in \left\{-\frac{N}{2}+1,...,\frac{N}{2}\right\}^2 \setminus \{(0,0)\}} \sum_{k \neq 0} \frac{4CN^2}{sup(|kN\xi'|, |kN\eta'|)^2} \\ &\leq \frac{4C}{N^2} \frac{\pi^2}{6} \sum_{(\xi,\eta) \in \left\{-\frac{N}{2}+1,...,\frac{N}{2}\right\}^2 \setminus \{(0,0)\}} \frac{1}{sup(|\xi'|, |\eta'|)^2} . \end{aligned}$$

Moreover, for any $(\xi,\eta) \in \left\{-\frac{N}{2}+1, ..., \frac{N}{2}\right\}^2 \setminus \{(0,0)\}$, there exists $l \in \mathbb{Z}$, satisfying $|l| \leq \frac{N}{2\, sup(|\xi'|,|\eta'|)}$, such that $(\xi,\eta) = l(\xi',\eta')$ (in fact $l = gcd(\xi,\eta)$). So, setting

$$S_1^N = \sum_{(\xi,\eta) \in \left\{-\frac{N}{2}+1,...,\frac{N}{2}\right\}^2 \setminus \{(0,0)\}} \frac{1}{sup(|\xi'|, |\eta'|)^2} ,$$

we have

$$\begin{aligned} S_1^N &\leq \sum_{\substack{(\xi',\eta') \in \left\{-\frac{N}{2}+1, ..., \frac{N}{2}\right\}^2 \setminus \{(0,0)\} \\ gcd(\xi',\eta') = 1}} \sum_{|l| \leq \frac{N}{2\, sup(|\xi'|,|\eta'|)}} \frac{1}{sup(|\xi'|, |\eta'|)^2} , \\ &\leq 4N \sum_{\substack{\frac{N}{2} \geq \xi' \geq \eta' \geq 0 \\ \xi' \neq 0,\ gcd(\xi',\eta') = 1}} \frac{1}{\xi'^3} \\ &\leq 4N \sum_{\frac{N}{2} \geq \xi' > 0} \frac{1+\xi'}{\xi'^3} = 4C'N \end{aligned}$$

with $C' = \sum_{\xi'=1}^{\infty} \frac{1+\xi'}{\xi'^3}$.

Therefore, for any $\varphi \in \mathcal{S}'(\mathbb{R}^2)$, there exists C'', such that

$$|\langle S^{K,N}, \varphi \rangle| \leq \frac{C''}{N},$$

which achieves the proof. □

This proposition shows that for a given reconstruction kernel h, that satisfies the hypotheses of Proposition 5.6, if we increase sufficiently the image size (we assume here that h is localized enough (in space domain) so that we can neglect the influence of the increase in the image size), then h is "essentially" supported by $[-\frac{1}{2}, \frac{1}{2}]^2$.

5.3 Conclusion

Both sections above show that linear reconstructions do not allow to reconstruct frequencies in a meaningful manner. Indeed, they simply periodize the initial spectrum before diminishing the values supported by the frequencies (in general, especially the high (created) ones). We have shown, with regard to the repartition of the non-cancelled frequencies, that the new frequencies are taking values that do not make sense (note here that we could probably have got the same conclusion regarding the phases of the created frequencies). Therefore, our conclusion is that we do have to cancel the "false information" supported by these frequencies. Thus, in order to keep as much information and sharpness as possible, we should use the zero-padding interpolation (which may yield an exact reconstruction [46]). However, we could also expect the reconstruction kernel to have nice properties in space domain (such as localization and positiveness). We suggest in Section 5.1 to use prolate spheroidal functions (see [28]) to deal with Heisenberg uncertainty principle. Doing this, we get a well localized reconstruction kernel. Moreover, the L^2 norm of the oscillations of the kernel is negligible with regard to the L^2 norm of the whole kernel. Therefore, we do not meet the artifacts due to the lack of positiveness of the kernel. Note that it could be interesting to try to see if it is possible, expecting a positive reconstruction kernel, to find one that has a correct spatial localization (note that the positiveness hypothesis can be replaced by a stronger one such as $\langle (x,y), \nabla h(x,y) \rangle \leq 0$, where h is the reconstruction kernel and $(x,y) \in \mathbb{R}^2$, or stronger).

Whatever the chosen method is, the compactly supported aspect of the reconstruction kernel yields infinitely differentiable results. Visually, the reconstructed images present blurred edges and very smooth zones. Such a behavior is damaging to these methods since edges in natural images look often discontinuous. More generally, leaving apart the framework of reconstructions that preserve cylindric images, the regularity of the results provided by a linear reconstruction is predetermined by the chosen kernel. Moreover,

this regularity is not adapted to the information (on the local regularity of the initial landscape), remaining in the sampled image. This leads us to the variational approach described in the next chapter. This is mainly driven by the idea that among the "possible images" we want to select one that has a "reasonable" regularity.

Chapter 6

Variational image oversampling

In this chapter we will focus on nonlinear oversampling methods. Formally, we have to talk about restorations, since we do take into account the whole degradation suffered by the image (including the convolution).

Let us introduce the framework and some notations that will be used all along the chapter. First, these restorations are based on functional minimization, so we turn to a finite dimensional case, in order to get proper results. Therefore, a sampled image u is assumed to be periodic of period N (for commodity we will assume in the following that N is even). This leads us to define the zoomed images on the torus of size N, $(N\mathbb{T})^2$ (noted $(\mathbb{T}_N)^2$).

In the following, in order to distinguish Fourier series from Discrete Fourier Transforms, we will denote $\hat{w}_{\frac{k}{N},\frac{l}{N}}$ by $\hat{w}(\frac{k}{N},\frac{l}{N})$ in the case of the Fourier series. Moreover, the frequency coordinates will often be written $(\frac{\xi}{N}+k,\frac{\eta}{N}+l)$, with $(\xi,\eta) \in \{-\frac{N}{2}+1,...,\frac{N}{2}\}^2$ and $(k,l) \in \mathbb{Z}^2$, to give prominence to the frequency on which it is copied during the sampling process.

Moreover, we do present the method in the case of a regularity criterion that is the total variation, but most of the results can be extended to other kinds of energies that would satisfy properties such as "lower semi-continuity", "compactness" and which satisfy

$$E(h * w) \leq \|h\|_1 E(w)\,,$$

for $h \in L^1((\mathbb{T}_N)^2)$. However, we do present this work in the case of the total variation since we do believe it is the most suitable for image reconstruction (see Section 2.2).

Let us now present the method under study and the associated results.

6.1 Total variation based restoration

As far as we know, such restorations have first been introduced in [23], while the use of the total variation in image processing was introduced in [44]. Our idea here is to apply a regularization approach to the problem of image zooming. With that in mind, we have first to define the set of all possible images of $L^2((\mathbb{T}_N)^2)$ that are sampled in the discrete N-periodic image $u \in l^\infty(\mathbb{Z}^2)$.

As we said in the introduction, we assume the sampled image u is deduced from a continuous one v by the composition of a convolution and a multiplication by a Dirac comb. So, the set of all the candidates to be the result of the restoration is defined by

Definition 6.1 *Let N be a strictly positive integer, $u \in l^\infty(\mathbb{Z}^2)$ a N-periodic function and $s \in L^2((\mathbb{T}_N)^2)$. We define $\mathcal{W}_{s,u}$, the set of all the functions $w \in L^2((\mathbb{T}_N)^2)$ that satisfy*

$$\forall (m,n) \in \{0,...,N-1\}^2,\ u_{m,n} = (s * w)(m,n)\,. \tag{6.1}$$

In other terms, $\mathcal{W}_{s,u}$ is the set of the images which yield u after a convolution with s and a sampling. In this definition, the smoothing s can be arbitrary, but in practice we mainly focus on two simple kernels yielding good properties when used to restore N-periodic cylindric functions (in axis or in any direction). These are the "mean kernel"

$$s^m(x,y) = 1_{]-\frac{1}{2},\frac{1}{2}]^2}(x,y) \tag{6.2}$$

for $(x,y) \in (\mathbb{T}_N)^2$ and the "frequency extrapolation kernel" (or "sinc") s^e defined by its Fourier series

$$\widehat{s^e}(\frac{k}{N},\frac{l}{N}) = 1_{|\{-\frac{1}{2}+\frac{1}{N},...,\frac{1}{2}\}^2}(\frac{k}{N},\frac{l}{N}) \tag{6.3}$$

for $(k,l) \in \mathbb{Z}^2$ (note that s^e belongs to $L^\infty((\mathbb{T}_N)^2)$ and consequently $L^2((\mathbb{T}_N)^2)$). In this latter case, frequencies of w higher than $\frac{1}{2}$ in modulus are simply set free by the constraint (6.1) (see (6.4) to follow).

Remark that, since the convolution and the sampling operator are linear, for any convolution kernel s, $\mathcal{W}_{s,u}$ is an affine sub-space of $L^2((\mathbb{T}_N)^2)$.

In order to interpret the degrees of freedom we have inside $\mathcal{W}_{s,u}$, we express (6.1) in the frequency domain. The Poisson formula, given in Proposition 1.1, yields

$$\hat{u}_{\xi,\eta} = \sum_{(k,l)\in\mathbb{Z}^2} \hat{s}(\frac{\xi}{N}+k,\frac{\eta}{N}+l)\,\widehat{w}(\frac{\xi}{N}+k,\frac{\eta}{N}+l)\,, \tag{6.4}$$

where $(\xi,\eta) \in \{-N/2+1,...,N/2\}^2$. Looking at (6.4), we see that the degrees of freedom

mentioned above simply are the repartition of $\hat{u}_{\xi,\eta}$ onto $\left(\widehat{w}(\frac{\xi}{N}+k,\frac{\eta}{N}+l)\right)_{k,l}$. Moreover, (6.4) gives us a sufficient condition for $\mathcal{W}_{s,u}$ not to be empty. In the following we will assume that $\hat{s}$ does not vanish on $\{-\frac{1}{2}+\frac{1}{N},...,\frac{1}{2}\}^2$, so that for any N-periodic $u \in l^\infty(\mathbb{Z}^2)$ the function u^c defined by

$$\widehat{u^c}(\frac{\xi}{N}+k,\frac{\eta}{N}+l) = \begin{cases} \frac{\hat{u}_{\xi,\eta}}{\hat{s}(\frac{\xi}{N},\frac{\eta}{N})} & \text{, if } (k,l)=(0,0) \\ 0 & \text{, otherwise,} \end{cases} \tag{6.5}$$

for $(\xi,\eta) \in \{-N/2+1,...,N/2\}^2$ and $(k,l) \in \mathbb{Z}^2$, belongs to $\mathcal{W}_{s,u}$.

At this point, we have to select an element of $\mathcal{W}_{s,u}$, given u and s. We propose here to choose the one that is the most "regular", in the sense that its total variation is minimal, say

$$Z(u) = argmin(|Dw|((\mathbb{T}_N)^2)), \text{ among } w \in \mathcal{W}_{s,u}\,. \tag{6.6}$$

One can refer to Chapter 2 for the properties of the total variation that will be used in the following and to [3, 17, 21] for general results.

6.1.1 Existence and uniqueness of a solution

Let us state a proposition ensuring the existence of a solution to (6.6). Remark that, despite the lack of generality, we are only able to state the existence (and therefore the results that will follow) in the space $L^2((\mathbb{T}_N)^2)$ (and not in $L^\infty((\mathbb{T}_N)^2)$). However, we do not have found any case (neither theoretical nor numerical) where the sup-norm of the result tends to infinity.

Proposition 6.1 *Let $N \in \mathbb{N}$, $u \in l^\infty(\mathbb{Z}^2)$ N-periodic and let $s \in L^2((\mathbb{T}_N)^2)$ such that $\hat{s}$ does not vanish on $\{-\frac{1}{2}+\frac{1}{N},...,\frac{1}{2}\}^2$ and $\hat{s}(k,l)=0$ for any $(k,l) \in \mathbb{Z}^2 \setminus \{(0,0)\}$, then (6.6) admits a solution $v \in \mathcal{W}_{s,u} \cap BV((\mathbb{T}_N)^2)$.*

Note that, looking at (6.4), $\hat{s}(k,l) = \hat{s}(\frac{0}{N}+k,\frac{0}{N}+l) = 0$, for any $(k,l) \in \mathbb{Z}^2 \setminus \{(0,0)\}$, simply forces functions of $\mathcal{W}_{s,u}$ to have the same mean-value.

Proof Let v_n be a sequence minimizing the total variation and satisfying the constraint (note that such a sequence exists since (6.5) defines a function of $\mathcal{W}_{s,u}$ which has a finite total variation). Remark that, since $v_n \in \mathcal{W}_{s,u}$ and $(\mathbb{T}_N)^2$ is bounded, v_n is in $L^1((\mathbb{T}_N)^2)$ and therefore in $BV((\mathbb{T}_N)^2)$. So, Poincaré inequalities (see Section 2.1) ensure that there exists $C>0$

$$\|v_n\|_2 \leq C\,|Dv_n|((\mathbb{T}_N)^2) + N\left|\int_{(\mathbb{T}_N)^2} v_n\right|.$$

So, since $\int_{(\mathbb{T}_N)^2} v_n$ is fixed, $\|v_n\|_2$, $\|v_n\|_1$ and $\|v_n\|_{BV}$ are bounded. Therefore, compactness theorems both in $BV((\mathbb{T}_N)^2)$ and $L^2((\mathbb{T}_N)^2)$ (see [21]) yield that there exists a subsequence v_{n_j} that converges in $L^1((\mathbb{T}_N)^2)$ and weakly in $L^2((\mathbb{T}_N)^2)$ to a function $v \in BV((\mathbb{T}_N)^2) \cap L^2((\mathbb{T}_N)^2)$.

It is easy to check that v is solution of (6.6). Indeed, the weak convergence in L^2 of v_{n_j} ensures that $v \in \mathcal{W}_{s,u}$ and the lower semi-continuity of the total variation ensures that $|Dv|((\mathbb{T}_N)^2) \leq \liminf_{j\to\infty} |Dv_{n_j}|((\mathbb{T}_N)^2)$. □

The "sinc" function s^e obviously falls under the scope of the above proposition. Concerning s^m, we have, for any $(k,l) \in \mathbb{Z}^2$,

$$\widehat{s^m}(k/N, l/N) = sinc(\pi k/N) sinc(\pi l/N)\,.$$

So s^m satisfies the hypotheses of the above proposition. Moreover, remark that for any $h \in L^2((\mathbb{T}_N)^2)$ such that $\hat{h}$ does not vanish on $\{-\frac{1}{2}+\frac{1}{N}, ..., \frac{1}{2}\}^2$, $h * s^e$ and $h * s^m$ also satisfy the hypotheses of Proposition 6.1.

We are not necessarily sure of the uniqueness of this solution, since the total variation is not strictly convex. Nevertheless, we can see that minimizers are "close" one to each other in the sense that for almost every point, where their gradients exist and are not null, they have the same gradient direction, as explained by S. Durand in [20].

Proposition 6.2 ("Weak Uniqueness") *Let v_1 and v_2 be two solutions of the problem (6.6). If we note*

$$\Gamma = \left\{(x,y) \in (\mathbb{T}_N)^2,\ v_1 \text{ and } v_2 \text{ are } C^1 \text{ at } (x,y) \text{ and } \nabla v_1(x,y) \neq 0\right\}\,,$$

for any $(x,y) \in \Gamma$, there exists $\lambda \geq 0$ such that

$$\nabla v_2(x,y) = \lambda \nabla v_1(x,y)\,.$$

Note that if v_1 and v_2 are both continuously differentiable on $(\mathbb{T}_N)^2$, then this proposition means that the connected components (in $\Gamma \cap \{(x,y) \in (\mathbb{T}_N)^2,\ \nabla v_2(x,y) \neq 0\}$) of the level lines of v_1 and v_2 are identical. Thus, both minima somehow differ in a local change of contrast (one can refer to [7] for an example of definition of contrast change related to level sets).

Proof Let us consider two minimizers u_1 and u_2. Since the total variation and the constraint are both convex, the image $(u_1+u_2)/2$ is also a minimizer and we have

$$|D(u_1+u_2)|((\mathbb{T}_N)^2) = |Du_1|((\mathbb{T}_N)^2) + |Du_2|((\mathbb{T}_N)^2).$$

Moreover, since for all $\Omega \in (\mathbb{T}_N)^2$,

$$|D(u_1 + u_2)|(\Omega) \leq |Du_1|(\Omega) + |Du_2|(\Omega)\,,$$

we must have, for all $(x, y) \in \Gamma$ (on which the minimizers are C^1),

$$|\nabla(u_1 + u_2)(x)| = |\nabla u_1(x)| + |\nabla u_2(x)|,$$

which implies the announced result. □

6.1.2 Total variation based restoration and cylindric functions

Both following propositions give sufficient conditions on s so that (6.6) defines a zoom that preserves cylindric functions. To do so, we construct a cylindric solution v' given a solution v. Unfortunately, we cannot guarantee all the solutions of (6.6) to be cylindric.

Proposition 6.3 *Let N be an integer, $u \in l^\infty(\mathbb{Z}^2)$ N-periodic and cylindric along an axis direction. For any kernel $s = h * s^m$ (see (6.2)), with $h \in L^2((\mathbb{T}_N)^2)$ such that $\hat{h}$ does not vanish on $\{-\frac{1}{2}+\frac{1}{N}, ..., \frac{1}{2}\}^2$, (6.6) admits a solution cylindric along the same axis direction.*

Proof The proof of this proposition is similar to the one of the next proposition. □

Proposition 6.4 *Let N be an integer, $(\alpha, \beta) \in \mathbb{R}^2 \setminus \{(0,0)\}$, $u \in l^\infty(\mathbb{Z}^2)$ N-periodic and cylindric along the direction (α, β). For any kernel $s = h * s^e$ (see (6.3)), with $h \in L^2((\mathbb{T}_N)^2)$ such that $\hat{h}$ does not vanish on $\{-\frac{1}{2} + \frac{1}{N}, ..., \frac{1}{2}\}^2$, (6.6) admits a solution cylindric along the same direction (α, β).*

Proof Let $v \in \mathcal{W}_{s,u}$ a solution of (6.6) (we know there exists one since $s = h * s^e$ satisfies the hypotheses of Proposition 6.1). Let $M \in \mathbb{R}$, we define the function

$$v_M(x, y) = \frac{1}{2M} \int_{-M}^{M} v(x - \beta t, y + \alpha t)dt\,, \tag{6.7}$$

for $(x, y) \in (\mathbb{T}_N)^2$.

We are now going to show that the limit of v_M, when M tends to infinity, exists, is a solution of (6.6) and is cylindric along the right direction. In order to do this, let us first estimate $|Dv_M|((\mathbb{T}_N)^2)$. We have for any $\varphi \in C_0^1((\mathbb{T}_N)^2)^2$, such that $\|\varphi\|_\infty \leq 1$ and any

$M > 0$

$$\begin{aligned}\int_{(\mathbb{T}_N)^2} v_M(x,y) div\varphi(x,y)dxdy &= \frac{1}{2M}\int_{(\mathbb{T}_N)^2}\int_{-M}^{M} v(x-\beta t, y+\alpha t) div\varphi(x,y)dtdxdy \\ &= \frac{1}{2M}\int_{-M}^{M}\int_{(\mathbb{T}_N)^2} v(x-\beta t, y+\alpha t) div\varphi(x,y)dxdydt \\ &\leq \frac{1}{2M}\int_{-M}^{M} |Dv|((\mathbb{T}_N)^2)dt \\ &\leq |Dv|((\mathbb{T}_N)^2)\,.\end{aligned}$$

So, for any $M > 0$,

$$|Dv_M|((\mathbb{T}_N)^2) \leq |Dv|((\mathbb{T}_N)^2).$$

Therefore, just as in the proof of Proposition 6.1, Poincaré inequalities, combined with the fact that, for any M, v_M has the same mean, ensure that $\|v_M\|_2$ and $\|v_M\|_{BV}$ are bounded. Thus, we can extract a sub-sequence $(v_{M_j})_{j\in\mathbb{N}}$ that converges in L^1, to a function $v' \in BV((\mathbb{T}_N)^2) \cap L^2((\mathbb{T}_N)^2)$ which satisfies

$$|Dv'|((\mathbb{T}_N)^2) \leq \liminf_{j\to\infty} |Dv_{M_j}|((\mathbb{T}_N)^2) \leq |Dv|((\mathbb{T}_N)^2).$$

In order to show that v' is a solution of (6.6), we still have to prove that v' belongs to $\mathcal{W}_{s,u}$. We are going to show, at the same time, that v' is cylindric of direction (α,β). Therefore, we compute for $j \in \mathbb{N}$ and $(k,l) \in \mathbb{Z}^2$,

$$\begin{aligned}\widehat{v_{M_j}}(\frac{k}{N},\frac{l}{N}) &= \hat{v}(\frac{k}{N},\frac{l}{N})\,\frac{1}{2M_j}\int_{-M_j}^{M_j} e^{-2i\pi(\beta\frac{k}{N}-\alpha\frac{l}{N})t}dt \\ &= \hat{v}(\frac{k}{N},\frac{l}{N})\; sinc\left(2\pi\frac{\beta k-\alpha l}{N}M_j\right)\,.\end{aligned}$$

Thus, since v_{M_j} converges in L^1 to v' (and so $\widehat{v_{M_j}}$ converges in l^∞ to $\widehat{v'}$), we have for any $(k,l) \in \mathbb{Z}^2$ such that $\beta k - \alpha l = 0$

$$\widehat{v'}(\frac{k}{N},\frac{l}{N}) = \lim_{j\to\infty} \widehat{v_{M_j}}(\frac{k}{N},\frac{l}{N}) = \hat{v}(\frac{k}{N},\frac{l}{N})$$

and for those such that $\beta k - \alpha l \neq 0$

$$\widehat{v'}(\frac{k}{N},\frac{l}{N}) = \lim_{j\to\infty} \widehat{v_{M_j}}(\frac{k}{N},\frac{l}{N}) = 0\,.$$

So v' is cylindric along the direction (α,β). Moreover, since v belongs to $\mathcal{W}_{s,u}$ and u is

cylindric along the direction (α, β), we are sure that $v' \in \mathcal{W}_{s,u}$. □

Remark that the advantage of the total variation based restoration over linear reconstructions (that preserves cylindric functions) is that it allows to extrapolate the frequencies out of $\{-\frac{1}{2}+\frac{1}{N}, ..., \frac{1}{2}\}^2$. Therefore, here we do not *a-priori* have to choose between "ringing" and "blurring" artifacts (see Chapter 7).

Note also that in the Proof of this proposition we have only used the form of the constraint and the fact that the total variation decreases after a convolution with a function h such that $\int_{(\mathbb{T}_N)^2} |h| = 1$. So, such a proposition can be obtained doing the same reasoning for other kind of energies like for instance $\int_{(\mathbb{T}_N)^2} |L(w)|^r$ where L is a differential operator and $r \geq 1$ is a real number.

6.2 Numerical approximation of the total variation based restoration

Let us first show two consistency propositions which ensure that a solution of (6.6) can be approximated numerically. With that in mind, we first define a problem, the solutions of which are computable and approximate a solution of (6.6).

Let N, u, s be such as in Proposition 6.1 and let $K > 1$ be an integer, we define $\mathcal{W}_{s,u}^K$ by

$$w \in \mathcal{W}_{s,u}^K \Longleftrightarrow \left\{ \begin{array}{l} w \in \mathcal{W}_{s,u} \text{ and} \\ \forall (k,l) \in \mathbb{Z}^2 \setminus \{-\frac{KN}{2}+1, ..., \frac{KN}{2}-1\}^2,\ \widehat{w}(\frac{k}{N}, \frac{l}{N}) = 0\,. \end{array} \right. \tag{6.8}$$

Since $\mathcal{W}_{s,u}^K$ is a finite dimensional affine space, its elements can be manipulated numerically. Therefore, we define the *band-limited approximating restoration* by

$$v^K = argmin(|Dw|((\mathbb{T}_N)^2)), \text{ among } w \in \mathcal{W}_{s,u}^K\,. \tag{6.9}$$

Note that such a minimum exists since $u^c \in \mathcal{W}_{s,u}^K$ (see (6.5)) and since we minimize a coercive and convex functional on $\mathcal{W}_{s,u}^K$ (a finite dimensional affine space). Note also that since functions of $\mathcal{W}_{s,u}^K$ are C^1 we have $|Dw|((\mathbb{T}_N)^2) = \int_{(\mathbb{T}_N)^2} |\nabla w|$, for any $w \in \mathcal{W}_{s,u}^K$. For any given $K > 1$, the associated band-limited approximating restoration represents a zoom of factor K (in the sense that the image resolution is increased by the factor K). Proposition 6.6 will prove that v^K can be used for K large to evaluate a solution of (6.6).

Unfortunately, we are not able to compute $\int_{(\mathbb{T}_N)^2} |\nabla w|$ (and so we cannot numerically minimize it), even for an image in $\mathcal{W}_{s,u}^K$. The problem is that even when $|\nabla w|$ is defined

everywhere (functions of $\mathcal{W}_{s,u}^K$ are band limited), we cannot integrate it on the torus. So, we estimate the integral with a Riemann summation and approximate the total variation by

$$E_{K'}(w) = \frac{1}{K'^2} \sum_{m,n=0}^{K'N-1} |\nabla w(\frac{m}{K'}, \frac{n}{K'})| \,.$$

We define the *solvable restoration* (the solution of which are numerically computable) by

$$v^{K,K'} = argmin(E_{K'}(w)), \text{ among } w \in \mathcal{W}_{s,u}^K \,. \tag{6.10}$$

Note, once again that $v^{K,K'}$ exists and that it can be estimated by a method similar to the one described in [11] (note that in [11] the image degradation is inclusive of noise).

The following proposition shows that a solution v^K of the band-limited approximating restoration (6.9) can be approximated by the sequence $(v^{K,K'})_{K' \geq K}$ when K' grows to infinity.

Proposition 6.5 *Let N and K be two integers (with $K > 1$), $u \in l^\infty(\mathbb{Z}^2)$ N-periodic and $s \in L^2((\mathbb{T}_N)^2)$ satisfying the hypotheses of the Proposition 6.1. For any $K' \geq K$, we note $v^{K,K'} \in L^2((\mathbb{T}_N)^2)$ a solution of (6.10). Then, there exists $v^K \in BV((\mathbb{T}_N)^2) \cap L^2((\mathbb{T}_N)^2)$ and a sub-sequence $(v^{K,K'_j})_{j \in \mathbb{N}}$ such that*

$$\lim_{j \to \infty} \|v^{K,K'_j} - v^K\|_1 = 0$$

and $(v^{K,K'_j})_{j \in \mathbb{N}}$ weakly converges in $L^2((\mathbb{T}_N)^2)$ to v^K. Moreover, for any such sub-sequence $(v^{K,K'_j})_{j \in \mathbb{N}}$, its limit v^K is solution of (6.9) and

$$\lim_{j \to \infty} E_{K'_j}(v^{K,K'_j}) = \int_{(\mathbb{T}_N)^2} |\nabla v^K| \,. \tag{6.11}$$

Proof In order to simplify notations we will forget the index K in $v^{K,K'}$ and denote it by $v^{K'}$, the prime symbol reminding us that the index K' refers to the minimization of $E_{K'}$.

Remark first that, since for any $w \in \mathcal{W}_{s,u}^K$, w is band limited, we have

$$\lim_{K' \to \infty} E_{K'}(w) = \int_{(\mathbb{T}_N)^2} |\nabla w| \,.$$

Therefore, $\lim_{K' \to \infty} E_{K'}(u^c)$ exists (where u^c is defined in (6.5)) and we know that

there exists $C > 0$ such that

$$E_{K'}(v^{K'}) \leq E_{K'}(u^c) \leq C\,. \tag{6.12}$$

Unfortunately, we do not have any compactness theorem for $E_{K'}$. However, we can boil down to compactness in BV since for any $w \in L^2((\mathbb{T}_N)^2)$, the frequency support of which is included in $\{-\frac{K}{2}+\frac{1}{N},...,\frac{K}{2}-\frac{1}{N}\}^2$,

$$\begin{aligned}\int_{(\mathbb{T}_N)^2} |w(x,y)|dxdy &= \int_{(\mathbb{T}_N)^2} \left| \frac{1}{N^2} \sum_{(k,l)\in\mathbb{Z}^2} \hat{w}(\frac{k}{N},\frac{l}{N}) e^{2i\pi(\frac{kx+ly}{N})} \right| dxdy \\ &\leq \sum_{(k,l)\in\mathbb{Z}^2} |\hat{w}(\frac{k}{N},\frac{l}{N})| \\ &\leq (KN)^2 \sup_{|k|,|l|<\frac{KN}{2}} |\hat{w}(\frac{k}{N},\frac{l}{N})|\,. \end{aligned} \tag{6.13}$$

Denoting $\hat{w}_{k,l}$ the discrete Fourier transform (adapted to images of size $K'N \times K'N$) of w. We have

$$\hat{w}_{k,l} = \sum_{m,n=0}^{K'N-1} w(\frac{m}{K'},\frac{n}{K'}) e^{-2i\pi\frac{km+ln}{K'N}} = K'^2 \hat{w}(\frac{k}{N},\frac{l}{N})\,,$$

since $\hat{w}$ is supported by $\{-\frac{K}{2}+\frac{1}{N},...,\frac{K}{2}-\frac{1}{N}\}^2$ and $K' \geq K$. Therefore, (6.13) yields

$$\int_{(\mathbb{T}_N)^2} |w| \leq \frac{K^2N^2}{K'^2} \sum_{m,n=0}^{K'N-1} |w(\frac{m}{K'},\frac{n}{K'})|\,.$$

Applying this to $\frac{\partial w}{\partial x}$ and $\frac{\partial w}{\partial y}$ for a $w \in \mathcal{W}^K_{s,u}$, we finally get

$$\int_{(\mathbb{T}_N)^2} |\nabla w| \leq C' E_{K'}(w)\,,$$

where C' does not depend on K'. This, combined with (6.12), yields

$$\int_{(\mathbb{T}_N)^2} |\nabla v^{K'}| \leq C'C\,.$$

We can yet do the same reasoning as the one presented in the proof of Proposition 6.1, which guarantees the existence of a sub-sequence $(v^{K'_j})_{j\in\mathbb{N}}$ and a function $v \in BV((\mathbb{T}_N)^2) \cap L^2((\mathbb{T}_N)^2)$, such that $v^{K'_j}$ converges in $L^1((\mathbb{T}_N)^2)$ and converges weakly in $L^2((\mathbb{T}_N)^2)$ to v.

We still have to prove that v is a solution of the band-limited approximating restoration (6.9). Note first that the weak convergence in L^2 ensures that $v \in \mathcal{W}_{s,u}^K$, since for all j, $v^{K'_j}$ do belong to $\mathcal{W}_{s,u}^K$.

Let us now prove (6.11). We decompose

$$E_{K'_j}(v^{K'_j}) - \int_{(\mathbb{T}_N)^2} |\nabla v| = E_{K'_j}(v^{K'_j}) - E_{K'_j}(v) + E_{K'_j}(v) - \int_{(\mathbb{T}_N)^2} |\nabla v| \,.$$

Therefore, since $\lim_{K' \to \infty} E_{K'}(v) = \int_{(\mathbb{T}_N)^2} |\nabla v|$, it is then sufficient to prove that

$$\lim_{j \to \infty} E_{K'_j}(v^{K'_j} - v) = 0$$

to get (6.11).

Let $w \in L^2((\mathbb{T}_N)^2)$, the Fourier series of which is supported by $\{-\frac{K}{2} + \frac{1}{N}, ..., \frac{K}{2} - \frac{1}{N}\}^2$, we have

$$E_{K'}(w) \leq \frac{1}{K'^2} \sum_{m,n=0}^{K'N-1} |\frac{\partial w}{\partial x}(\frac{m}{K'}, \frac{n}{K'})| + \frac{1}{K'^2} \sum_{m,n=0}^{K'N-1} |\frac{\partial w}{\partial y}(\frac{m}{K'}, \frac{n}{K'})| \,.$$

So, analyzing both summations separately, we have, since $K' \geq K$,

$$\frac{1}{K'^2} \sum_{m,n=0}^{K'N-1} |\frac{\partial w}{\partial x}(\frac{m}{K'}, \frac{n}{K'})| = \frac{1}{K'^2} \sum_{m,n=0}^{K'N-1} \left| \frac{2\pi}{(K'N)^2} \sum_{k,\, l=-\frac{K'N}{2}+1}^{\frac{K'N}{2}} \frac{k}{K'N} \hat{w}_{k,l} e^{2i\pi \frac{km+ln}{K'N}} \right| \,.$$

Thus, since $\hat{w}_{k,l} = 0$ for $|k|$ or $|l|$ strictly larger than $\frac{KN}{2}$, we have

$$\begin{aligned} \frac{1}{K'^2} \sum_{m,n=0}^{K'N-1} |\frac{\partial w}{\partial x}(\frac{m}{K'}, \frac{n}{K'})| &\leq \frac{1}{K'^2} \sum_{m,n=0}^{K'N-1} \frac{\pi K^2}{K'^2} \sup_{k,l} |\hat{w}_{k,l}| \\ &\leq \frac{\pi N^2 K^2}{K'^2} \sup_{k,l} |\hat{w}_{k,l}| \,. \end{aligned}$$

Once again, we just remark that, since $K' \geq K$, we have $\hat{w}_{k,l} = K'^2 \hat{w}(\frac{k}{N}, \frac{l}{N})$ and we obtain

$$\frac{1}{K'^2} \sum_{m,n=0}^{K'N-1} |\frac{\partial w}{\partial x}(\frac{m}{K'}, \frac{n}{K'})| \leq \pi N^2 K^2 \int_{(\mathbb{T}_N)^2} |w| \,.$$

So, there exists $C > 0$, which does not depend on K', such that for any $w \in L^2((\mathbb{T}_N)^2)$,

the Fourier series of which is supported by $\{-\frac{K}{2}+\frac{1}{N},...,\frac{K}{2}-\frac{1}{N}\}^2$, we have

$$E_{K'_j}(w) \leq C \int_{(\mathbb{T}_N)^2} |w| \,.$$

Applying this to $(v^{K'_j} - v)$ yields $\lim_{j\to\infty} E_{K'_j}(v^{K'_j} - v) = 0$.

Therefore, (6.11) holds and for any $w \in \mathcal{W}^K_{s,u}$, we have

$$\int_{(\mathbb{T}_N)^2} |\nabla w| = \lim_{j\to\infty} E_{K'_j}(w) \geq \lim_{j\to\infty} E_{K'_j}(v^{K'_j}) = \int_{(\mathbb{T}_N)^2} |\nabla v| \,,$$

which achieves the proof. □

The following proposition shows that $(v^K)_{K\in\mathbb{N}}$ allows us to approximate a solution v of (6.6).

Proposition 6.6 *Let N be an integer, $u \in l^\infty(\mathbb{Z}^2)$ N-periodic and $s \in L^2((\mathbb{T}_N)^2)$ satisfying the hypotheses of the Proposition 6.1. If for any $K > 1$, we note $v^K \in L^2((\mathbb{T}_N)^2)$ a solution of (6.9), we know that there exists $v \in \mathcal{W}_{s,u}$ and a sub-sequence $(v^{K_j})_{j\in\mathbb{N}}$ such that*

$$\lim_{j\to\infty} \|v^{K_j} - v\|_1 = 0$$

and $(v^{K_j})_{j\in\mathbb{N}}$ weakly converges in L^2 to v. Moreover, for any such sub-sequence $(v^{K_j})_{j\in\mathbb{N}}$, its limit v is solution of (6.6) and

$$\lim_{j\to\infty} \int_{(\mathbb{T}_N)^2} |\nabla v^{K_j}| = |Dv|((\mathbb{T}_N)^2) \,.$$

Proof Note first that the sequence $(|Dv^K|((\mathbb{T}_N)^2))_{K\in\mathbb{N}}$ decreases. So, the same reasoning as the one presented in the proof of the Proposition 6.1 yields that there exists $v \in BV((\mathbb{T}_N)^2) \cap L^2((\mathbb{T}_N)^2)$ and a sub-sequence $(v^{K_j})_{j\in\mathbb{N}}$ such that v_{K_j} converges in L^1 and weakly converges in L^2 to v. Moreover, we have

$$|Dv|((\mathbb{T}_N)^2) \leq \liminf_{j\to\infty} |Dv^{K_j}|((\mathbb{T}_N)^2) \,.$$

Once again, the weak convergence in L^2 ensures that $v \in \mathcal{W}_{s,u}$. Nevertheless, we still have to prove that $|Dv|((\mathbb{T}_N)^2)$ is minimum among the functions of $\mathcal{W}_{s,u}$. For that, we are going to build a sequence of functions, indexed by K, of elements of $\mathcal{W}^K_{s,u}$ and which minimizes the total variation.

Let $K > 1$ be an integer, we define for any $(k,l) \in \mathbb{Z}^2$

$$\hat{h}_K(\frac{k}{N},\frac{l}{N}) = \begin{cases} (1-\frac{|2k|}{KN})(1-\frac{|2l|}{KN}) & \text{, for } |k| \text{ and } |l| \leq \frac{KN}{2} \\ 0 & \text{, otherwise.} \end{cases}$$

For any $K>1$, $h_K \in L^2((\mathbb{T}_N)^2) \cap L^1((\mathbb{T}_N)^2)$ and $\int_{(\mathbb{T}_N)^2} |h_K| = 1$, indeed $\int_{(\mathbb{T}_N)^2} h_K = 1$ since $\hat{h}_K(0,0)=1$ and $h_K \geq 0$ since it is the convolution of two positive functions (which are obtained by convolving the Fourier series of a function with itself). We define an operator P_K from $\mathcal{W}_{s,u}$ onto $\mathcal{W}^K_{s,u}$ by

$$P_K(w) = h_K * w + w'_K$$

where $w \in \mathcal{W}_{s,u}$ and w'_K is defined as follows: $\widehat{w'_K}$ is supported by $\{-\frac{1}{2}+\frac{1}{N},...,\frac{1}{2}\}^2$ and for any $(\xi,\eta) \in \{-\frac{N}{2}-1,...,\frac{N}{2}\}^2$,

$$\widehat{w'_K}(\frac{\xi}{N},\frac{\eta}{N}) = \frac{1}{\hat{s}(\frac{\xi}{N},\frac{\eta}{N})} \sum_{(k',l')\in\mathbb{Z}^2} \hat{s}(\frac{\xi}{N}+k',\frac{\eta}{N}+l') \hat{w}(\frac{\xi}{N}+k',\frac{\eta}{N}+l') \left[1-\hat{h}_K(\frac{\xi}{N}+k',\frac{\eta}{N}+l')\right].$$

It is easy to check using (6.4) and (6.8) that $P_K(w) \in \mathcal{W}^K_{s,u}$ for any $w \in \mathcal{W}_{s,u}$. Let us show that $P_K(w)$ converges to w in $L^2(\mathbb{R}^2)$, when K tends to infinity. Let $K>3$, we have

$$\|k_K * w - w\|_2^2 = \frac{1}{N^2} \sum_{(k,l)\in\mathbb{Z}^2} |\hat{w}(\frac{k}{N},\frac{l}{N})|^2 \left|1-\hat{h}_K(\frac{k}{N},\frac{l}{N})\right|^2 .$$

Let us now denote $C_K = KN\left(1-(1-\frac{1}{logK})^{\frac{1}{2}}\right)$ and split the sum into two pieces: S_1, the sum over all the indexes whose magnitudes are below C_K and S_2 the sum over the reminding indexes.

Due to the particular form of $\hat{h}$, we have, for indexes k and l which concern the sum S_1, $\left|1-\hat{h}_K(\frac{k}{N},\frac{l}{N})\right| \leq \frac{1}{logK}$. This yields,

$$S_1 \leq \frac{1}{(logK)^2}\|w\|_2^2 ,$$

which guarantees that $\lim_{K\to\infty} S_1 = 0$. Concerning S_2, we get

$$S_2 \leq \sum_{|k| \text{ or } |l|>C_K} |\hat{w}(\frac{k}{N},\frac{k}{N})|^2 ,$$

since $\left|1 - \hat{h}_K(\frac{k}{N}, \frac{l}{N})\right| \leq 1$. Therefore $\lim_{K\to\infty} S_2 = 0$ and we get

$$\lim_{K\to\infty} \|k_K * w - w\|_2 = 0\,.$$

The same kind of calculation yields

$$\lim_{K\to\infty} \|w'_K\|_2 = 0$$

and we finally have

$$lim_{K\to\infty} \|P_K(w) - w\|_2 = 0\,.$$

We are now going to show that $\lim_{K\to\infty} |DP_K(w)|((\mathbb{T}_N)^2)$ exists and is smaller than $|Dw|((\mathbb{T}_N)^2)$. This is basically a consequence of the fact that $|D(h_K * w)|((\mathbb{T}_N)^2) \leq |D(w)|((\mathbb{T}_N)^2)$ and that $|Dw'_K|((\mathbb{T}_N)^2)$ tends to 0 when K tends to infinity. Let us detail this.

Let $w \in \mathcal{W}_{s,u}$ and $\varphi \in C_0^1((\mathbb{T}_N)^2)^2$ such that $\|\varphi\|_\infty \leq 1$. We have, noting $h_K * \varphi = (h_K * \varphi_1, h_K * \varphi_2)$,

$$\begin{aligned}\int_{(\mathbb{T}_N)^2} P_K(w)\, div(\varphi) &= \int_{(\mathbb{T}_N)^2} w\, div(h_K * \varphi) + \int_{(\mathbb{T}_N)^2} w'_K\, div(\varphi)\,,\\ &\leq |Dw|((\mathbb{T}_N)^2) + \int_{(\mathbb{T}_N)^2} w'_K\, div(\varphi)\,.\end{aligned}$$

So, since w'_K and $div(\varphi)$ belong to $L^2((\mathbb{T}_N)^2)$, we can compute $I_1 = \int_{(\mathbb{T}_N)^2} w'_K\, div(\varphi)$ in frequency domain and this yields the upper bound (we note $\varphi = (\varphi_1, \varphi_2)$, $\overline{\hat{\varphi}_i}$ the complex conjugate of $\hat{\varphi}_i$, for $i = 1,\ 2$)

$$\begin{aligned}|I_1| &= \frac{2\pi}{N^2}\left|\sum_{-\frac{N}{2}+1\leq\xi,\eta\leq\frac{N}{2}} \widehat{w'_K}(\frac{\xi}{N},\frac{\eta}{N})\,[\frac{\xi}{N}\,\overline{\hat{\varphi}_1(\frac{\xi}{N},\frac{\eta}{N})} + \frac{\eta}{N}\,\overline{\hat{\varphi}_2(\frac{\xi}{N},\frac{\eta}{N})}]\right|\\
&\leq 2\pi\|w'_K\|_2 \left(\sum_{-\frac{N}{2}+1\leq\xi,\eta\leq\frac{N}{2}} \left|\frac{\xi}{N}\hat{\varphi}_1(\frac{\xi}{N},\frac{\eta}{N}) + \frac{\eta}{N}\hat{\varphi}_2(\frac{\xi}{N},\frac{\eta}{N})\right|^2\right)^{\frac{1}{2}}\\
&\leq 2\pi\|w'_K\|_2\ \left(\|\varphi_1\|_2^2 + \|\varphi_2\|_2^2\right)^{\frac{1}{2}}\\
&\leq 2\sqrt{2}\,\pi N\,\|w'_K\|_2.\end{aligned}$$

Therefore, for any $\varepsilon > 0$ and any $w \in \mathcal{W}_{s,u}$ there exists $K_\varepsilon > 1$ such that for $K \geq K_\varepsilon$

$$|D\,P_K(w)|((\mathbb{T}_N)^2) \leq |Dw|((\mathbb{T}_N)^2) + \epsilon\,.$$

So, since $|Dw|((\mathbb{T}_N)^2) \leq \liminf_{K\to\infty} |D\,P_K(w)|$, we have for any $w \in \mathcal{W}_{s,u}$

$$\lim_{K\to\infty} |D\,P_K(w)|((\mathbb{T}_N)^2) = |Dw|((\mathbb{T}_N)^2). \tag{6.14}$$

So, in particular, for a solution w of (6.6), we have

$$|Dw|((\mathbb{T}_N)^2) \leq |Dv^{K_j}|((\mathbb{T}_N)^2) \leq |D\,P_{K_j}(w)|((\mathbb{T}_N)^2)$$

and then $|Dw|((\mathbb{T}_N)^2) = \lim_{j\to\infty} |Dv^{K_j}|((\mathbb{T}_N)^2)$.
This, at last, guarantees

$$|Dv|((\mathbb{T}_N)^2) \leq \lim_{j\to\infty} |Dv^{K_j}|((\mathbb{T}_N)^2) = |Dw|((\mathbb{T}_N)^2) \leq |Dv|((\mathbb{T}_N)^2)\,,$$

which finishes the proof. □

Remark first that we could have stated, in the case of the band-limited approximating restoration (6.9), some propositions similar to Proposition 6.2 (the "weak uniqueness") and Proposition 6.4 (that deals with the preservation of cylindric images for (6.6)). So, since any function $w \in \mathcal{W}^K_{s,u}$ is continuously differentiable and since for any such function $\{(x,y) \in (\mathbb{T}_N)^2,\ \nabla w = 0\}$ is of null measure, we can expect any solution v^K of (6.9) to be cylindric, given an initial cylindric data. Therefore, a solution v of (6.6) obtained as a limit of a sub-sequence $(v^{K_j})_{j\in\mathbb{N}}$ is also cylindric.

Now, as we said in the introduction of this section, we can only compute a solution of the solvable restoration (given by (6.10)). We are now going to show the consequence of the change in the minimizing energy on the behavior of the restoration when dealing with cylindric images.

Proposition 6.7 *Let N, K, K' be some integers with $K' \geq K > 1$, $(\alpha,\beta) \in \mathbb{Z}^2\setminus\{(0,0)\}$, $u \in l^\infty(\mathbb{Z}^2)$ N-periodic and cylindric along the direction (α,β). For any kernel $s = h * s^e$ with $h \in L^2((\mathbb{T}_N)^2)$ such that $\hat{h}$ does not vanish on $\{-\frac{1}{2}+\frac{1}{N},...,\frac{1}{2}\}^2$, the solvable restoration (6.10) admits a solution whose Fourier series is supported by*

$$S_{\alpha',\beta'} = \left\{(k,l) \in \{-\frac{K}{2}+\frac{1}{N},...,\frac{K}{2}-\frac{1}{N}\}^2,\ \beta' k - \alpha' l \in K'\mathbb{Z}\right\},$$

where $(\alpha',\beta') \in \mathbb{Z}^2$ are such that $\alpha' \wedge \beta' = 1$ ($\wedge$ denotes the largest common divisor) and (α',β') defines the same direction as (α,β).

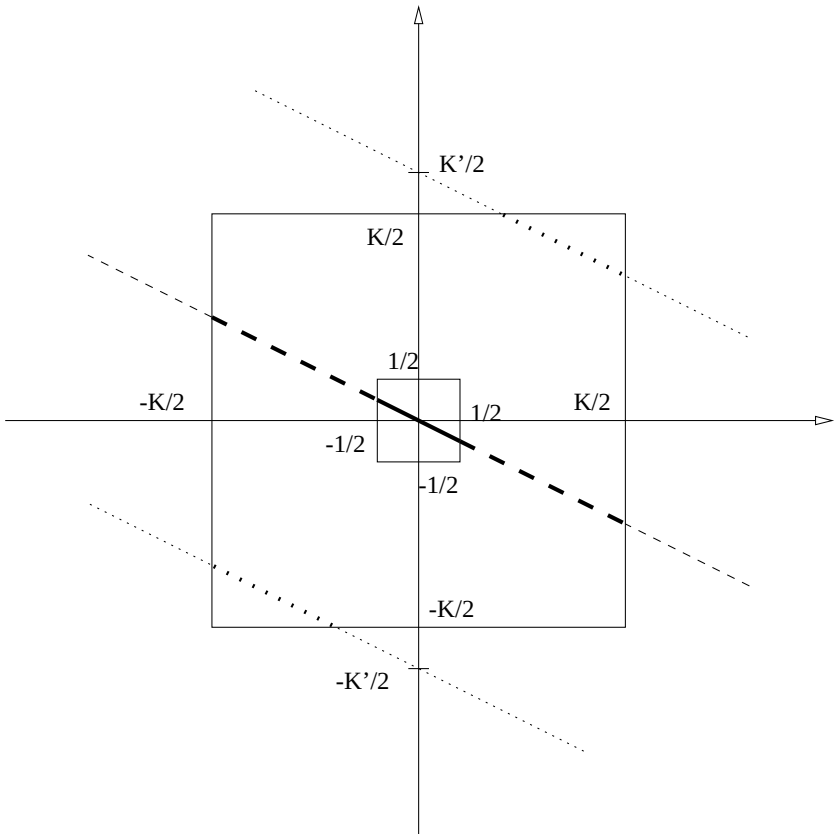

Figure 6.1: The solid thick line represents the initial spectrum support (cylindric along the direction $(2,-1)$). The dashed lines (thick and thin) represent the restriction to the direction $(2,-1)$ of the possible spectrum support after minimizing $E_{K'}$. The dotted lines (thick and thin) represent the restriction to wrong directions of the possible spectrum support after minimizing $E_{K'}$. The thick lines (solid, dashed and dotted) represent the possible spectrum support after minimizing $E_{K'}$ among $\mathcal{W}_{s,u}^K$.

Remark that, modulo the uniqueness (we could state a proposition similar to Proposition 6.2 in the case of (6.10)), this proposition means that the results of the solvable restoration are not fully cylindric (see the thick line on Figure 6.1).

Moreover, for $(\alpha,\beta)\in\mathbb{Z}^2\setminus\{(0,0)\}$, we can define $(\alpha',\beta')\in\mathbb{Z}^2$ a pair representing the same direction as (α,β), but such that $\alpha'\wedge\beta'=1$. Then, since $S_{\alpha',\beta'}$ is included in $S_{\alpha,\beta}$, the use of such a pair (α',β') in the statement of Proposition 6.7 yields a stronger result.

Proof The proof is similar to the one of Proposition 6.4, except that we have to take care of the fact that $E_{K'}(w)$ only takes into account the values of w on a discrete set.

Let $(\alpha',\beta')\in\mathbb{Z}^2$ be such as in the proposition.

Let $K'\geq K$, $v\in\mathcal{W}_{s,u}^K$ a solution of (6.10) and $M\in\mathbb{N}$, we define the function

$v_M \in L^2((\mathbb{T}_N)^2)$, in frequency domain, by

$$\widehat{v_M}(\frac{k}{N},\frac{l}{N}) = \hat{v}(\frac{k}{N},\frac{l}{N})\,\frac{1}{2M+1}\sum_{t=-M}^{M} e^{-2i\pi\frac{(k\beta'-l\alpha')}{K'N}t}\,, \tag{6.15}$$

for any $(k,l)\in\mathbb{Z}^2$.

There is an analogy between this v_M and the one defined by (6.7) that is that for any $(m,n)\in\{0,...,K'N-1\}^2$

$$v_M(\frac{m}{K'},\frac{n}{K'}) = \frac{1}{2M+1}\sum_{t=-M}^{M} v(\frac{m}{K'}-\beta' t,\ \frac{n}{K'}+\alpha' t)\,. \tag{6.16}$$

Indeed, since $v\in\mathcal{W}^K_{s,u}$ and $K'\geq K$, we have

$$\begin{aligned}(\widehat{v_M})_{k,l} &= K'^2\widehat{v_M}(\frac{k}{N},\frac{l}{N})\\ &= K'^2\hat{v}(\frac{k}{N},\frac{l}{N})\,\frac{1}{2M+1}\sum_{t=-M}^{M} e^{-2i\pi\frac{(k\beta'-l\alpha')}{K'N}t}\\ &= \hat{v}_{k,l}\,\frac{1}{2M+1}\sum_{t=-M}^{M} e^{-2i\pi\frac{(k\beta'-l\alpha')}{K'N}t}\,,\end{aligned}$$

which in space domain yields (6.16).

Similarly, we also have for any $(m,n)\in\{0,...,K'N-1\}^2$

$$\nabla v_M(\frac{m}{K'},\frac{n}{K'}) = \frac{1}{2M+1}\sum_{t=-M}^{M}\nabla v(\frac{m}{K'}-\beta' t,\ \frac{n}{K'}+\alpha' t)$$

and so

$$E_{K'}(v_M)\leq E_{K'}(v)$$

(note that it is the point where the v_M defined by (6.7) fails).

Remark that $\left\{w\in L^2((\mathbb{T}_N)^2),\ Supp(\hat{w})\subset\{-\frac{K}{2}+\frac{1}{N},...,\frac{K}{2}-\frac{1}{N}\}\right\}$ is a finite dimensional space and that $E_{K'}(w)=0$ implies $\int_{(\mathbb{T}_N)^2}|\nabla w|=0$. So there exists $C>0$ such that for any $w\in L^2((\mathbb{T}_N)^2)$ satisfying $Supp(\hat{w})\subset\{-\frac{K}{2}+\frac{1}{N},...,\frac{K}{2}-\frac{1}{N}\}$

$$\int_{(\mathbb{T}_N)^2}|\nabla w|\leq C E_{K'}(w)\,.$$

So, $\int_{(\mathbb{T}_N)^2}|\nabla v_M|$ is bounded and similarly to Proposition 6.4, we know that there exists

v_{M_j} that converges in $L^1((\mathbb{T}_N)^2)$ to a function $v' \in BV((\mathbb{T}_N)^2) \cap L^2((\mathbb{T}_N)^2)$.

Moreover, as shown before, there exists $C' > 0$ such that for any $w \in L^2((\mathbb{T}_N)^2)$, such that $Supp(\hat{w}) \subset \{-\frac{K}{2} + \frac{1}{N}, ..., \frac{K}{2} - \frac{1}{N}\}$

$$E_{K'}(w) \leq C' \int_{(\mathbb{T}_N)^2} |w| \, .$$

So, $\lim_{j\to\infty} E_{K'}(v_{M_j} - v') = 0$ and

$$E_{K'}(v') = \lim_{j\to\infty} E_{K'}(v_{M_j}) \leq E_{K'}(v) \, .$$

Moreover, since v_{M_j} converges to v' in $L^1((\mathbb{T}_N)^2)$, looking at (6.15), we finally have for any $(k, l) \in \mathbb{Z}^2$

$$\widehat{v'}(\frac{k}{N}, \frac{l}{N}) = \begin{cases} \hat{v}(\frac{k}{N}, \frac{l}{N}) & \text{, if } (k\beta' - l\alpha') \in K'N\mathbb{Z} \\ 0 & \text{, otherwise.} \end{cases}$$

This ensures that $v' \in \mathcal{W}^K_{s,u}$ and finishes the proof of the announced result. □

Remark however that the solution v' of the solvable restoration (6.10) given in the proof of the proposition satisfies

$$v'(\frac{m}{K'}, \frac{n}{K'}) = v'(\frac{m}{K'} - \beta' t, \frac{n}{K'} + \alpha' t) \, ,$$

for any $(m, n) \in \{0, ..., K'N - 1\}^2$ and any $t \in \mathbb{Z}$.

Remark once again that we could have stated a proposition similar to Proposition 6.4 (which ensures the preservation of cylindric function for (6.6)) in the case of the band-limited approximating restoration (6.9). So, this proposition has to be regarded under the scope of Proposition 6.5 (a consistency proposition) which guarantees that for K' large the cylindric aspect of the result is preponderant. Moreover, we have

Corollary 6.1 *Let N and K be two integers and $(\alpha, \beta) \in \mathbb{Z}^2 \setminus \{(0, 0)\}$. There exists $K' \geq K$ beyond which the solutions of (6.10) are cylindric along the direction (α, β), for any kernel $s = h * s^e$ (see (6.2)), with $h \in L^2((\mathbb{T}_N)^2)$ such that $\hat{h}$ does not vanish on $\{-\frac{1}{2} + \frac{1}{N}, ..., \frac{1}{2}\}^2$ and any $u \in l^\infty(\mathbb{Z}^2)$ N-periodic and cylindric along the direction (α, β).*

Indeed, looking at the definition of $S_{\alpha',\beta'}$ (see Proposition 6.7), we see that for K' large the lines $\beta' k - \alpha' l = \pm K'$ do not intersect the square $\{-\frac{K}{2} + \frac{1}{N}, ..., \frac{K}{2} - \frac{1}{N}\}^2$ (see figure 6.1). Therefore, for K' large, $S_{\alpha',\beta'}$ is reduced to the trace of the line $\beta' k - \alpha' l = 0$ on $\{-\frac{K}{2} + \frac{1}{N}, ..., \frac{K}{2} - \frac{1}{N}\}^2$ and the solutions of (6.10) are cylindric along the direction (α, β).

Note also that the case $K' = K$ is sufficient to preserve the functions cylindric along the axis directions (the cases where $(\alpha, \beta) = (1, 0)$ or $(\alpha, \beta) = (0, 1)$).

6.2.1 The fully discrete total variation based restoration

Similarly to Section 5.2, we will briefly present a very practical aspect of the total variation based restoration. Once again, the initial data belongs to $\mathbb{R}^{N^2}$ while the restored image is in $\mathbb{R}^{(KN)^2}$ for $K > 1$, an integer. This case is almost the one presented as the "solvable restoration" (see (6.10)) in Section 6.2 (the difference lies in frequencies $\{\frac{KN}{2}\} \times \{-\frac{KN}{2} + 1, ..., \frac{KN}{2}\}$ and $\{-\frac{KN}{2} + 1, ..., \frac{KN}{2}\} \times \{\frac{KN}{2}\}$).

In such a case, given $K > 1$ and $s \in \mathbb{R}^{(KN)^2}$, we define the set of the possible restorations

$$\begin{aligned} \mathcal{W} &= \left\{ w \in \mathbb{R}^{(KN)^2}, \forall (m,n) \in \{0, ...N-1\}^2,\ u_{m,n} = s * w_{Km,Kn} \right\}, \\ &= \left\{ w \in \mathbb{R}^{(KN)^2}, \forall (\xi,\eta) \in \{-\frac{N}{2} + 1, ..., \frac{N}{2}\}^2, \right. \\ &\qquad \left. \hat{u}_{\xi,\eta} = \frac{1}{K^2} \sum_{k,\,l=0}^{K-1} \hat{s}_{\xi+kN,\eta+lN}\ \hat{w}_{\xi+kN,\eta+lN} \right\}, \end{aligned}$$

where $*$ denotes the discrete convolution, periodized at images border.

Let us illustrate this very practical case. We display on Figure 6.2 the nature of the constraint on two simple examples of kernel s (note that these are signal examples and that we take $K = 2$). In both cases, the spatial support of the smoothing kernel is less than the original pixel size. Therefore, the constraint on the values of w_{2m} and w_{2m+1} does not depend on the values of w_{2n} and w_{2n+1} for $n \neq m$. They are only linked by the regularity criterion. Remark that this is not the case when the spatial support of s is larger than the original pixel size.

Assume we minimize E_K over $\mathcal{W}$, we could state a proposition similar to Proposition 6.7 (that deals with the "solvable restoration" of cylindric functions) by taking $K' = K$ and modifying the behavior on frequencies $\{\frac{KN}{2}\} \times \{-\frac{KN}{2} + 1, ..., \frac{KN}{2}\}$ and $\{-\frac{KN}{2} + 1, ..., \frac{KN}{2}\} \times \{\frac{KN}{2}\}$.

Let us now introduce the example of the restoration of a simple Heavyside function. We are going to show, in a general framework, that the Heavyside function is a result of the total variation minimization, when the initial data is also a Heavyside function. That is a point where other kinds of energies can fail (see example in the following section).

Example 6.1. Let us consider a signal v of size $2N$

$$v(l) = \begin{cases} 0 & \text{, if } 0 \leq l \leq N, \\ 1 & \text{, otherwise.} \end{cases}$$

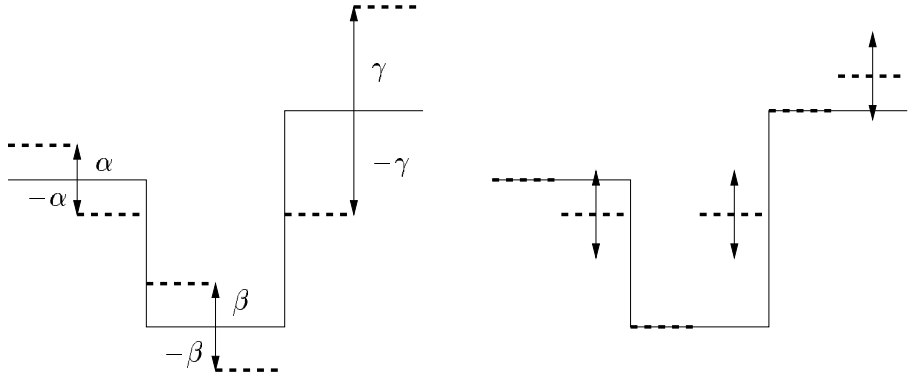

s is the mean over two adjacent pixels s is a Dirac delta function

----- pixels of the oversampled signal

_____ pixels of the initial signal

Figure 6.2: Elements of $\mathcal{W}$ in the 1D case with $K = 2$.

Let $s \in \mathbb{R}^{(2N)}$ and assume its support is an interval whose size is smaller than N. Assume also that s is strictly positive on its support and that $\sum_{m=0}^{2N} s(m) = 1$. Let us consider $u \in \mathbb{R}^N$ such that for any $m \in \{0, ...N-1\}$, $u_m = (s * v)_{2m}$.

We are now going to prove that v minimizes $\sum_{m=0}^{2N-1} |w_{m+1} - w_m|$ among functions of $\mathcal{W}$.

Indeed, let us denote $I_0 = \{m,\ u(m) = 0\}$, and $I_1 = \{m,\ u(m) = 1\}$ (note that these are not empty). Moreover, for any $0 \leq m < N$, we note C_m the interval of indices which are concerned by the convolution leading to u_m.

Let $w \in \mathcal{W}$, for any $m \in I_0$, and any $n \in C_m$ if $w_n \neq 0$ then their exists $j \in C_m$ such that $w_j < 0$ (otherwise $(s * w)_m \neq 0$). In the same way, for any $m \in I_1$, and any $n \in C_m$ if $w_n \neq 1$ then their exists $j \in C_m$ such that $w_j > 1$ (otherwise $(s * w)_m \neq 1$). Therefore $E_1(w) \geq 1$ for any $w \in \mathcal{W}$. So, since $v \in \mathcal{W}$ and $E_1(w) = 1$, v minimizes E_1 among function of $\mathcal{W}$.

6.3 Linear reconstructions associated with some variational restorations

As we said previously, most of the results presented above are also true for restorations based on minimization of other kinds of energies. In this section, we are going to study a particular case which yields a linear reconstruction.

Indeed, there is an important link between linear reconstructions and some variational

minimization of the form

$$Z_L(u) = argmin \left(\int_{(\mathbb{T}_N)^2} |L(w)|^2 \right), \text{ among } w \in \mathcal{W}_{s,u}, \tag{6.17}$$

where L is a linear and translation invariant operator (note that variational minimization of the same kind have already been introduced in [27]).

In order to describe this link, let us focus on the particular case where $L = \nabla$. This leads us to search solutions of

$$Z(u) = argmin \left(\int_{(\mathbb{T}_N)^2} |\nabla w|^2 \right), \text{ among } w \in \mathcal{W}_{s,u}. \tag{6.18}$$

Let us state the a proposition which gives the explicit form of a solution of (6.18). Note that this proposition could be stated in the case of Z_L for most of the linear and translation invariant operator L (we will make this clear after the proof of the proposition).

Proposition 6.8 *Let $N \in \mathbb{N}$, $u \in l^\infty(\mathbb{Z}^2)$ N-periodic and let $s \in L^2((\mathbb{T}_N)^2)$ such that $\hat{s}$ does not vanish on $\{-\frac{1}{2} + \frac{1}{N}, ..., \frac{1}{2}\}^2$, then (6.18) defines a linear, translation invariant operator continuous from $\{u \in l^\infty(\mathbb{Z}^2),\ u$ is N-periodic$\}$ to $L^2((\mathbb{T}_N)^2)$. Moreover, (6.18) admits a unique solution v given by:*

for any $(\xi, \eta) \in \{-\frac{N}{2} - 1, ..., \frac{N}{2}\}^2 \setminus \{(0,0)\}$ and any $(k,l) \in \mathbb{Z}^2$,

$$\hat{v}(\frac{\xi}{N} + k, \frac{\eta}{N} + l) = \frac{\bar{\hat{s}}(\frac{\xi}{N} + k, \frac{\eta}{N} + l)}{[(\frac{\xi}{N} + k)^2 + (\frac{\eta}{N} + l)^2]\psi(\frac{\xi}{N}, \frac{\eta}{N})} \hat{u}_{\frac{\xi}{N}, \frac{\eta}{N}},$$

where $\bar{\hat{s}}$ denotes the complex conjugate of $\hat{s}$ and

$$\psi(\frac{\xi}{N}, \frac{\eta}{N}) = \sum_{(k,l) \in \mathbb{Z}^2} \frac{|\hat{s}(\frac{\xi}{N} + k, \frac{\eta}{N} + l)|^2}{(\frac{\xi}{N} + k)^2 + (\frac{\eta}{N} + l)^2}$$

and for any $(k,l) \in \mathbb{Z}^2$,

$$\hat{v}(k,l) = \begin{cases} \frac{\hat{u}_{0,0}}{\hat{s}_{0,0}} & , \text{for } (k,l) = (0,0), \\ 0 & \text{otherwise.} \end{cases}$$

The proof of this proposition is a direct consequence of the following lemma

Lemma 6.1 *Let $C > 0$, $(d_k)_{k \in \mathbb{Z}}$ be a sequence of real numbers larger than C, $(s_k)_{k \in \mathbb{Z}} \in l^2(\mathbb{Z})$ be a non identically null sequence of complex numbers and $u \in \mathbb{C}$. The problem of*

minimizing $E(\mathbf{w}) = \sum_{k\in\mathbb{Z}} d_k|w_k|^2$, *under the constraint that* $\mathbf{w} = (w_k)_{k\in\mathbb{Z}} \in \mathbb{C}^{\mathbb{Z}}$, *belongs to* $l^2(\mathbb{Z})$ *and satisfies* $\sum_{k\in\mathbb{Z}} s_k w_k = u$, *has a unique solution* $\mathbf{v} = (v_k)_{k\in\mathbb{Z}} \in \mathbb{C}^{\mathbb{Z}}$ *of the form*

$$v_k = \frac{\bar{s_k}}{d_k\left(\sum_{k'\in\mathbb{Z}} \frac{|s_{k'}|^2}{d_{k'}}\right)} u\,. \tag{6.19}$$

Proof First of all E is a coercive and strictly convex functional and E is minimized on a convex set, so we are sure that there exists a minimum and that it is unique. Second, if we index the real and imaginary part of w_k, s_k and u by respectively r and i, we are minimizing

$$E(w) = \sum_{k\in\mathbb{Z}} d_k({w_{k,r}}^2 + {w_{k,i}}^2)\,,$$

under the constraint

$$\begin{cases} \sum_{k\in\mathbb{Z}} (s_{k,r}w_{k,r} - s_{k,i}w_{k,i}) = u_r\,, \\ \sum_{k\in\mathbb{Z}} (s_{k,i}w_{k,r} + s_{k,r}w_{k,i}) = u_i\,. \end{cases}$$

So, the theorem of the Lagrange multipliers (see [22]) ensures that if $\mathbf{v}$ is the minimum, there exist λ_r and λ_i such that for any $k \in \mathbb{Z}$

$$\begin{cases} \frac{\partial E}{\partial w_{k,r}}(\mathbf{v}) = 2d_k v_{k,r} = \lambda_r s_{k,r} + \lambda_i s_{k,i}\,, \\ \frac{\partial E}{\partial w_{k,i}}(\mathbf{v}) = 2d_k v_{k,i} = -\lambda_r s_{k,i} + \lambda_i s_{k,r}\,. \end{cases} \tag{6.20}$$

Then, putting these expressions of $w_{k,r}$ and $w_{k,i}$ into the constraint, we find

$$\begin{cases} \lambda_r = \frac{2u_r}{\sum_{k'\in\mathbb{Z}} \frac{|s_{k'}|^2}{d_{k'}}}\,, \\ \lambda_i = \frac{2u_i}{\sum_{k'\in\mathbb{Z}} \frac{|s_{k'}|^2}{d_{k'}}}\,. \end{cases}$$

Using the expressions of λ_r and λ_i in (6.20), yields (6.19).

It easy to check that this $\mathbf{v}$ satisfies the constraint and belongs to $l^2(\mathbb{Z})$. Moreover, we have for any $\mathbf{w} \in \mathbb{C}^{\mathbb{Z}}$ satisfying the constraint

$$\begin{aligned} E(\mathbf{v}) &= \sum_{k\in\mathbb{Z}} d_k \left| \frac{\bar{s_k}}{d_k\left(\sum_{k'\in\mathbb{Z}} \frac{|s_{k'}|^2}{d_{k'}}\right)} u \right|^2\,, \\ &= \left(\sum_{k'\in\mathbb{Z}} \frac{|s_{k'}|^2}{d_{k'}}\right)^{-1} |u|^2\,, \end{aligned}$$

so we have

$$\begin{aligned} E(\mathbf{v}) &\leq \left(\sum_{k' \in \mathbb{Z}} \frac{|s_{k'}|^2}{d_{k'}}\right)^{-1} \left(\sum_{k \in \mathbb{Z}} |\frac{s_k}{\sqrt{d_k}}| |\sqrt{d_k} w_k|\right)^2 , \\ &\leq \sum_{k \in \mathbb{Z}} d_k |w_k|^2 = E(\mathbf{w}) . \end{aligned}$$

□

Proof of the Proposition 6.8 Expressing $\int_{(\mathbb{T}_N)^2} |\nabla w|^2$ in Fourier domain, for $w \in \mathcal{W}_{s,u}$, we have

$$\int_{(\mathbb{T}_N)^2} |\nabla w|^2 = \frac{(2\pi)^2}{N^2} \sum_{(\xi,\eta) \in \{-\frac{N}{2}-1,\dots,\frac{N}{2}\}^2} W_{\xi,\eta} ,$$

with

$$W_{\xi,\eta} = \sum_{(k,l) \in \mathbb{Z}^2} \left[(\frac{\xi}{N} + k)^2 + (\frac{\eta}{N} + l)^2 \right] |\hat{w}(\frac{\xi}{N} + k, \frac{\eta}{N} + l)|^2 ,$$

for $(\xi, \eta) \in \{-N/2+1, ..., N/2\}^2$. Therefore, for all $(\xi, \eta) \in \{-N/2+1, ..., N/2\}^2$, solutions of (6.18) minimizes $W_{\xi,\eta}$ under the constraint

$$\hat{u}_{\xi,\eta} = \sum_{(k,l) \in \mathbb{Z}^2} \hat{s}(\frac{\xi}{N} + k, \frac{\eta}{N} + l)\, \widehat{v}(\frac{\xi}{N} + k, \frac{\eta}{N} + l) .$$

For $(\xi, \eta) \neq (0, 0)$, the preceding lemma applies and yields the expected form for $\hat{w}$.

For $(\xi, \eta) = (0, 0)$, we minimize $W_{0,0}$, which does not depend on $\hat{w}(0, 0)$ (but depends on all the other $\hat{w}(k, l)$), under a constraint which is satisfied when the whole $\hat{u}_{0,0}$ is distributed onto $\hat{w}(0, 0)$. So, the unique possible solution is the one given in the proposition.

The fact that this w is really a solution is obvious given Lemma 6.1.

Note that this solution is obviously translation invariant and linear. Moreover, the operator Z defined by (6.18) is continuous from $\{u \in l^\infty(\mathbb{Z}^2),\ u \text{ is N-periodic}\}$ to $L^2((\mathbb{T}_N)^2)$ (this directly follows from the form of the solution and the fact that $\hat{s}$ does not vanish on $\{-\frac{1}{2} - \frac{1}{N}, ..., \frac{1}{2}\}$). □

As we said previously, Proposition 6.8 can be generalized to find solutions of problems of the form (6.17). Indeed, the only property we use in the demonstration is that $\int |\nabla w|^2$

is the integral of the modulus of a differential operator raised at the power 2. Thus if we note $L(w) = h * w$ and if there exists $C > 0$ such that $|\hat{h}(\frac{k}{N}, \frac{l}{N})|^2 \geq C$ for $(k,l) \neq (0,0)$, we simply have to replace, in Proposition (6.8), $(\frac{\xi}{N}+k)^2 + (\frac{\eta}{N}+l)^2$ by $|\hat{h}(\frac{\xi}{N}+k, \frac{\eta}{N}+l)|^2$. Note that this holds for any differential operator.

Note also that, when $\hat{s} \in l^1$, the interpolation defined by (6.18) can be extended to $l^\infty(\mathbb{Z}^2)$ (by interpolating the Fourier series of the convolution kernel) in such a way that it satisfies the hypotheses of the Propositions 5.2 and 5.3. Therefore, since we can see in Proposition 6.8 that it puts 0 at lost frequencies (where $\hat{s} = 0$), Propositions 5.2 and 5.3 yields result similar to Proposition 6.3 and 6.4 but adapted to problem (6.18).

Remark also that for any linear and translation invariant interpolation operator (defined by an h such that $|\nabla h| \in L^2((\mathbb{T}_N)^2)$ and $\hat{h}(\frac{\xi}{N}, \frac{\eta}{N}) \neq 0$ for any $(\xi, \eta) \in \{-N/2+1, ..., N/2\}^2)$, (6.18) applied with the kernel

$$\hat{s}(\frac{\xi}{N}+k, \frac{\eta}{N}+l) = \frac{\left((\frac{\xi}{N}+k)^2 + (\frac{\eta}{N}+l)^2\right) \quad \bar{\hat{h}}(\frac{\xi}{N}+k, \frac{\eta}{N}+l)}{\sum_{(k',l')\in\mathbb{Z}^2} \left[(\frac{\xi}{N}+k')^2 + (\frac{\eta}{N}+l')^2\right] |\hat{h}(\frac{\xi}{N}+k', \frac{\eta}{N}+l')|^2},$$

defines the same reconstruction as the linear and translation invariant one simply defined by h.

Therefore, this analysis gives a parallel between linear, translation invariant reconstructions and solutions of (6.18). This parallel can be used to describe linear reconstructions, but makes useless the use of (6.18) to reconstruct images.

At last, let us come back to the example, dealing with a 1D Heavyside function, developed in the preceding section.

Example 6.2. We are going to estimate an approximation of the reconstruction of a Heavyside signal.

Let $N > 0$ be an integer and v be the signal of size $4N$ given by

$$v_m = \begin{cases} 0 & \text{, if } 0 \leq m \leq 2N\,, \\ 1 & \text{, otherwise.} \end{cases}$$

We also define $s(m) = 0.5$ for $m = 0$ or 1, and $s(m) = 0$ otherwise. Therefore, the subsampled signal u of $\mathbb{R}^{2N}$ is equal to 0 for m in $\{0, ..., N\}$ and 1 anywhere else.

We simplify the minimization problem and look for α_0 such that the signal w^{α_0} minimizes $E(w) = \sum_{m=0}^{4N-1} |w_{m+1} - w_m|^2$ within the family of signals w^α (see Figure 6.3), such

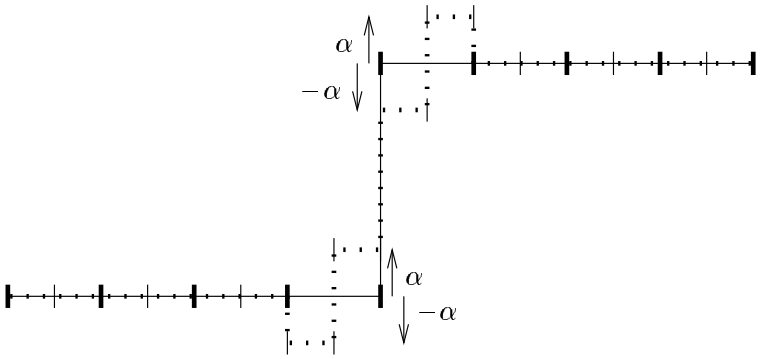

Figure 6.3: Part of a function w^α. $\sum_{m=0}^{4N} |w_{m+1} - w_m|^2$ is smaller for the dot signal than for the heavyside function.

that

$$w_m^\alpha = \begin{cases} 0 & \text{, if } 0 \leq m \leq 2N-2\,, \\ -\alpha & \text{, if } m = 2N-1\,, \\ \alpha & \text{, if } m = 2N\,, \\ 1-\alpha & \text{, if } m = 2N+1\,, \\ 1+\alpha & \text{, if } m = 2N+2\,, \\ 1 & \text{, otherwise.} \end{cases}$$

Note that such a w^α is sampled in u and

$$E(w^\alpha) = 14\alpha^2 - 4\alpha + 1$$

which is minimum for $\alpha_0 = \frac{1}{7}$.

So, one can see that there exists some signals that have an energy E lower than the Heavyside function v, that oscillate more than v and that lead to the same subsampled function u. This example illustrates the argument given in Section 2.2, as well as the fact that $\int_{(\mathbb{T}_N)^2} |\nabla w|^2$ is not a good measure of regularity, (see figure 6.3).

Chapter 7

Experiments

We illustrate in this chapter some propositions and the methods described above. The methods are the duplication interpolation, the bicubic reconstruction (see [39]), the "zero padding" interpolation, a reconstruction using a Prolate function and the total variation based restoration (these are respectively presented on figures from up to down and from left to right). Moreover, unless specified, the presented experiments are zooms of level 4 (the initial image numbers of row and of column are multiplied by 4) and they are generally displayed both in space and frequency domain. In this latter case, the presented images are the spectrum modulus raised to the power 0.01.

Figure 7.1 displays zooms of an initial image (see Figure 7.1.a) which is cylindric along the direction $(1, 3)$. Note that we only display the same extracted part of the zoomed images. Images 7.1.b and 7.1.c, which correspond to the duplication and the bicubic reconstructions, do present oscillating edges. In the same time, images 7.1.d and 7.1.e, which correspond to the "zero-padding" and the linear reconstruction defined by the prolate function, does not. This illustrates Proposition 5.3, since the convolution kernels associated with the duplication and bicubic reconstructions do not have Fourier transforms supported by $]-\frac{1}{2},\frac{1}{2}[^2$, while the "sinc" and the prolate functions do. In the same way, image 7.1.f is a part of the total variation based restoration associated with the "sinc function" ($s = s^e$) and does not have oscillating edges. Moreover, image 7.1.d oscillates more than the initial image while image 7.1.e does not (but it is very blurred). We can see that the total variation restoration (Figure 7.1.f), owing to its ability to extrapolate frequencies, has a sharp result which oscillates less than the initial image.

Figure 7.2 represents the Fourier series of the duplication interpolation of the image 7.1.a (a part of which is displayed on Figure 7.1.b), one can see its periodical structure preventing from the preservation of the 1D nature of image 7.1.a. Note that the same observation could have been made on the spectrum of the bicubic reconstruction. On the other hand, looking at Figure 7.3, we can see the ability of the total variation based restoration to prolong the initial structure out of $]-\frac{1}{2},\frac{1}{2}[^2$ ($]-\frac{1}{2},\frac{1}{2}[^2$ is represented by

the black square in the center of the figure). Moreover, we observe on this spectrum the property announced in Proposition 6.7. Indeed, we took the same value for K and K' and we can see that the Fourier series of the result is essentially supported by $S_{1,3}$ (see Proposition 6.7).

We display on Figure 7.4 the same zooming methods as the ones of Figure 7.1, in the case of an image representing a triangle. We can make about this figure the same comments as one made about Figure 7.1. Moreover, remark that the horizontal edge of the triangle is accurately restored by all the linear reconstructions. This is basically due to the fact that all the associated kernel satisfy the hypotheses of Proposition 5.2. Moreover, we can see a limit of our model on Figure 7.4.e. Indeed, we remark some oscillations on the edges in the vicinity of the triangle's corners. These are due to the need, of the total variation, to erode the corners in order to decrease. Figure 7.5 displays the spectrum of the images of Figure 7.4. Figure 7.5.a and 7.5.b illustrate Proposition 5.2 (the periodizations of the vertical white line are located at the same places as the vertical black ones, therefore they are canceled and the horizontal edge is correctly restored). Moreover, 7.5.e shows that the total variation restoration is the only one which tends to prolong the initial structures of the spectrum.

We display on Figure 7.6 the same zooming methods as the ones of Figure 7.1, in the case of an image representing an ellipse. The ellipse is clearly a limit case of the cylindric model, since the curvature of its edge is never null. This experiments shows that the results based on the modeling of edges by cylindric functions still apply to other kinds of edges, since the conclusions of the preceding experiments still hold. Looking at Figure 7.7 we see that the total variation based restoration permits to extend the initial spectrum much better than the duplication or any other linear method that periodizes it.

Figure 7.8 illustrates Proposition 6.4. It represents a small part of zooms of level 8 of a natural image (a woman photograph; note that the contrast has highly been modified). The difference in all these total variation based restorations holds in the filter s used to define $\mathcal{W}_{s,u}$ (up-down: the size of the frequencial support of s decrease, see the right part of Figure 7.8). On Figure 7.8.a, the value are fixed every height point, the other points are free of any constraint and the "number of constraint points" increase until Figure 7.8.d, where the constraint corresponds to the case $s = s^e$ (see Proposition 6.4). We see on Figure 7.8 that the zones, that suffer of "significant" constraint, are visible on Figures 7.8.a, 7.8.b, 7.8.c, but not on Figure 7.8.d. This highlights the need of the hypothesis "$s = h * s^e$" in Proposition 6.4.

In order to estimate the relevance of our analysis in the case of a real world images, we display on Figure 7.9 the same reconstruction/restoration methods in the case of an image provided by the C.N.E.S.. A part of this image presents oscillations that are essentially cylindric and for which are valid the comments made for Figure 7.1. Moreover, looking at this oscillating zone on Figures 7.9.a and 7.9.b, we remark that visually, it is corrupted by an oscillation (in a wrong direction). This artifact is due to the spectrum periodization

and is visually similar to the artifacts usually caused by aliasing. Furthermore, 7.9.e shows a shortcoming of the total variation based restoration that is that it tends to create homogeneous zones (even if the linear part on the left of the cylindric structure is well restored). We display on Figure 7.10 the spectra of the images of Figure 7.9. We observe here the frequency translation of most of the artifact seen on the spatial representation. In particular, the ability of the total variation based restoration to preserve cylindric images is translated in its ability to prolong the initial spectrum structure to the new spectral domain.

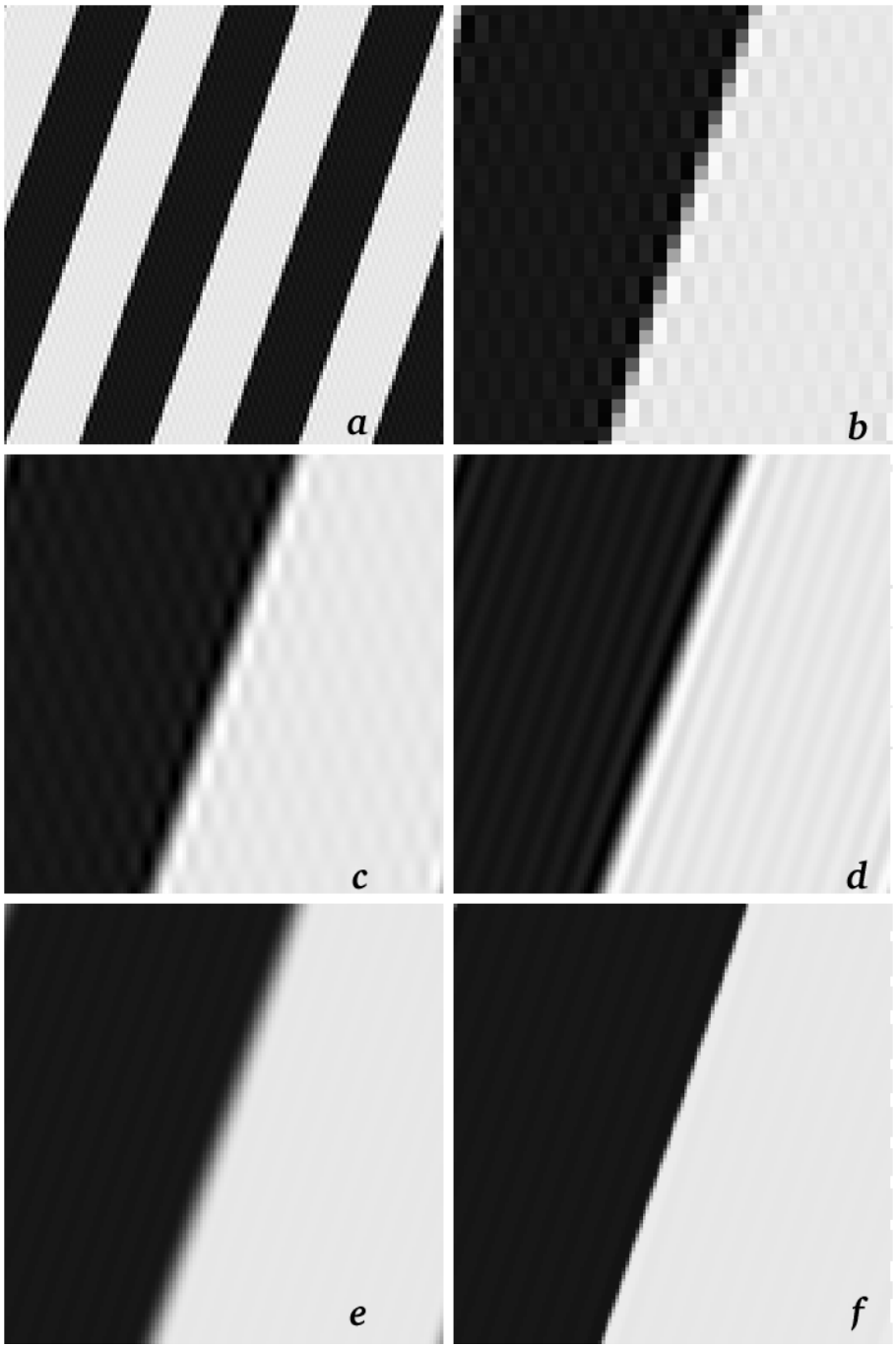

Figure 7.1: a: The initial image (cylindric along the direction $(1, 3)$). Part of the images zoomed by a factor 4 by: b: the duplication interpolation; c: the cubic convolution reconstruction; d: the "zero-padding" interpolation; e: the reconstruction using the Prolate function; f: the total variation based restoration.

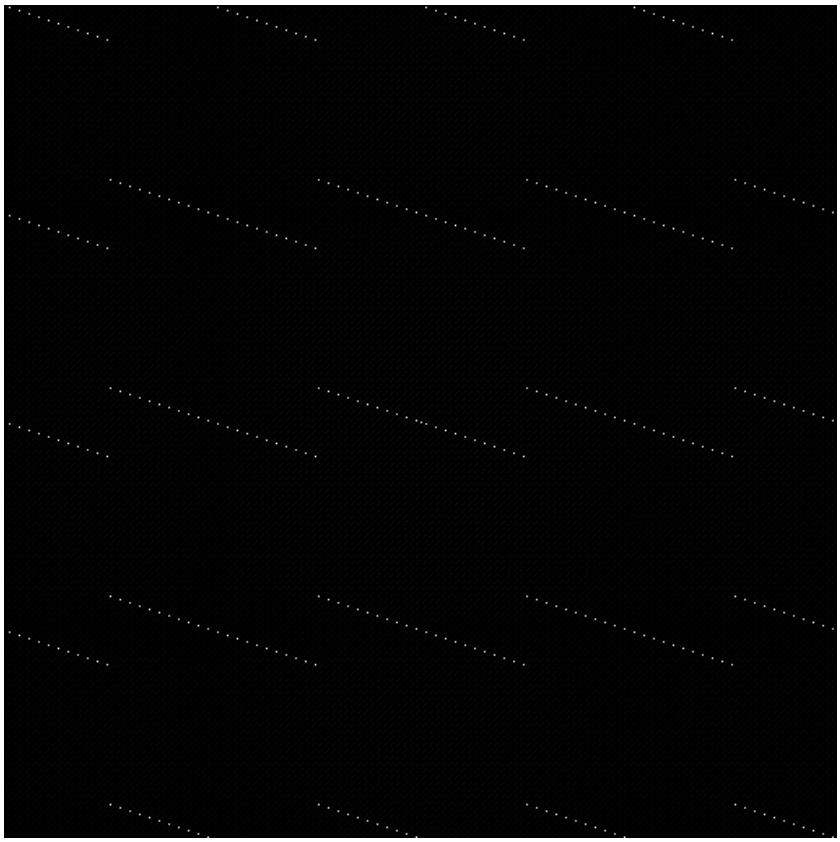

Figure 7.2: Spectrum of the duplication interpolation, a part of which is displayed on Image 7.1.b.

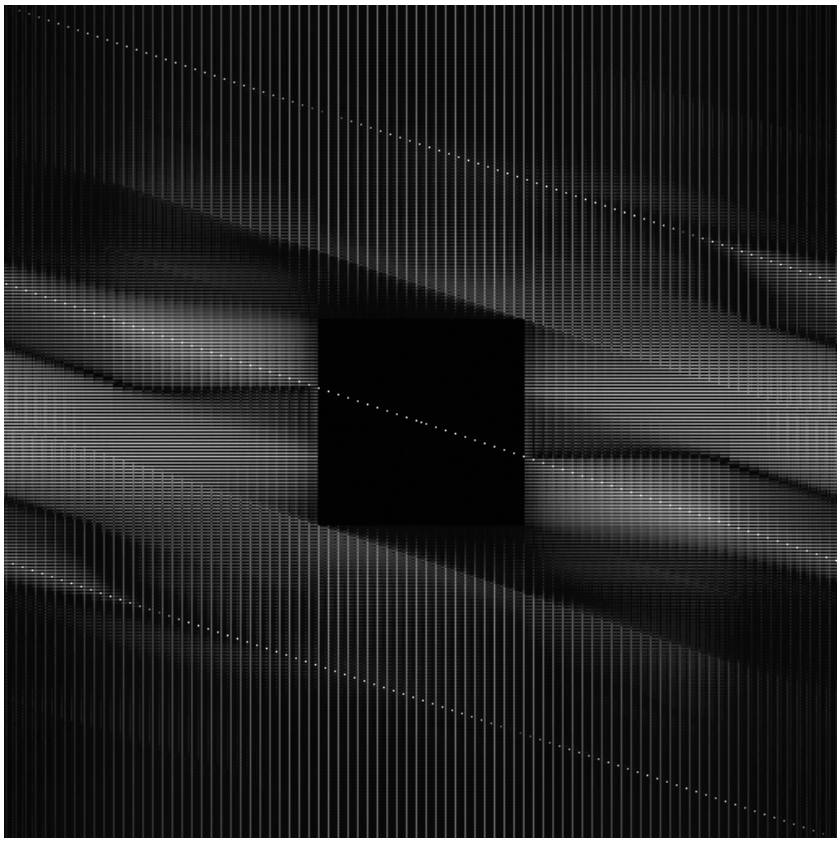

Figure 7.3: Spectrum of the Total Variation based restoration, a part of which is displayed on Image 7.1.f.

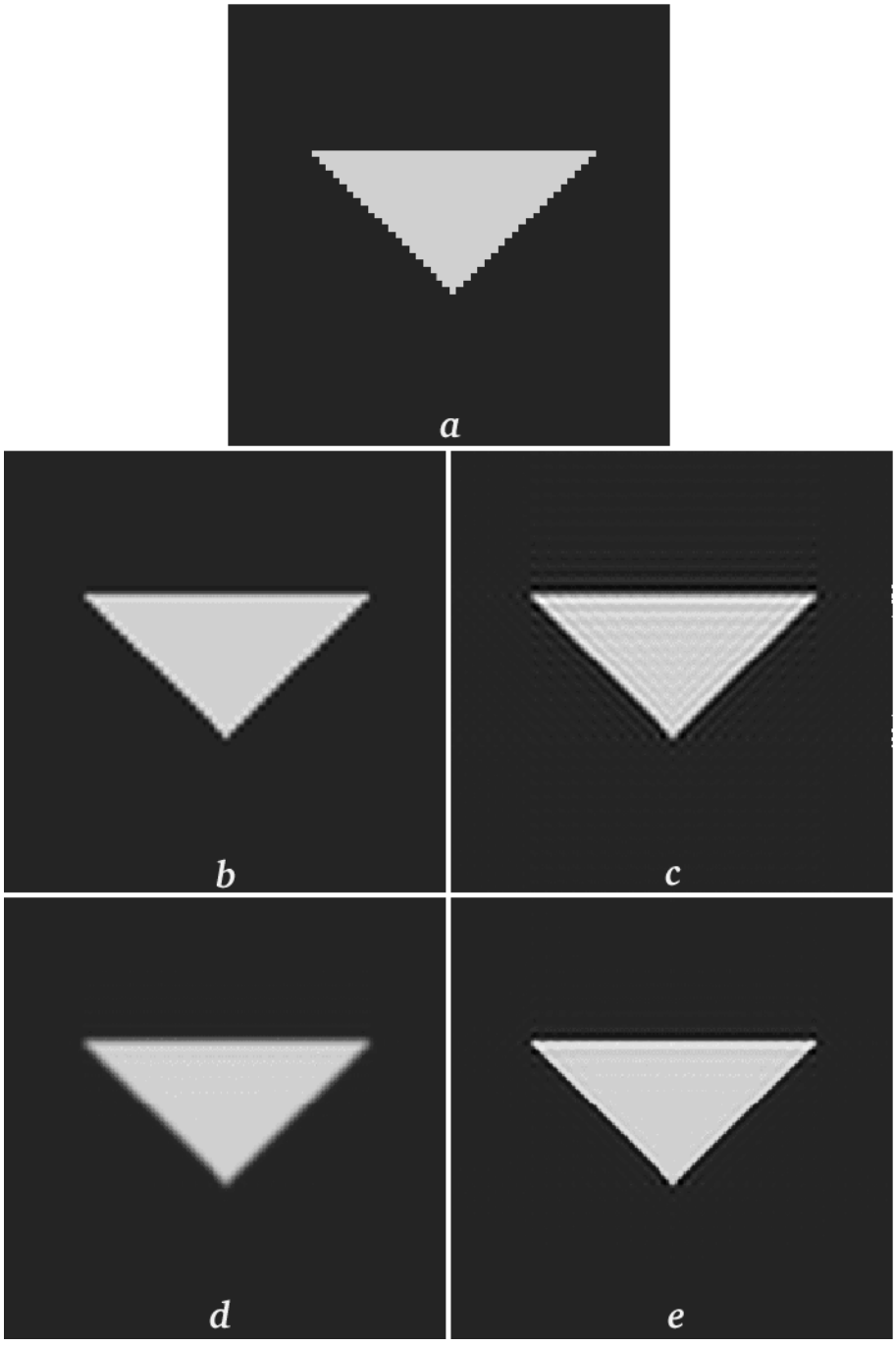

Figure 7.4: Image zoomed by a factor 4 by: a: the duplication interpolation; b: the cubic convolution reconstruction; c: the "zero-padding" interpolation; d: the reconstruction using the Prolate function; e: the total variation based restoration.

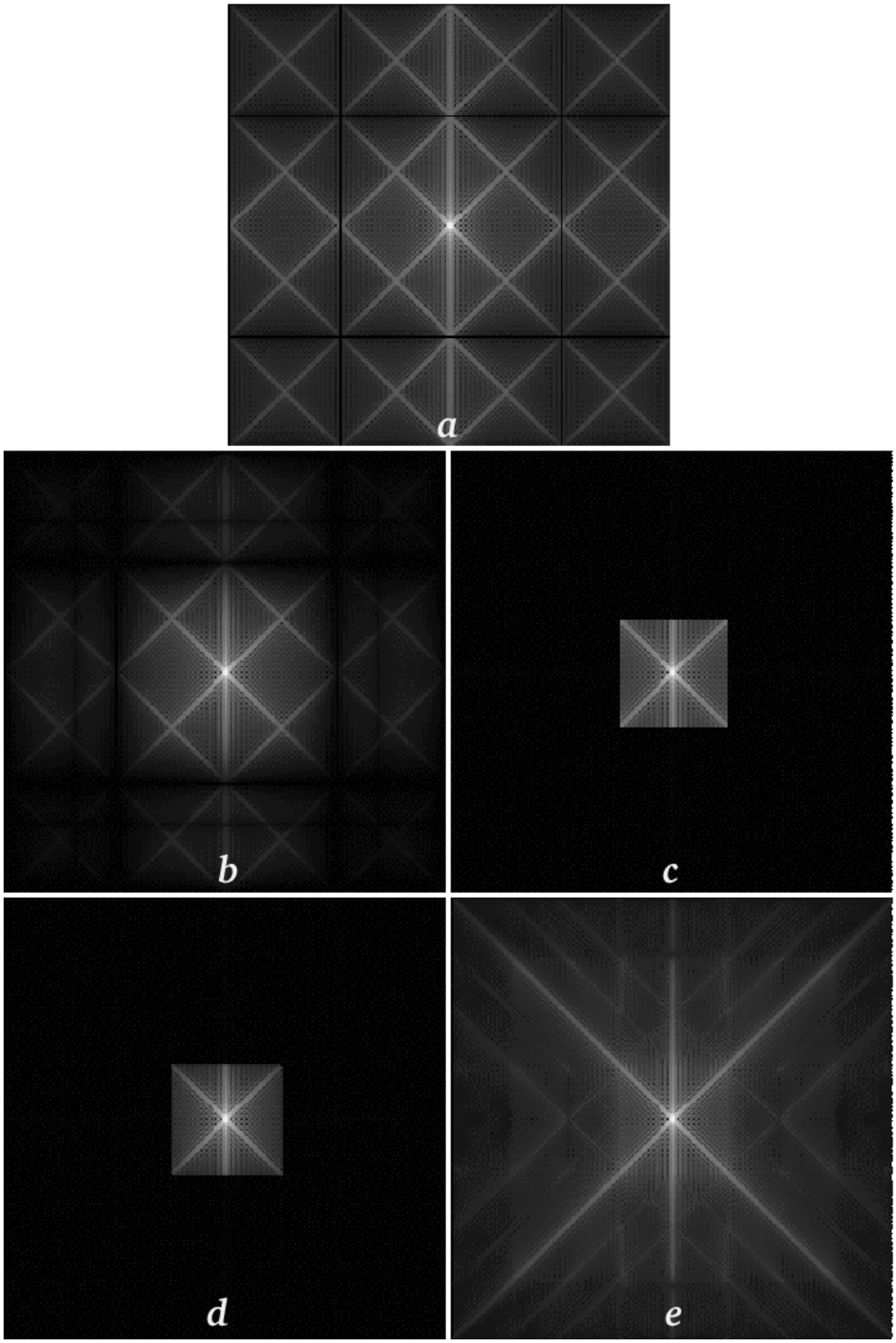

Figure 7.5: Spectra of the images displayed on Figure 7.4.

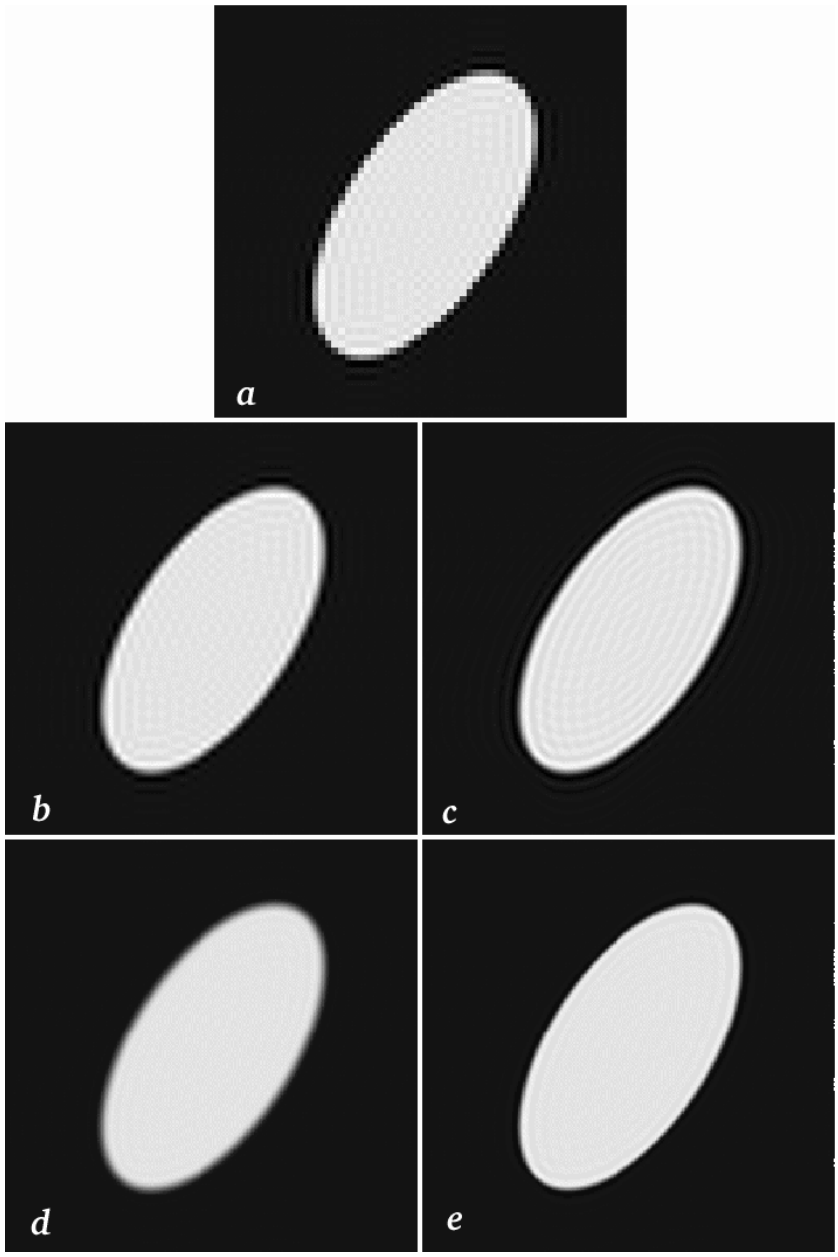

Figure 7.6: Image zoomed by a factor 4 by: a: the duplication interpolation; b: the cubic convolution reconstruction; c: the "zero-padding" interpolation; d: the reconstruction using the Prolate function; e: the total variation based restoration.

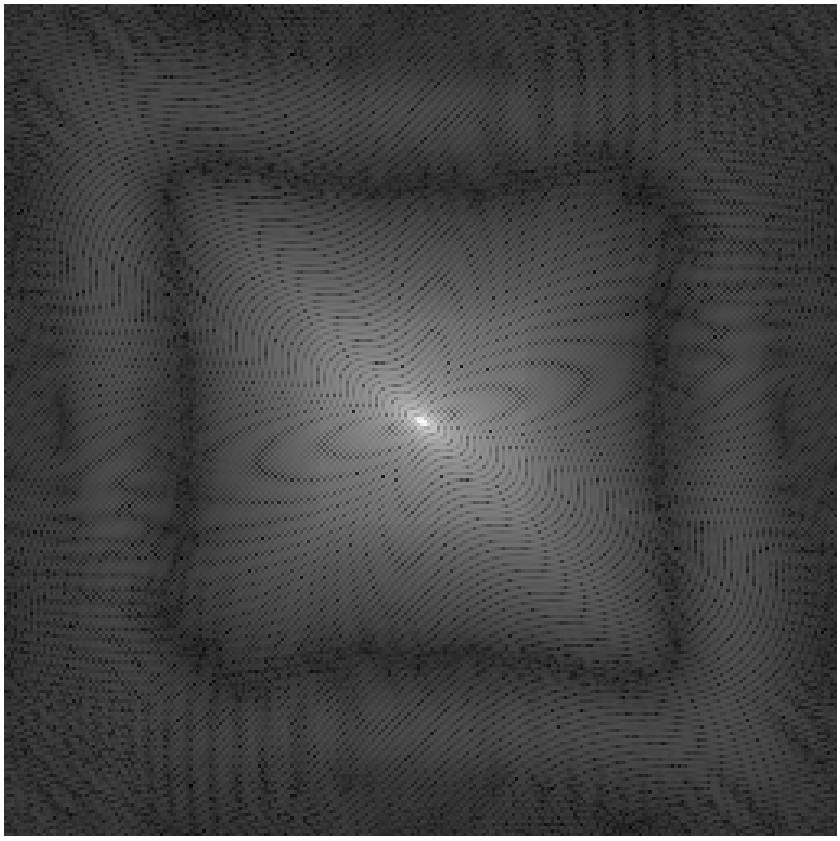

Figure 7.7: Spectrum of the total variation based restoration displayed on Figure 7.6.e.

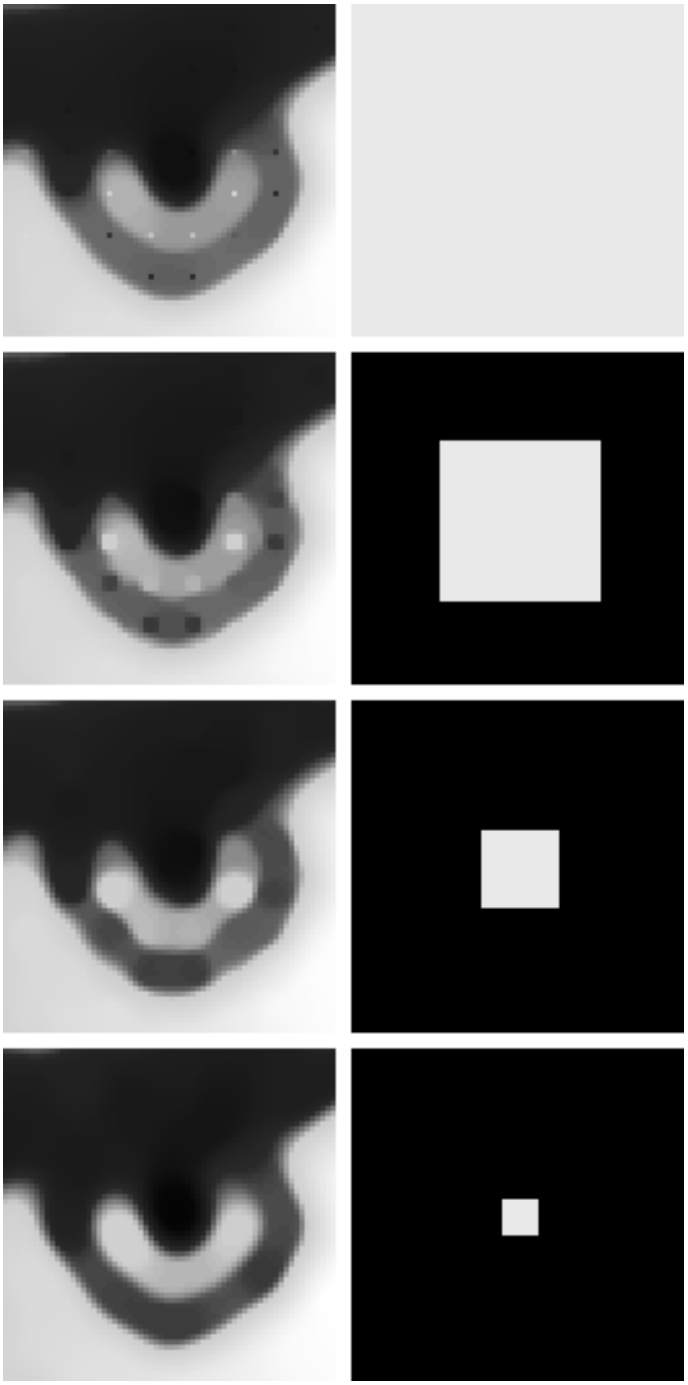

Figure 7.8: Left: the images restored with the total variation restoration (zooms of level 8; the contrast has been modified); Right: the Fourier transform of the kernel s used to restore the image on the left (i.e. this latter belongs to $\mathcal{W}_{s,u}$).

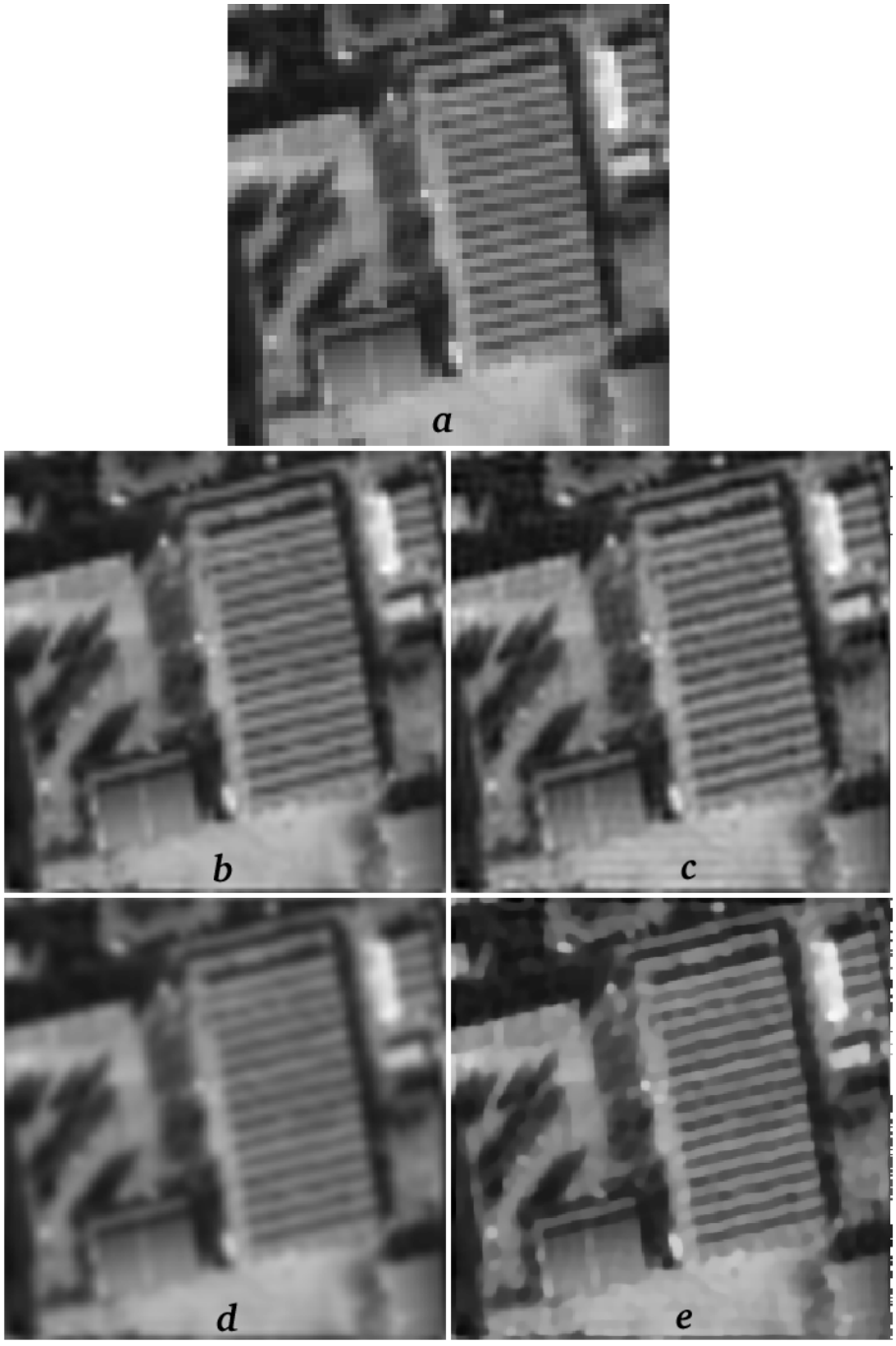

Figure 7.9: Image zoomed by a factor 4 by: a: the duplication interpolation; b: the cubic convolution reconstruction; c: the "zero-padding" interpolation; d: the reconstruction using the Prolate function; e: the total variation based restoration.

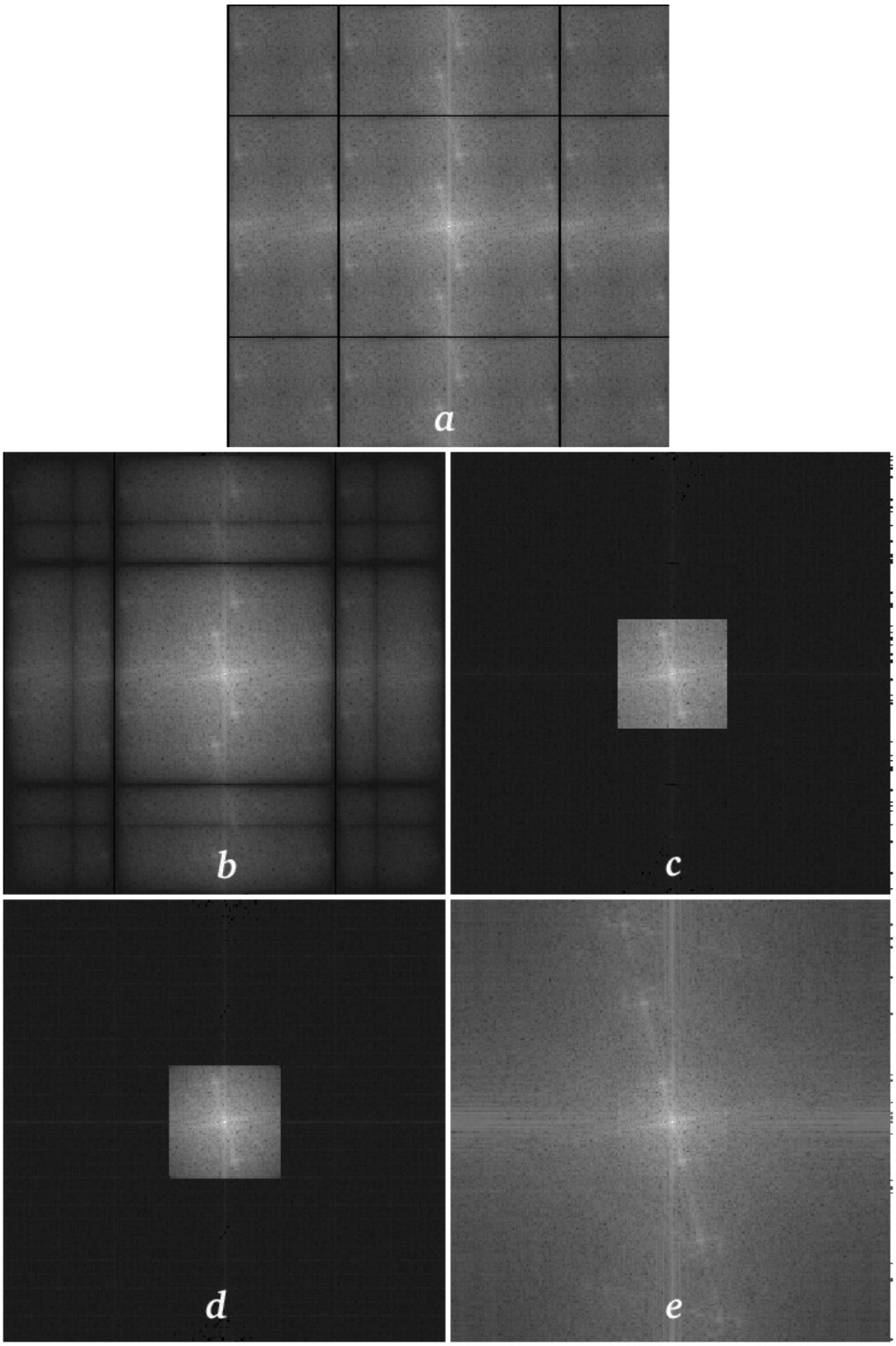

Figure 7.10: Spectra of the images displayed on Figure 7.9.

Part III

Image deblurring

Chapter 8

Introduction

This part deals with two complementary methods in image deblurring: a nonlinear shrinkage of wavelet-packets coefficients that is called Fixed Chosen Noise Restoration (FCNR) and a variational method (known as Rudin-Osher-Fatemi method)[1].

We do distinguish deblurring from reconstruction, restoration, and interpolation, in the fact that the degradation model that deblurring methods try to invert, contains noise. Mathematically speaking, given Ω an open set of $\mathbb{R}^2$, we assume u is defined, for $(m,n) \in \Omega \cap \mathbb{Z}^2$, by

$$u_{m,n} = (s * v)(m,n) + b_{m,n} \, , \tag{8.1}$$

where s and v map $\mathbb{R}^2$ onto $\mathbb{R}$, and b is a noise. In practice, the noise is white and is considered Gaussian of standard variation σ. S will sometime denote the convolution operator with s. Moreover, similarly to the previous part, we only consider the case $\Omega = \mathbb{R}^2$ or the case where we identify Ω to the torus of size N, $(N\mathbb{T})^2$ (noted $(\mathbb{T}_N)^2$).

Taking the noise into account leads us to simplify the problem and therefore to look for a result defined over the same sampling grid (we will however show that the Rudin-Osher-Fatemi method permits to construct oversampled deblurred images; Experiments will show that this is only interesting in the cases where the noise is low).

Remark that, since the deblurred image is defined on the sampling grid, and since we do want neither aliasing nor useless blurring, our goal should be to approximate a function of the form

$$\tilde{v}_{m,n} = (\tilde{s} * v)(m,n) \, ,$$

[1]Very recent papers deal with the equivalence between wavelet shrinkage methods and variational methods (see [9, 13, 26]). The superiority of the wavelet based methods is therefore on a numerical point of view. Our purpose here is, among other things, to show that, in some situations, a variational method might remain more adapted.

for $(m,n) \in \Omega \cap \mathbb{Z}^2$ and a given function $\tilde{s}$ (think about the prolate functions [28] or about some functions of the kind). However, this does not have any impact on the formalism, since we do still note the convolution kernel s (instead of a modified s taking into account $\tilde{s}$).

Note that, even when the blurring defined by s is "invertible" (in the sense that $\hat{s}$ does not vanishes (inside $\{-\frac{N}{2}+1,...,\frac{N}{2}\}^2$ when $\Omega = (\mathbb{T}_N)^2$ or $]-\frac{1}{2},\frac{1}{2}]^2$ when $\Omega = \mathbb{R}^2$)), such a problem is known to be ill-posed. Indeed, let us assume that there exists an inverse operator S^{-1} defined, for $(m,n) \in \Omega \cap \mathbb{Z}^2$, by

$$\left(S^{-1}(u)\right)_{m,n} = \left(\frac{1}{\hat{s}}\hat{u}\right)^{\vee}_{m,n},$$

where $u^{\vee}$ denotes the inverse Fourier transform of u (defined over $\Omega \cap \mathbb{Z}^2$). Applying S^{-1} to (8.1), we obtain, for $(m,n) \in \Omega \cap \mathbb{Z}^2$, when neglecting the aliasing[2] (and therefore assuming s cancels efficiently the high frequencies),

$$\left(S^{-1}(u)\right)_{m,n} = v_{m,n} + \left(\frac{\hat{n}}{\hat{s}}\right)^{\vee}_{m,n}. \tag{8.2}$$

This equation expresses the fact that the noise might blow up at the frequencies for which $\hat{s}$ vanishes, or becomes very small.

Several approaches have been used to recover v (or $\tilde{s} * v$) over $\Omega \cap \mathbb{Z}^2$. The reader is referred to [4] for most of the linear ones and to [16, 25] for overviews on the subject. In a few words, the first approach consists in enhancing images without regard to the convolution kernel [29]. The other methods are based on regularization approaches of the problem: using statistical properties (Wiener[3] and Kalman filters) or regularity measurements of the images such as the entropy ([16] and included references), the Total Variation [44] or the characterization of Besov spaces by wavelets coefficients [18, 19].

---

[2] Otherwise, we would have

$$\left(S^{-1}(u)\right)_{m,n} = v_{m,n} + \left(\frac{\hat{n}}{\hat{s}}\right)^{\vee}_{m,n} + \text{"aliasing term"}.$$

However, similarly to Chapter 1 we cannot afford aliasing, since it may appear like information. Therefore, it is reasonable to assume that it is negligible.

[3] The Wiener filter is used, as a reference, in the Section 11. It is the optimal (in the sense of the l^2 norm) linear deblurring given the assumed covariance Φ of the initial landscape. The Fourier transform of the Wiener filter is given by

$$\frac{\hat{\Phi}\,\hat{s}^*}{\hat{\Phi}|\hat{s}|^2 + \sigma^2}. \tag{8.3}$$

We detail in the following two approaches of the problem. Looking back at (8.2), note that the difficulty in image deblurring is directly related to the issue of denoising an image with a highly colored noise. Our first objective can therefore be to control the noise in order to obtain a restored image with a white noise of reasonable standard deviation (note that white noises are perceptually less disturbing than colored ones). This leads us to the FCNR method which was first introduced by B. Rougé in [41] and is formalized in the next chapter.

Although it is very efficient to restore an image after an "invertible" blur (when $\hat{s}$ does not cancel (inside $\{-\frac{N}{2}+1, ..., \frac{N}{2}\}^2$ when $\Omega = (\mathbb{T}_N)^2$ or $]-\frac{1}{2}, \frac{1}{2}]^2$ when $\Omega = \mathbb{R}^2$)), this technique appears to be limited in the case when the blurring is no longer "invertible". Indeed, if $\hat{s}$ vanishes on some part of the Fourier domain, the information supported by these frequencies is lost during the degradation and replacing it by zero creates Gibbs effects.

The Rudin-Osher-Fatemi variational method, described in Chapter 10 has the ability to reconstruct the lost frequencies, in a reliably manner, and therefore avoids the Gibbs effects. This ability to rebuild lost frequencies can, in a way similar to the one introduced in the preceding part, be used to obtain deblurred images defined on a grid thinner than the sampling one.

The complementarity of these two methods is highlighted in Section 11.1 where they are applied to the restoration of satellites SPOT 1 and SPOT 5 images. Then, experiments on the ability of Rudin-Osher-Fatemi variational method to simultaneously deblur and oversample images are given in Section 11.2 and show that such methods can be applied to remove aliasing.

Chapter 9

Fixed chosen noise restoration (FCNR)

The Fixed Chosen Noise Restoration, which was introduced by B. Rougé in [40, 41], is inspired from Donoho and Johnstone's wavelet shrinkage method which consists in thresholding the coefficients of a noisy image in a wavelet basis [18, 19].

From the decomposition of the image in an orthonormal basis $\psi_{j,n}$,

$$u_0 = \sum_{j \in \mathcal{J}} \sum_{k \in \mathcal{K}} \langle u_0, \psi_{j,k} \rangle \psi_{j,k},$$

shrinkage methods denoise the image by applying the following formula

$$u_1 = \sum_{j \in \mathcal{J}} \sum_{k \in \mathcal{K}} \tau_\lambda(\langle u_0, \psi_{j,k} \rangle) \psi_{j,k},$$

where the soft-thresholding function τ_λ is given by

$$\tau_\lambda(x) = \begin{cases} x - sgn(x)\lambda & if\ |x| \geq \lambda\,, \\ 0 & if\ |x| < \lambda\,, \end{cases} \tag{9.1}$$

and the threshold λ depends on the characteristics of the noise. In the case of a Gaussian noise, Donoho and Johnstone [18] chose a threshold which is proportional to the standard deviation σ of the noise,

$$\lambda = \sigma \sqrt{2log\ N},$$

where N is the number of samples of the image. For N large, the L^∞-norm of the noise is known to have a high probability of being close to λ [5].

Looking at (8.2), it seems opportune, in the case of a deblurring, to adapt the denoising

to frequencies. The deconvolution does indeed emphasize the noise at the frequencies for which $\hat{s}$ is small (in general, high frequencies). However, since fine scale wavelets (which are located in high frequencies) are badly concentrated in the Fourier domain, a strategy of an adapted wavelet thresholding is impossible. Wavelets are not appropriate for the deblurring which needs a high resolution in frequency.

On the other hand, they are very well adapted to denoising since they concentrate the energy of the image over few coefficients (this is not the case of Fourier coefficients which offer an optimal resolution in frequency).

Wavelet-packets are a good alternative to wavelets since they offer a good resolution in frequency and a decomposition in "wavelets style" coefficients which ensures an efficient denoising.

9.1 The wavelet-packets

Let us start this section with a short introduction to wavelet-packets theory. For more details the reader is referred to [15]. We consider a pair of quadrature mirror filters (m_0, m_1), with

$$m_0(\xi) = \frac{1}{\sqrt{2}} \sum_{k \in \mathbb{Z}} c_k e^{-ik\xi} ,$$

with $(c_k)_{k\in\mathbb{Z}} \in l^2(\mathbb{Z})$, and

$$m_1(\xi) = \frac{1}{\sqrt{2}} \sum_{k \in \mathbb{Z}} d_k e^{-ik\xi} ,$$

where $(d_k)_{k\in\mathbb{Z}} \in l^2(\mathbb{Z})$ and is connected with a multiresolution analysis (for instance, $d_k = (-1)^k c_{1-k}$; see [35]).

The basic wavelet-packets $w_n(x)$ are defined by recursion. We start with $w_0(x)$ which is the unique $L^1 \cap L^2$-solution of the equation

$$w_0(x) = \sqrt{2} \sum_{k \in \mathbb{Z}} c_k w_0(2x - k), \tag{9.2}$$

under the normalization constraint

$$\int_{\mathbb{R}} w_0(x)\ dx = 1.$$

This function w_0 is actually the scaling function or father wavelet, usually denoted φ, associated with the connected multiresolution analysis. The other w_n's are then defined

as follows

$$w_{2m}(x) = \sqrt{2} \sum_{k \in \mathbb{Z}} c_k w_m(2x - k), \tag{9.3}$$

$$w_{2m+1}(x) = \sqrt{2} \sum_{k \in \mathbb{Z}} d_k w_m(2x - k). \tag{9.4}$$

The properties of the quadrature mirror filters ensure that, for all $j \in \mathbb{N}$, the family $\{2^{-j/2} w_m(2^{-j}x - k),\ k \in \mathbb{Z}\}$ is an orthonormal basis of

$$E_m^j := \overline{span\{2^{-j/2} w_m(2^{-j}x - k),\ k \in \mathbb{Z}\}}^{L^2(\mathbb{R})}$$

with the scalar product $\langle u, v \rangle = \int_{\mathbb{R}} u(x)\, \bar{v}(x)\, dx$. Moreover, we have

$$\forall j \in \mathbb{N}, \forall m \in \mathbb{N}, \quad E_m^j = E_{2m}^{j+1} \oplus E_{2m+1}^{j+1}, \tag{9.5}$$

and thus

$$\forall j \in \mathbb{N}, \qquad E_0^0 = \oplus_{m=0}^{2^j - 1} E_m^j$$

which means that, for all $j \in \mathbb{N}$, $\{2^{-j/2} w_m(2^{-j}x - k),\ k \in \mathbb{Z}, m = 0, 1, \cdots, 2^j - 1\}$ is an orthonormal basis of E_0^0. Hence, the wavelet-packets theory provides us with a collection of orthonormal bases of a Hilbert space E_0^0 that we can identify with $l^2(\mathbb{Z})$. Looking at (9.5), let us observe that there are many other bases than the ones just mentioned, which involve several values of j. Yet, we will here restrict ourselves to the bases associated with a unique level of decomposition j.

All this can also be expressed in the Fourier domain. Equations (9.3) and (9.4) become

$$\hat{w}_{2m}(2\xi) = m_0(\xi)\, \hat{w}_m(\xi),$$

$$\hat{w}_{2m+1}(2\xi) = m_1(\xi)\, \hat{w}_m(\xi),$$

which implies

$$\hat{w}_m(2^j \xi) = M_m^j(\xi)\, \hat{w}_0(\xi),$$

with $m = \sum_{l=0}^{2^{j-1}} \epsilon_l 2^l$ ($\epsilon_l \in \{0, 1\}$) and $M_m^j(\xi) = \prod_{l=0}^{2^{j-1}} m_{\epsilon_l}(2^l \xi)$. The identification of E_0^0 with $l^2(\mathbb{Z})$ is translated by the identification of $\hat{u}$ the Fourier transform of a function

$u \in E_0^0$, with $m \in L^2(\mathbb{T})$ such that

$$\hat{u}(\xi) = m(\xi)\, \hat{w}_0(\xi).$$

The same way, the Fourier transform of the functions $u \in E_m^j$ will be of the form $m(\xi)\, 2^{j/2} \hat{w}_m(2^j \xi)$ where $m \in L^2(\mathbb{T})$. Therefore, using the notable property of the quadrature mirror filters, $|m_0(\xi)|^2 + |m_1(\xi)|^2 = 1$, we obtain, for any $u \in E_0^0$

$$\begin{array}{rcl} \hat{u}(\xi) & = & \sum_{m=0}^{2^j-1} |M_m^j(\xi)|^2 m(\xi)\, \hat{w}_0(\xi) \\ & = & \sum_{m=0}^{2^j-1} m(\xi)\, \overline{M_m^j(\xi)}\, \hat{w}_m(2^j \xi) \end{array} \tag{9.6}$$

which expresses u as the linear combination of its projections onto the spaces E_m^j. Let us observe that when $|m_0|^2$ is well localized around $[-\pi/2, \pi/2]$ $(mod\ 2\pi)$ (and therefore $|m_1|^2$ around $[\pi/2, 3\pi/2]$ $(mod\ 2\pi)$), $|M_m^j|^2$ will be localized around an interval of length $2^{-j}\pi$. Therefore, equation (9.6) provides us with a horizontal slicing of the time-frequency plane by the spaces E_m^j, imitating in some sense the Fourier transform.

The optimal slicing would be obtained with the filter $m_0(\xi) = \sum_{l \in \mathbb{Z}} \chi_{[-\pi/2, \pi/2]}(\xi + 2l\pi)$ (χ_A denotes the characteristic function of a set A) that we will call, in the sequel, Shannon filter. However, it does not generate wavelet-packets in the sense they have been defined above since there is no L^1-solution of the associated scaling equation (9.2). A Shannon basis is however defined by starting with $\hat{w}_0 = \chi_{[-\pi, \pi]}$.

Going back to the time domain, note that we get from the decomposition of a signal into the wavelet basis of E_m^j to its projection onto E_{2m}^{j+1} and E_{2m+1}^{j+1}, with the benefit of the operators T_0 and T_1 defined as follows

$$\forall u \in l^2(\mathbb{Z}), \quad \begin{array}{rcl} T_0(u)(k) & = & \sum_{l \in \mathbb{Z}} c_{2k-l} u(l) \\ T_1(u)(k) & = & \sum_{l \in \mathbb{Z}} d_{2k-l} u(l) \end{array} \tag{9.7}$$

and which satisfy the following property

$$\sum_{k \in \mathbb{Z}} u(k) w_{m,k}^j = \sum_{k \in \mathbb{Z}} T_0(u)(k) w_{2m,k}^{j+1} + \sum_{k \in \mathbb{Z}} T_1(u)(k) w_{2m+1,k}^{j+1},$$

with $w_{m,k}^j(x) = w_m(2^j x - k)$. The reconstruction is done with the dual operators $T_0^\star$ and $T_1^\star$,

$$T_0^\star(T_0(u)) + T_1^\star(T_1(u)) = u.$$

The 2D-wavelet-packets are obtained by tensor product but that, for convenience, we will think out in 1D in the sequel.

9.2 Study framework and approximations

B. Rougé proposed another approach than Donoho and Johnstone's [18] and consequently the restoration is not optimal in Donoho's sense. The approach is driven by the remark that it is impossible to remove all the noise from an image without loosing a lot of data (it is impossible to completely separate noise and image structure). Therefore, our goal should not be to remove the noise but to control it.

Our aim should be here to obtain a restored image with a Gaussian noise. It is therefore necessary to find a method of denoising that leaves a noise of the form $S(n_0)$ where n_0 is Gaussian so that further deconvolution leaves a white noise. The other possibility is to transform a colored noise $S^{-1}(n)$ into a Gaussian noise when the deblurring is done before the denoising.

To apply a wavelet-packet shrinkage method as it will be introduced below, we need to make the following assumption. We assume that the deconvolved noise $S^{-1}(n)$ is "almost" Gaussian on the support of the packets E_m^j. This means that the wavelet-packets we use are very well localized in frequency variable. However, since the wavelet-packets do not give rise to a partition of the Fourier domain with arbitrary precision, even for a large j, the restoration would be all the more successful that $1/\hat{s}$ does not oscillate too much.

We must however use wavelet-packets that are very well localized in the Fourier domain. With that in mind, the Shannon basis (associated with Shannon filter (see Section 9.1)) appears to be an optimal choice. Yet, it is not applicable since the coefficients of the filter are not decreasing fast enough (such a basis is not suited to denoising). Consequently, we will use cubic spline wavelets which have exponential decay and are well localized in frequency. They will therefore offer a good compromise.

Remark now that when the "localization assumption" is satisfied, we can as well approximate S by an operator which is diagonal in the wavelet-packets basis. Moreover, since wavelets associated with the same packet are deduced one from another by a translation, the eigenvalues of S are almost constant on this packet. Note therefore that deblurring by multiplying the projection of the image over every packet by a constant, ensures that the deconvolved noise is Gaussian on the packets.

Let us focus on the error made in this approximation. We start from a signal $U = \sum_{k\in\mathbb{Z}} u(k)\, w_0(.-k) \in E_0^0$. For any $j \in \mathbb{N}$ and $m \in \mathbb{N}$, the projection of U on E_m^j is given by

$$P_m^j U = \sum_{k\in\mathbb{Z}} T_m^j(u)(k)\; w_m^j(.-k),$$

where $T_m^j = T_{\epsilon_{j-1}} \circ \cdots \circ T_{\epsilon_0}$ with $(\epsilon_0, \cdots, \epsilon_{j-1}) \in \{0,1\}^j$ and $m = \sum_{l=0}^{j-1} \epsilon_l 2^l$.

The error made in the direction of each wavelet-packet is therefore given by

$$T_m^j(S^{-1}(u)) - C_m^j T_m^j(u).$$

Therefore, its L^2-norm is minimized by

$$C_m^j = \frac{\langle T_m^j(S^{-1}(u)), T_m^j(u)\rangle}{\|T_m^j(u)\|_2^2}\,.$$

This formula is usable for users who have a statistical estimation of the images they deal with. But as the deblurring is relatively stable with regard to the variations of C_ϵ, it is more convenient to approximate these latter by values which are independent of u.

9.3 The fixed chosen noise restoration

Once again, the FCNR comes from the remark that it might be worthwhile to find a method of restoration that returns an image with a Gaussian noise of known standard deviation. Indeed, a low contrast texture drowned in a strong noise might still be detected by the eye of an observant, even when the standard deviation of the noise is much larger than the intensity of the contrast of the texture. Using a method which consists in thresholding the coordinates of the image in a given basis might erase this texture since its coordinates might be under the threshold. The thresholding is therefore not appropriate to recover an image with a lot of textures.

Hence, it seems advisable to replace the soft-thresholding (of Donoho and Johnstone's methods) by an invertible function that does not erase any data.

One way to match this constraint, together with the objective of recovering an image with a Gaussian noise, is to replace the soft-thresholding function (see (9.1)) by the following

$$\tilde{\tau}_{\lambda_1,\lambda_2}(x) = \begin{cases} (\lambda_2/\lambda_1)\, x & if\ |x| \le \lambda_1\,, \\ x + sgn(x)\,(\lambda_2 - \lambda_1) & if\ |x| > \lambda_1\,. \end{cases} \tag{9.8}$$

This function has to be read "shrink from λ_1 to λ_2".

Remark also that the method is very close to the classical thresholding defined by τ (see (9.1)) since we have, for $|x| \ge \lambda_1$,

$$\tilde{\tau}_{\lambda_1,\lambda_2}(x) = \tau_{\lambda_1-\lambda_2}(x).$$

Unlike the thresholding, this function applied on the coordinates of a noisy image, does replace, in homogeneous zones, the Gaussian noise of standard deviation σ by a Gaussian noise of standard deviation $(\lambda_2/\lambda_1)\,\sigma$ (modulo a negligible part of the noise - see Figures 9.1, 9.2 and 9.3).

The choice of the parameter λ_2/λ_1 is therefore very clear. The role of λ_1 is more subjective. Indeed, if the noise is bounded, it seems natural to take λ_1 equal to this

bound. In the case of a Gaussian noise, we can take $\lambda_1 = \sigma\sqrt{logN}$ where N is the number of samples of the image (or the packet when it is applied on E_m^j). However, if the noise is not bounded (or if its bound is too large) we have to chose λ_1 in a pragmatic way.

As it was mentioned above, we are going to adapt the shrinkage to wavelet-packets. Therefore, from a noisy image u_0 whose wavelet-packets decomposition is

$$u_0 = \sum_{\substack{m \in \mathbb{N} \\ k \in \mathbb{Z}}} \langle u_0, w_{m,k}^j \rangle w_{m,k}^j,$$

with $w_{m,k}^j(x) = w_m(2^j x - k)$, we obtain a denoised image

$$u_1 = \sum_{\substack{m \in \mathbb{N} \\ k \in \mathbb{Z}}} \tilde{\tau}_{{\lambda_1}^{j,m}, {\lambda_2}^{j,m}}(\langle u_0, w_{m,k}^j \rangle) w_{m,k}^j.$$

The parameters ${\lambda_1}^{j,m}$ and ${\lambda_2}^{j,m}$ depend naturally on the standard deviation σ of the noise but they also depend on the wavelet-packet $w_{m,k}^j$ and the filter $\hat{s}$. Note that, since we get from $w_{m,k}^j$ to $w_{m,0}^j$ by translation and since the noise is Gaussian, there are no reasons for ${\lambda_1}^{j,m}$ and ${\lambda_2}^{j,m}$ to depend on parameter k.

Let us choose to make the deblurring after denoising (note that when it is done by multiplying the projection of the image on each packet by a constant (see Section 9.2) the obtained result does actually not depend on that chosen order).

We will also assume, in the following, that S is approximated by a diagonal operator in the wavelet-packet basis and we will denote by $\frac{1}{C_m^j}$ the approximating eigenvalue for the packet E_m^j (the method can easily be generalized to the case when S is not approximated).

Let us denote $\sigma^{j,m}$ the standard deviation of the noise, after shrinkage and before deblurring, on each packet E_m^j. In order to obtain an image with a "Gaussian" noise ("Gaussian" has to be understood as Gaussian modulo a negligible part (see Figure 9.3)) of standard deviation σ_0 on homogeneous zones, we must therefore solve

$$\sigma_0 = C_m^j \, \sigma^{j,m}. \tag{9.9}$$

Let us assume we have found $\lambda_1^{j,m}$ such that

$$(C_m^j)^2 \int_{\lambda_1^{j,m}}^{\infty} (x - \lambda_1^{j,m})^2 e^{-\frac{x^2}{2\sigma^2}} dx$$

is negligible compared to $(\sigma_0)^2$ (Heuristically: on Figure 9.3 the part of the function beyond λ_2 is "negligible" compared with the rest of the function). Then, we can assume

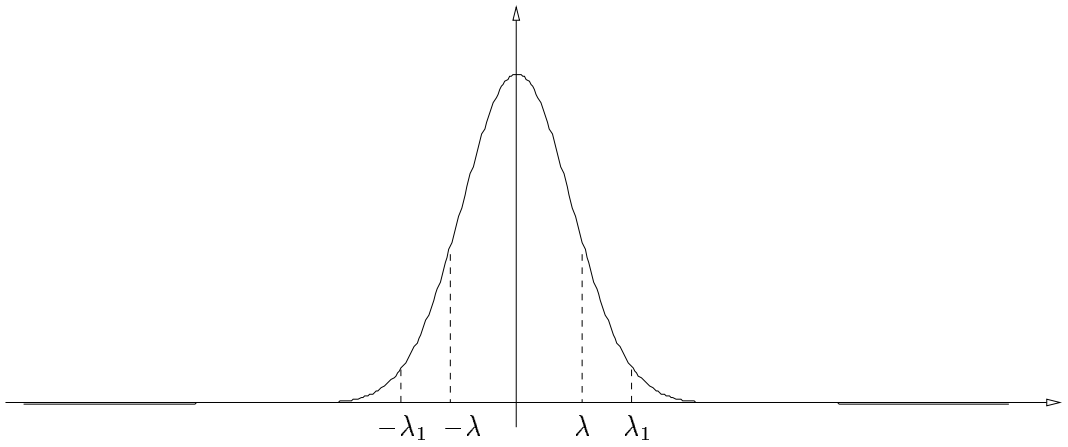

Figure 9.1: Noise histogram before restoration.

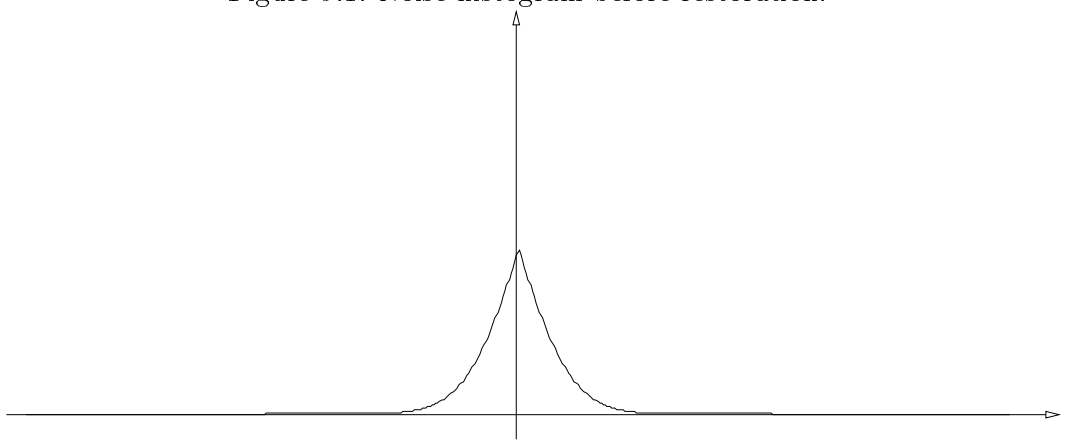

Figure 9.2: Noise histogram in homogeneous zones after a soft-thresholding (with τ_λ).

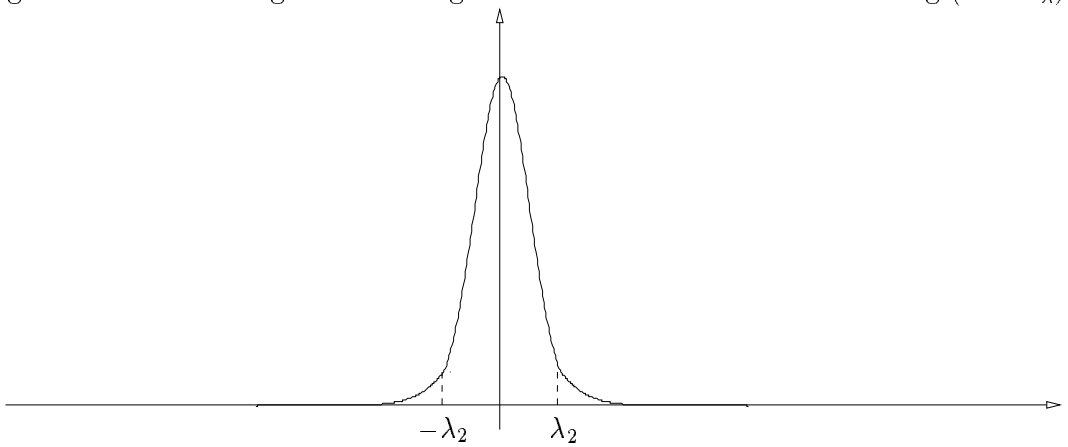

Figure 9.3: Noise histogram in homogeneous zones after a shrinkage with the function $\tilde{\tau}_{\lambda_1,\lambda_2}$.

that, for any $\lambda_2 \leq \lambda_1^{j,m}$, the standard deviation of the noise after the shrinkage defined by $\tilde{\tau}_{\lambda_1^{j,m},\lambda_2}$ is almost $\frac{\lambda_2}{\lambda_1^{j,m}}\sigma$. So, letting

$$\lambda_2^{j,m} = \frac{\lambda_1^{j,m}\sigma_0}{C_m^j\,\sigma},$$

$\tilde{\tau}_{\lambda_1^{j,m},\lambda_2^{j,m}}$ yields a standard deviation $\sigma^{j,m}$ that satisfies (9.9)(modulo the famous negligible part).

Remark that when S is not invertible, C_m^j can be infinite. Thus, to generalize the method to non-invertible S's, we must let $\tilde{\tau}_{\infty,\lambda_2}(x) = 0$ for any real values of x and λ_2. The packets associated with an infinite first parameter are canceled by the restoration.

Remark finally that if we keep in memory the parameters $\lambda_1^{j,m}$ and $\lambda_2^{j,m}$ this method is invertible in the sense that we can recover the blurred and noisy image from the restored image (if S is itself invertible). There is therefore no loss of data.

Moreover, in order to fight against the lack of independence in translation of the wavelet-packets decomposition, one can apply the same treatment on several translated versions of the image and, afterwards, make the mean of all the restored images [14].

9.4 Multi-level shrinkage

The model we have presented in the preceding section is not fully satisfactory since the basis we use does not decorrelate the noise from the significant signal very well. Indeed, the support of the wavelets in a fine frequency decomposition is too large. On the other hand, if the wavelet packet decomposition is stopped at a higher level, the noise will be more decorrelated, but the basis will not be adapted to the deconvolution since it will not have a fine frequency decomposition and thus $\mathcal{F}(S^{-1}(n))$ will not be "uniform" enough on the support of the $\hat{w}_k^j$'s. We are meeting here Heisenberg uncertainty principle.

The way we have chosen to get round this difficulty is to shrink wavelet coefficients at different levels of the decomposition. With that in mind, we remark that

$$\forall \lambda_1, \lambda_2, \lambda_3 \in \mathbb{R}, \quad \tilde{\tau}_{\lambda_2,\lambda_3} \circ \tilde{\tau}_{\lambda_1,\lambda_2} = \tilde{\tau}_{\lambda_1,\lambda_3}. \tag{9.10}$$

Let us explain this more clearly in the case of a 1D-signal. Assume we want to shrink at the level j of the decomposition. Every packet E_m^j, for $m = 0, ..., 2^j - 1$, is associated with two parameters ${\lambda_1}^{j,m}$ and ${\lambda_2}^{j,m}$. Note that the multiplication of a couple $({\lambda_1}^{j,m}, {\lambda_2}^{j,m})$ by a constant $c > 1$ only modifies the result on a negligible part of the noise. Therefore, assuming the noise is "small" with regard to initial signal, we can normalize the couples $({\lambda_1}^{j,m}, {\lambda_2}^{j,m})$'s in such a way that for any $m = 0, ..., 2^j - 1$, ${\lambda_1}^{j,m} = \lambda_1$, for an appropriate λ_1 (for instance $\lambda_1 = max({\lambda_1}^{j,m})$).

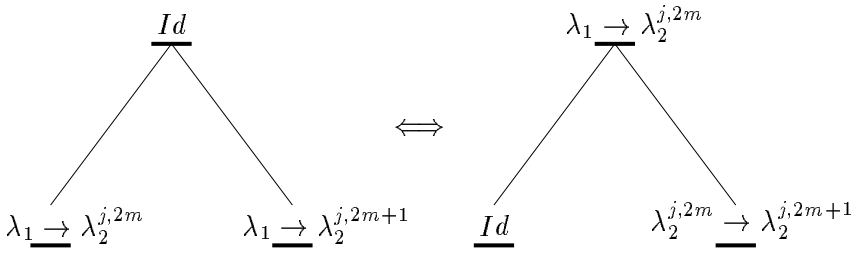

Figure 9.4: Two ways of shrinking the packet $E_m^{j-1} = E_{2m}^j \oplus E_{2m+1}^j$ (it is a case where $\lambda_2^{j,2m+1} \geq \lambda_2^{j,2m}$).

Therefore, we boil down to the case where every packet E_m^j, for $m = 0, ..., 2^j - 1$, is associated with two parameters λ_1 and ${\lambda_2}^{j,m}$.

Let us denote, for $m = 0, ..., 2^{j-1} - 1$,

$$\lambda_2^{j-1,m} = min\{\lambda_2^{j,2m}, \lambda_2^{j,2m+1}\}.$$

We can, since the shrinkage satisfies (9.10), shrink first the packet E_{2m}^j (respectively E_{2m+1}^j) from λ_1 to $\lambda_2^{j-1,m}$, and then from $\lambda_2^{j-1,m}$ to $\lambda_2^{j,2m}$ (respectively from $\lambda_2^{j-1,m}$ to $\lambda_2^{j,2m+1}$). Hence, the packets E_{2m}^j and E_{2m+1}^j are first shrunk in the same way. Therefore, since the noise is "Gaussian", this shrinkage can, as well, be made in the wavelet basis $\{w_m(2^{j-1}x - k),\ k \in \mathbb{Z}\}$ associated with the packet $E_m^{j-1} = E_{2m}^j \oplus E_{2m+1}^j$. More precisely, instead of applying

$$\tilde{\tau}_{\lambda_1,\lambda_2^{j,2m}} = \tilde{\tau}_{\lambda_2^{j-1,m},\lambda_2^{j,2m}} \circ \tilde{\tau}_{\lambda_1,\lambda_2^{j-1,m}},$$

on Ej_{2m}, we apply $\tilde{\tau}_{\lambda_1,\lambda_2^{j-1,m}}$ on E_m^{j-1} and then $\tilde{\tau}_{\lambda_2^{j-1,m},\lambda_2^{j,2m}}$ on E_{2m}^j (idem for E_{2m+1}^j see Figure 9.4).

Note that we can likewise apply $\tilde{\tau}$ at every level of the decomposition, starting from the higher levels and going up to the lower ones. Note also that these arguments are also valid when we do the deconvolution before the denoising.

Remark also that, since the shrinkage is made at every level, we do not need to compute the best basis that is the wavelet-packets basis the most adapted to the operator S (the basis in which S is the most diagonal), but that it might have been interesting from a numerical point of view [26],[33].

In addition to the reasons explained above, this technique of shrinking at different levels will also give a better preservation of the structures of the signal because the shrinkage is made in different bases.

9.5 Numerical implementation

Let (m_0, m_1) denote the 1D-QMF associated with the cubic spline wavelets [33]. The 2D-QMF (respectively, wavelet-packets) are obtained by tensorial product $m_{\epsilon_1,\epsilon_2} = m_{\epsilon_1} \times m_{\epsilon_2}$ with $\epsilon_i \in \{0, 1\}$ (respectively, $w^j_{m,n} = w^j_m \times w^j_n$). From then on, we present the algorithm in the 2D point of view.

The passing from $\mathbb{Z}^2$ to a finite grid (the support of the image) is done by periodization.

Let us consider the case when S is approximated by a diagonal operator in the wavelet-packets basis. For numerical reasons, we will not use the basis associated with the finest frequency level. Indeed, wavelet-packets w_n for n large, are in general badly localized in the Fourier domain. Hence, there is no advantage in getting too far in the decomposition since we will not gain any precision in frequency. This has led us to stop it at the fifth level. Therefore, the enhancement $C^5_{m,n}$, that is applied to the packet indexed by (m, n) of the fifth level, has to be estimated.

To facilitate the measurement, the 1D QMF (m_0, m_1) is approximated by the Shannon filters $(\sum_{k\in\mathbb{Z}} \chi_{[-\pi/2,\pi/2]}(. + 2k\pi), \sum_{k\in\mathbb{Z}} \chi_{[\pi/2,3\pi/2]}(. + 2k\pi))$. The iterated filters $M^5_{m,n}$ are also some characteristic functions, and we denote $S^5_{m,n}$ their support. As it was said in section 9.2, even if the optimum $C^5_{m,n}$'s depend on the image u, they are estimated by[1]

$$C^5_{m,n} = card(S^5_{m,n}) \left(\sum_{(k,l)\in S^5_{m,n}} |\hat{s}(k, l)| \right)^{-1},$$

where $card(S^5_{m,n})$ denotes the cardinal of $S^5_{m,n}$.

This enhancement is well defined unless $\hat{s}$ is identically null on $S^5_{m,n}$. However, when it is very large (or when it is not defined), we make the associated packet vanish since it

[1]Remark that when the deblurring is done without approximation, the standard deviation of the noise on each packet is enhanced by

$$\|M^5_{m,n}/\hat{s}\|_2,$$

where

$$M^5_{m,n}(\xi) = \prod_{l=0}^{4} m_{\epsilon_l}(2^l\xi),$$

with $(m, n) = \sum_{l=0}^{4} \epsilon_l 2^l$. Therefore the enhancement $C^5_{m,n}$ can be approximated by

$$C^5_{m,n} = card(S^5_{m,n})^{-1} \left(\sum_{(k,l)\in S^5_{m,n}} \frac{1}{|\hat{s}(k, l)|^2} \right)^{\frac{1}{2}},$$

Such $C^5_{m,n}$'s are less "stable" (they are not finite when $\hat{s}$ vanishes on $S^5_{m,n}$) than the one we propose. If $\hat{s}$ vanishes on $S^5_{m,n}$, the coefficients on the packet are replaced by zero.

should contain essentially noise without information.

We then compute λ_1 such that, for any (m,n) satisfying $C^5_{m,n} \neq \infty$,

$$(C^5_{m,n})^2 \int_{\lambda_1}^{\infty} (x-\lambda_1)^2 e^{-\frac{x^2}{2\sigma^2}} dx$$

is negligible compared to $(\sigma_0)^2$. Note that in practice λ_1 is a parameter. We are now able to estimate

$$\lambda_2^{5,m,n} = \frac{\lambda_1 \sigma_0}{C^5_{m,n}\,\sigma},$$

However, since the packets $E^5_{0,0}$ does not need to be shrunk (it corresponds to very low frequencies), we let

$$\lambda_2^{5,0,0} = 0.$$

In order to shrink at the higher levels, we let

$$\lambda_2^{j,m,n} = \min_{\epsilon_1,\epsilon_2 \in \{0,1\}} (\lambda_2^{j+1,2m+\epsilon_1,2n+\epsilon_2}),$$

for $j = 4,3,2,1,0$ (note that $\lambda_2^{j,0,0} = 0$). Therefore, every packet $E^{j+1}_{2m+\epsilon_1,2n+\epsilon_2}$ is associated with the parameters

$$(\lambda_1^{j+1,2m+\epsilon_1,2n+\epsilon_2}, \lambda_2^{j+1,2m+\epsilon_1,2n+\epsilon_2}) = (\lambda_2^{j,m,n}, \lambda_2^{j+1,2m+\epsilon_1,2n+\epsilon_2})$$

for $j = 0,1,2,3,4$.

The wavelet-packets coefficients $(u^1_{m,n})_{k,l}$ of the image at the 1^{st} level are then computed and they are shrunk with respect to the rule exposed above. The operation is next repeated at the next levels until the fifth one. That is, for $j = 1,2,3,4$,

$$u^{j+1}_{2m+\epsilon_1,2n+\epsilon_2} = T_{\epsilon_1} \times T_{\epsilon_2}(\tilde{u}^j_{m,n}),$$

with

$$(\tilde{u}^j_{m,n})_{k,l} = \tilde{\tau}_{\lambda_1^{j,m,n},\lambda_2^{j,m,n}} \left((u^j_{m,n})_{k,l}\right).$$

Then, after deblurring, the reconstruction is done directly from level 5 to 0 with the help of the dual operators $T_m^{5\,\star} \times T_n^{5\star}$.

$$u = \sum_{m,n} T_m^{5\,\star} \times T_n^{5\star}(C^5_{m,n}\tilde{u}^5_{m,n}).$$

Chapter 10

Variational deblurring

The second approach we are proposing is highly related to the one introduced by Rudin, Osher and Fatemi in [44, 45]. This is a variational approach which has the significant advantage on the one presented in the preceding chapter that it can reconstruct some lost frequencies. We will essentially give arguments that show that we reconstruct low frequencies in a meaningful manner (the rebuilding of the high frequencies has already been commented in Chapter 6).

Once again, the sampled images are assumed to be periodic of period N (for commodity we will assume in the following that N is even). The reconstructed images are therefore defined on the torus of size N, $(N\mathbb{T})^2$ (noted $(\mathbb{T}_N)^2$). In the following, in order to distinguish Fourier series from Discrete Fourier Transforms, we will denote $\hat{w}_{\frac{k}{N},\frac{l}{N}}$ by $\hat{w}(\frac{k}{N},\frac{l}{N})$ in the case of the Fourier series.

10.1 Rudin-Osher-Fatemi variational method adapted to oversampling

Rudin-Osher-Fatemi variational method consists in selecting a function that minimizes the total variation, among the ones that could be degraded into the blurred image. This problem is usually solved under its unconstrained variational form that is

$$\text{Minimize } |Dw|((\mathbb{T}_N)^2) + \lambda \int_{(\mathbb{T}_N)^2} |s * w - u|^2 ,$$

where λ is a Lagrange multiplier [8, 10, 11, 44, 45].

We present in the following a modified version of this method. Indeed, we will consider the sampling as being a part of the degradation process. This has the significant advantage to make possible the restoration on a grid thinner than the original sampling

one. Therefore, the method is based on the minimization of the functional

$$E(w) = |Dw|((\mathbb{T}_N)^2) + \lambda \sum_{m,n=0}^{N-1} |(s * w)_{m,n} - u_{m,n}|^2 , \tag{10.1}$$

among functions $w \in BV((\mathbb{T}_N)^2) \cap L^2((\mathbb{T}_N)^2)$. Note that λ can probably be interpreted as a Lagrange multiplier (in a way similar to the one describe in [10]). However, we will only consider λ as a parameter. It is clear that a λ large leads to a noisy image with sharp edges. Conversely, for a weak λ, the image is strongly denoised but blurred. Note also that, in practice, we can only expect to oversample the image in cases where the noise is low.

Of course, most of the results presented in Chapter 6 still hold in the case of the minimization of (10.1). The rest of the section is devoted to the statement of these results. We will not give the details of the proofs, since they are very similar[1] to the one of Chapter 6.

Therefore, concerning existence, we have

Proposition 10.1 *Let $N \in \mathbb{N}$, $u \in l^\infty(\mathbb{Z}^2)$ N-periodic and let $s \in L^2((\mathbb{T}_N)^2)$ such that $\hat{s}(k,l) = 0$ for any $(k,l) \in \mathbb{Z}^2 \setminus \{(0,0)\}$, then E defined by (10.1) admits a minimum v among functions of $BV((\mathbb{T}_N)^2) \cap L^2((\mathbb{T}_N)^2)$.*

Note that the hypothesis " $\hat{s}(k,l) = 0$ for any $(k,l) \in \mathbb{Z}^2 \setminus \{(0,0)\}$" could be replaced by a constraint on the mean of the result.

Note also that we cannot guarantee the uniqueness of the result since the functional is not strictly convex. However, we have the following proposition which combines a proposition similar to Proposition 6.2 and another one given in [10].

Proposition 10.2 *Let v_1, $v_2 \in BV((\mathbb{T}_N)^2) \cap L^2((\mathbb{T}_N)^2)$ minimizing (10.1). We have*

$$\forall (m,n) \in \{0,...,N-1\}^2, \ (s * v_1)_{m,n} = (s * v_2)_{m,n} .$$

Moreover, if we note

$$\Gamma = \left\{ (x,y) \in (\mathbb{T}_N)^2, \ v_1 \text{ and } v_2 \text{ are } C^1 \text{ at } (x,y) \text{ and } \nabla v_1(x,y) \neq 0 \right\} ,$$

for any $(x,y) \in \Gamma$, there exists $t \geq 0$ such that

$$\nabla v_2(x,y) = t \nabla v_1(x,y) .$$

[1] The main additional argument is that the weak L^2 convergence of a sequence $w^k \in L^2((\mathbb{T}_N)^2)$ ensures the pointwise converse of the sequence $(s * w^k)$ for $s \in L^2((\mathbb{T}_N)^2)$.

Similarly to Chapter 6, this proposition shows that two minima are "close" one from each other.

Let us now state the minimization problems that approximate the minimization of (10.1), among functions of $BV((\mathbb{T}_N)^2) \cap L^2((\mathbb{T}_N)^2)$, in such a way that we can compute and manipulate the results with a computer.

Therefore, we define, for an integer $K \geq 1$

$$\mathbb{B}_K = \left\{ w \in L^2((\mathbb{T}_N)^2),\ \hat{w} \text{ is supported by } \{-\frac{KN}{2}+1, ..., \frac{KN}{2}\}^2 \right\}. \tag{10.2}$$

We also define, for two integers K and K' with $K' \geq K \geq 1$, and for $w \in \mathbb{B}_K$

$$E_{K'}(w) = \frac{1}{K'^2} \sum_{m,n=0}^{K'N-1} |\nabla w(\frac{m}{K'}, \frac{n}{K'})| + \lambda \sum_{m,n=0}^{N-1} |(s * w)_{m,n} - u_{m,n}|^2 .$$

Note that the minimization of E_1 among functions of $\mathbb{B}_1$ yields the discrete form of the Rudin-Osher-Fatemi functional.

Remark, once again, that we could, in a way similar to Section 6.2, obtain a consistency proposition saying that results of the minimization of E (see (10.1)) among functions of $\mathbb{B}_K$ can be used to approximate a result of the minimization of E (see (10.1)) among functions of $BV((\mathbb{T}_N)^2) \cap L^2((\mathbb{T}_N)^2)$.

Similarly, we could say that the results of the minimization of $E_{K'}$ among functions of $\mathbb{B}_K$, for a given $K \geq 1$, can be used to approximate a result of the minimization of E (see (10.1)) among functions of $\mathbb{B}_K$.

Remark finally that we can state propositions similar to Proposition 6.4 and 6.7 of Chapter 6 (dealing with cylindric functions preservation). Of course, it is artificial to deal with cylindric functions in a noisy case. Let us however state

Proposition 10.3 *Let N be an integer, $(\alpha, \beta) \in \mathbb{R}^2 \setminus \{(0,0)\}$, $u \in l^\infty(\mathbb{Z}^2)$ N-periodic and cylindric along the direction (α, β). For any kernel $s \in L^2((\mathbb{T}_N)^2)$ whose Fourier transform is supported by $\{-\frac{1}{2}+\frac{1}{N}, ..., \frac{1}{2}\}^2$, (10.1) admits a minimum cylindric along the same direction (α, β).*

This result can of course be extended to most of the variational methods [2]. This result ensures not to have drawbacks in the restorations due to the lack of informations between points of the sampling grid.

[2] at least those using a lower-semicontinuous regularity measure (in our case the total variation), that decreases after a convolution with a kernel in L^1 and satisfies a compactness theorems (so that a solution exists)).

This proposition clearly claims in favor of a degradation based on a kernel s whose Fourier transform is supported by $\{-\frac{1}{2}+\frac{1}{N},...,\frac{1}{2}\}^2$. Indeed, images issued from such a degradation model can be oversampled (in a "reasonable way") by variational methods.

However, if the Fourier transform of s does not satisfy the hypothesis of the above proposition, experiments will show that it is more efficient to replace s by $\tilde{s}$, satisfying this hypothesis, than using s to define the functional. Indeed, doing this, the aliasing is considered as a noise and tends to be removed (see Section 11.2).

10.2 Spectrum interpolation

We are now going to leave the framework of image restoration for the one of frequency interpolation. This does appear to be unrealistic (since we will assume we interpolate frequencies over a compact set) but provides us with nice examples and a good intuition of the way frequencies are reconstructed. This also permits to illustrate the way Rudin-Osher-Fatemi variational method behaves when the kernel s vanishes inside $\{-\frac{1}{2}+\frac{1}{N},...,\frac{1}{2}\}^2$.

10.2.1 Theoretical aspect of the spectrum interpolation

Let us focus on the following problem. Given $v \in BV((\mathbb{T}_N)^2) \cap L^2((\mathbb{T}_N)^2)$, and $\mathcal{K}$ a bounded set of $\mathbb{Z}^2$, we

$$\text{Minimize } |Dw|((\mathbb{T}_N)^2), \text{ with } \hat{w}_{\frac{k}{N},\frac{l}{N}} = \hat{v}_{\frac{k}{N},\frac{l}{N}} \text{ for all } (k,l) \in \mathbb{Z}^2 \setminus \mathcal{K}\,. \tag{10.3}$$

Once again, existence of a solution does not pose any problem. We also have the usual behavior concerning uniqueness. Note that, in the particular case of spectrum interpolation, we can give the following example where two different solutions can be found. Let $v := (x,y) \in (\mathbb{T}_N)^2 \mapsto |cos(\frac{K}{N}x)| \in BV((\mathbb{T}_N)^2) \cap L^2((\mathbb{T}_N)^2)$, for a given $K \in \mathbb{Z}$. Assume we minimize $|Dw|((\mathbb{T}_N)^2)$ under the constraint $\hat{w}_{\frac{k}{N},\frac{l}{N}} = \hat{v}_{\frac{k}{N},\frac{l}{N}}$ for $(k,l) \notin \{(-K,0),(K,0)\}$. We can easily check that $(x,y) \mapsto |cos(\frac{K}{N}x)| + \alpha\, cos(\frac{K}{N}x)$ is a solution of (10.3), for every $\alpha \in [-1,1]$ (see Figure 10.1 which represents the profiles of two minima).

First of all, remark that the method cannot restore textures whose Fourier transform is located on $\mathcal{K}$. Secondly, the total variation based spectrum interpolation does not consist in interpolating the lost part of the spectrum of the image by interpolating the neighboring frequencies. Indeed, if $\hat{v}$ vanishes in the vicinity of $\mathcal{K}$, the minimum might be reached by a function whose restriction of the Fourier transform to $\mathcal{K}$ is not trivial. For instance, if $v := (x,y) \mapsto cos\, x \in BV((\mathbb{T}_N)^2) \cap L^2((\mathbb{T}_N)^2)$, and $\mathcal{K} = \{(-K,0),(K,0)\}$ where K is an odd integer larger than 1, the minimizer is $x \mapsto cos\, x - \alpha\, cos(Kx)$ where $\alpha \geq 1/K^2$ (compare the extrema). The reconstruction depends therefore on the whole spectrum of the image.

This remark shows however that the method is, in general, not very efficient in the

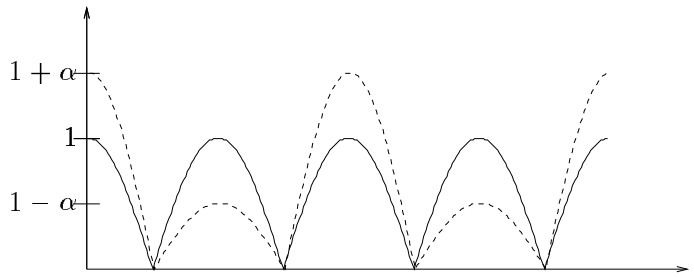

Figure 10.1: The functions $x \mapsto |cos(x)|$ (solid line) and $x \mapsto |cos(x)| + \alpha\, cos(x)$ (with $\alpha \in [-1, 1]$) have the same Total Variation.

restoration of textures. Whereas the following proposition proves that it is more powerful to restore edges.

Proposition 10.4 *If $v \in BV((\mathbb{T}_N)^2) \cap L^2((\mathbb{T}_N)^2)$ is piecewise constant and $0 \notin \mathcal{K}$, then v is the unique solution of (10.3).*

Proof. This property comes from the fact that if $w \in BV(\Omega)$ is band limited (and is therefore C^1), we have

$$|D(v+w)|((\mathbb{T}_N)^2) = |Dv|((\mathbb{T}_N)^2) + \int_{(\mathbb{T}_N)^2} |\nabla w| > |Dv|((\mathbb{T}_N)^2),$$

if $\int_{(\mathbb{T}_N)^2} |\nabla w| \neq 0$. Moreover, $0 \notin K$ ensures that if w is constant, $w \equiv 0$. □

This proposition shows to evidence the main behavior of the frequency interpolation defined by (10.3) that is its ability to reconstruct edges. We will see on experiments (see Chapter 11) that this behavior still appears in the case of the Rudin-Osher-Fatemi restoration.

Unfortunately, this proposition cannot be generalized to piecewise affine functions. For instance, in the case of functions of one variable, if $v := x \mapsto |x - x_0|\chi_{[-\pi,0]}(x) + x\, \chi_{[0,\pi]}(x)$ $(mod\ 2\pi)$ and $\mathcal{K} = \{-K, K\}$ where K is an odd integer, the minimizer is $w := x \mapsto v(x) + \alpha\, cos(Kx)$ for an $\alpha > 1/K$ (see Figures 10.2 and 10.3).

We have seen that the total variation is well suited to reconstruct edges but that it may fails in restoring textured zones. We must however moderate this remark since the textures are, in general, very different from one zone of the image to another. Therefore, we can expect that they will somehow make up for one another in order to reconstruct the initial textures. This opinion can be supported by the following 1D example.

Let N, $K \geq 1$ be two integers. We let $\mathcal{K} = \{-K, K\}$ and we define $v := x \mapsto \sum_{l=0}^{N-1} \chi_{[2\pi l, 2\pi(l+1)]}(x)\, cos(Kx + 2\pi l/N) \in BV(\mathbb{T}_N) \cap L^2(\mathbb{T}_N)$ (on v are present different

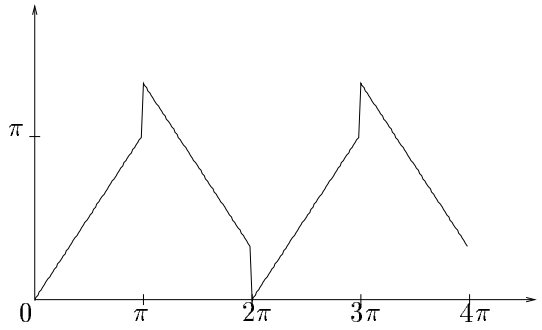

Figure 10.2: The piecewise affine function $u_\infty(x)$.

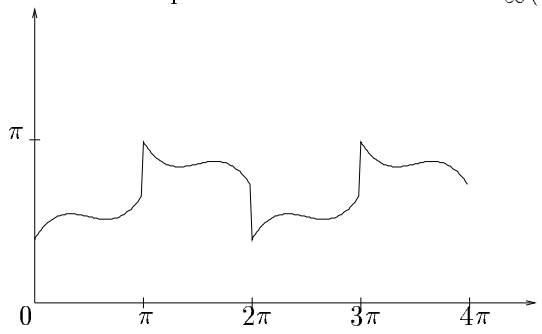

Figure 10.3: The function $u_\infty(x) + \alpha cos(x)$ with α minimizing the Total Variation.

phases of the same frequency). In such a situation, we can show that v is the solution of (10.3). Indeed, let us say it is $x \mapsto v(x) + \alpha\, cos(Kx + \varphi)$ with $\alpha, \varphi \in \mathbb{R}$. We can easily check that $x \mapsto v(x) + \alpha\, cos(Kx + \varphi + 2\pi kl/N)$ are also some minimizers for any $l \in \mathbb{Z}$. Moreover, since the set of minimizers is convex, we see that $v(x) = (1/N) \sum_{l=1}^{N} (v(x) + \alpha\, cos(kx + \varphi + 2\pi kl/N))$ is a minimizer. Then, making a reasoning similar to the one that leads to Proposition 10.2 (the derivatives of the minimizers have the same sign at almost every point of $\mathbb{T}_N$), we show that v is the only solution of (10.3).

The case $K = 1$ is the most interesting. Remark that $v - cos$ vanishes over the whole interval $(0, 2\pi)$ but the "parasitic" cosine makes the total variation increase on the complementary interval in such a way that the minimizer is v.

More generally, we can expect that, if the phases of the textures are well distributed, the reconstruction will be successful. Similar arguments can also be applied to the case when the frequencies are well-distributed.

The reasoning above does not apply to the case of images supported by a finite grid. We will however see on the following experiments that the behavior described in this section seems to make sense.

Figure 10.4: Reference Image with zones on which statistics are computed.

10.2.2 Experiments on spectrum interpolation

The experiment consists in solving (10.3) in the case when v is the image of reference displayed on Figure 10.4 (its creation process is fully described in Chapter 11 to follow) and the compact $\mathcal{K}$ is represented by the dark part of Figure 10.5.d.

The difference between the restored image and the reference is measured with the l^1 and l^2 norms. Moreover, in order to evaluate the ability of the method to restore every kind of structures, we focus the comparison on four zones which correspond to very different families of structures (see Figure 10.4). These zones are:

- The first zone represents an oscillatory texture. This structure is well localized in high frequencies. This shows the ability of the algorithm to recover highly correlated textures.

- The second zone is nearly homogeneous.

- The third zone contains a strong edge which may produce a Gibbs effects after the restoration.

- The fourth zone contains lots of sharp structures and thus does represent the quality of the sharpening.

		Degraded image	Restored image
Image	l^1	4.7	3.9
	l^2	6.5	5.7
Zone 1	l^1	3.6	4
	l^2	4.6	5.2
Zone 2	l^1	2	1.5
	l^2	2.6	2
Zone 3	l^1	3.6	2.5
	l^2	4.7	3.9
Zone 4	l^1	7	6.3
	l^2	9.2	8.5

Table 10.1: Errors between the images and the reference, on the zones defined on Figure 10.4.

Table 10.1 contains the error measurements when the "degraded image" (the one with zero at lost frequencies) and the restored one (the solution of (10.3)) are compared with the reference. Observe that all the measures are better for the restored image except the one concerning the first zone (which contains a texture). This clearly illustrates the announced behaviors.

For convenience of the display, the same experiment has also been applied on an extracted part of the initial image. The result is displayed on Figure 10.5. It focuses on the main correction brought by the restoration that is the significant reduction of Gibbs effects. Moreover, observe that the restoration retrieves some structures of the spectrum that had been lost during the degradation. This also illustrates the analysis made in Chapter 6 about cylindric functions.

10.3 Pixelization and approximation of the functional

The Achilles'heel of Rudin-Osher-Fatemi method is the well-known "stair-case" effect which, in dimension 2, is generalized by the creation of large homogeneous zones on the image (this phenomenon is also known as "pixelization"). This may have for consequence the loss of low contrast textures (see experiments of Section 10.2.2).

Let us try to explain this and report briefly the work of Nikolova on the subject. In order to simplify notations, we just look at the discrete form of the 1D Rudin-Osher-Fatemi functional

$$E(w) = \sum_{m=0}^{N-1} |w_{m+1} - w_m| + \lambda \sum_{m=0}^{N-1} |(s * w)_m - (u)_m|^2,$$

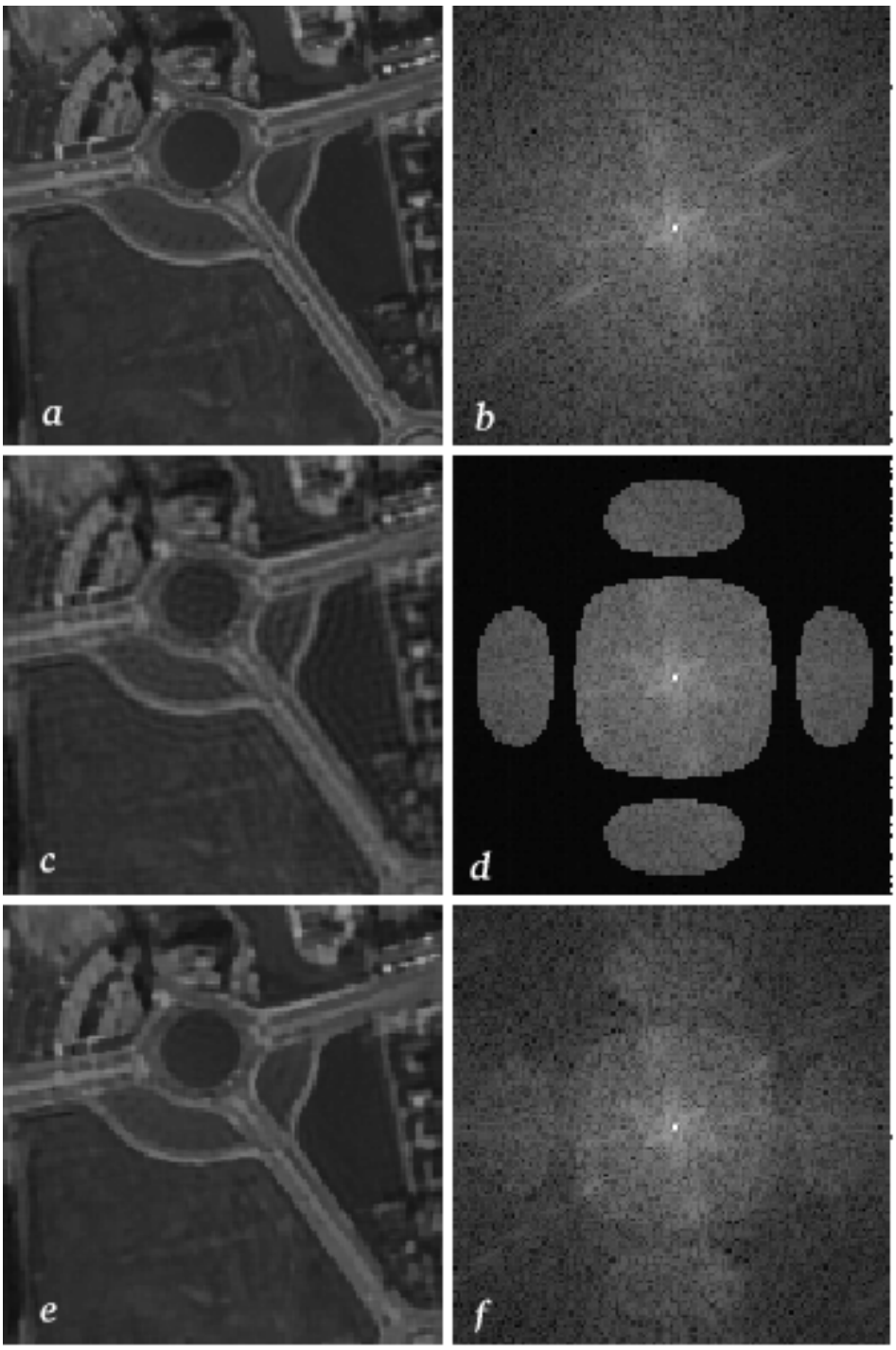

Figure 10.5: Right-Left: an aerial photograph and its spectrum. Up-Down: u; u_0 whose Fourier transform is equal to the one of u except for frequencies of $\frac{1}{N}\mathcal{K}$; and the restored image.

Nikolova showed in [37] that this effect is due to a lack of regularity at the origin of the function $x \mapsto |x|$ used to estimate $\sum_{m=0}^{N-1} |w_{m+1} - w_m|$. More precisely, this phenomenon can be explained, in the case of 1D discrete signal by the presence of a hidden soft-thresholding of the derivative of the signal.

Indeed, letting $d = Dw$ with $d_m = (Dw)_m = w_{m+1} - w_m$, and noting S the operator of convolution with s, we minimize

$$\tilde{E}(d) = \sum_{m=0}^{N-1} |d_m| + \lambda \sum_{m=0}^{N-1} |(SD^{-1}d)_m - (u)_m|^2.$$

Expressing a "Euler equation" for $\tilde{E}$, we can observe that the minimum d satisfies

$$d_m = 0 \text{ when } |2(SD^{-1})_m^T.(SD^{-1}d - u)| < \frac{1}{\lambda},$$

and we shall have, otherwise

$$2(SD^{-1})_m^T.(SD^{-1}d - u) = -\frac{sign(d_m)}{\lambda},$$

where $(SD^{-1})_m^T$ is the m^{th} column of SD^{-1}. In the particular case when $S = D$, the soft-thresholding appears very clearly

$$\begin{cases} d_m = 0 & \text{when } |u_m| < \frac{1}{2\lambda} \\ d_m = u_m - \frac{1}{2\lambda} sign(u_m) & \text{otherwise} \end{cases}$$

Nikolova's remark suggests us to smooth the functional. Several variations have been made on the model. One of the most standard is the following.

$$\text{Minimize } E_\beta(w) = \int \varphi_\beta(|\nabla w|) + \lambda \sum_{m,n=0}^{N-1} |(s * w)_{m,n} - (u)_{m,n}|^2$$

where φ_β is a regular approximation of the absolute value function as, for example, $\varphi_\beta(t) = \sqrt{\beta + t^2}$. This method will provide us with a better restitution of the low contrast textures and an image with less pixelization but it has the drawback to diffuse the gray levels on the surface of the image when the gradient is small. Nevertheless it is a good approximation of the original model for β small (see [1]).

10.4 Numerical implementation

We are now going to describe the algorithm we have used in order to do the experiments. Assume we have an image u, defined on $\{0, ..., N-1\}^2$, and a convolution kernel s whose Fourier transform is known over $\{-\frac{KN}{2}+1, ..., \frac{KN}{2}\}$, for a given $K \geq 1$. For $K' \geq K$ and $\lambda \in \mathbb{R}$, we would like to minimize among $w \in \mathbb{B}_K$ (see (10.2))

$$E_\beta(w) = \sum_{m,n=0}^{K'N-1} \varphi_\beta\Big(|\nabla w(\frac{m}{K'}, \frac{n}{K'})|\Big) + \lambda \sum_{\xi,\eta=-\frac{N}{2}+1}^{\frac{N}{2}} \left| \left(\sum_{(k,l)\in A_\xi \times A_\eta} \hat{s}_{\xi+kN,\eta+lN}\ \hat{u}_{\xi+kN,\eta+lN} \right) - \hat{u}_{\xi,\eta} \right|^2,$$

where A_ξ denotes the set of "aliased frequencies" that is

$$A_\xi = \left\{ k \in \mathbb{Z}, \xi + kN \in \{-\frac{KN}{2}+1, ..., \frac{KN}{2}\} \right\}.$$

Note that in order to estimate $\nabla w(\frac{m}{K'}, \frac{n}{K'})$ in a faithful way, with regard to the model describe in Section 10.1, we should compute (for instance, for the derivative with respect to the first variable)

$$\frac{\partial w}{\partial x}(\frac{m}{K'}, \frac{n}{K'}) = \left(2i\pi \frac{k}{N} \widehat{w}(\frac{k}{N}, \frac{l}{N}) \right)^\vee (\frac{m}{K'}, \frac{n}{K'})$$

where $^\vee$ denotes the inverse Fourier transform and $(m, n) \in \{0, ..., K'N-1\}^2$.

However, in order to gain in computational complexity, we have approximated the estimation of ∇w by finite differences. This leads us to struggle against the lack of isotropy of the gradient. The total variation will therefore be approximated by the sum of four terms corresponding to four different directions of the gradient.

We use the notations:

1. $x_m = mh$, $y_n = nh$, for $m, n = 0, 1, \cdots, K'N$ and $h = \frac{1}{K'}$;

2. $u_{m,n} = u(x_m, y_n)$;

3. $\Delta^x_+ u_{m,n} = u_{m+1,n} - u_{m,n}$ and $\Delta^x_- u_{m,n} = u_{m,n} - u_{m-1,n}$;

4. $\Delta^y_+ u_{m,n} = u_{m,n+1} - u_{m,n}$ and $\Delta^y_- u_{m,n} = u_{m,n} - u_{m,n-1}$.

The function E_β is calculated as follows.

$$\begin{aligned} 4E_\beta(u) &= \sum_{m,n=0}^{N-1} \left(\varphi_\beta\Big(\sqrt{(\Delta_+^x u_{m,n})^2 + (\Delta_+^y u_{m,n})^2}\Big) + \varphi_\beta\Big(\sqrt{(\Delta_-^x u_{m,n})^2 + (\Delta_+^y u_{m,n})^2}\Big) \right. \\ &\quad \left. + \varphi_\beta\Big(\sqrt{(\Delta_+^x u_{m,n})^2 + (\Delta_-^y u_{m,n})^2}\Big) + \varphi_\beta\Big(\sqrt{(\Delta_-^x u_{m,n})^2 + (\Delta_-^y u_{m,n})^2}\Big) \right) \\ &\quad + 4\,\lambda \sum_{\xi,\eta=-\frac{N}{2}+1}^{\frac{N}{2}} \left| \left(\sum_{(k,l)\in A_\xi \times A_\eta} \hat{s}_{\xi+kN,\eta+lN}\ \hat{u}_{\xi+kN,\eta+lN} \right) - \hat{u}_{\xi,\eta} \right|^2, \end{aligned}$$

taking $\Delta_+^x u_{m,n}$, $\Delta_-^x u_{m,n}$, $\Delta_+^y u_{m,n}$, $\Delta_-^y u_{m,n}$ equal to 0 on the edges of the image, when this is necessary.

This functional is minimized with a gradient descent algorithm. We start from u^0 the "sinc interpolation" of the blurred image (we extend its spectrum, with null frequencies, out of $\{-\frac{N}{2}+1, ..., \frac{N}{2}\}^2$). To get u^{j+1} from u^j, the gradient of the function E_β at u^j, $\nabla E_\beta(u^j)$, is calculated. $\nabla E_\beta(u^j)$ is then orthogonally projected in such a way that it keeps unchanged the frequencies out of $\{-\frac{KN}{2}+1, ..., \frac{KN}{2}\}^2$ (by letting $\widehat{\nabla E_\beta(u^j)}(\frac{k}{N}, \frac{l}{N}) = 0$ for $(k,l) \notin \{-\frac{KN}{2}+1, ..., \frac{KN}{2}\}^2$). Noting $\widetilde{\nabla E}_\beta(u^j)$ the result of the projection, the optimal amplitude of the variation of the image in the direction $-\widetilde{\nabla E}_\beta(u^j)$ is then estimated by the resolution of

$$\min_{s>0} E_\beta(u^j - s\ \widetilde{\nabla E}_\beta(u^j))$$

using a dichotomy method. Once the optimal amplitude s_0 is calculated, we let

$$u_{j+1} = u^j - s_0\ \widetilde{\nabla E}_\beta(u^j)\,,$$

and the process is iterated.

Note that when $\hat{s}_{k,l} = 0$ for $(k,l) \in \{-\frac{KN}{2}+1, ..., \frac{KN}{2}\}^2 \setminus \{-\frac{N}{2}+1, ..., \frac{N}{2}\}^2$ (s satisfies the assumption of Proposition 10.3) the data fidelity term can equivalently be expressed under the form

$$\sum_{k,l=-\frac{KN}{2}+1}^{\frac{KN}{2}} |\hat{s}_{k,l}\ \hat{u}_{k,l} - \hat{u}_{k,l}|^2\,.$$

In such a case, the algorithm is known to converge (see [11]). The reader can refer to T. Chan (at UCLA) for a general study on the minimization of Rudin-Osher-Fatemi functional.

Note that in order to speed the convergence up, we can start from a deblurred version

of u instead of u. Moreover, it is better to start with a large β and let it decrease to 0.

Chapter 11

Numerical results and comparison

The experiments have been split into two sections. The first one only contains images deblurring without oversampling. It is the result of an evaluation, which has been made with the CNES, between FCNR and Rudin-Osher-Fatemi method. This leads to the conclusion that the FCNR is better suited for cases where the convolution kernel does not cancel inside $\{-\frac{N}{2}+1, ..., \frac{N}{2}\}$ (because of its ability to have natural looking results), while the Rudin-Osher-Fatemi method is better suited for the opposite case (because of its ability to interpolate lost frequencies).

The second part shows that Rudin-Osher-Fatemi method can be used to deconvolve and oversample images at the same time. This can provide a way to remove aliasing from an image. However, such a method only applies to cases where the noise is very low.

11.1 Image deblurring without oversampling

11.1.1 The experiment description

In order to compare the two methods described above they have been put in competition in a very practical situation that is the restoration of satellite SPOT images. We will, moreover, consider two models of degradations which correspond to two different satellites: SPOT 5 and a specific mode of SPOT 1.

Moreover, to compare the restored images quantitatively and objectively, we have to measure them in front of a reference. For that reason, the blurred images have been re-created artificially from an airplane image. However, in order to take into account the whole degradation suffered by the images (including aliasing, even if it is small), the airplane image must be oversampled. Consequently, the restored images cannot be compared directly with the sharp image since they have not the same scale of sampling. The reference image has therefore been constructed from the oversampled image by convolving it with a prolate function (see [28]) and afterwards making a subsampling. The obtained reference has an optimal resolution without aliasing. This is the best image we can expect

Figure 11.1: Reference Image with the zones on which statistics are computed.

to obtain from the degraded ones.

The difference between the restored images and the reference is measured with the l^1 and l^2 norms. Moreover, in order to evaluate the ability of each method to restore every kind of structure, we also focus the comparison on four zones which correspond to very different families of structures (see Figure 11.1).

- The first zone represents an oscillatory texture. This structure is well localized in high frequency. It gives information about the quality of the high frequency recovery. Moreover, this shows the ability of the algorithm to recover highly correlated textures.
- The second zone is nearly homogeneous. It permits to measure the ability of the method to remove noise.
- The third zone contains a strong edge which may produce Gibbs effect after the restoration.
- The fourth zone contains lots of sharp structures and thus does represent the quality of the sharpening.

In order to illustrate the difficulty to restore blurred and noisy images, a Wiener filter has also been applied on the images (see (8.3) or [4]). We have tried to fix the parameter of

the filter (more properly, the assumed variance of the noise) such that the restored images have about the same quantity of noise in the homogeneous regions as the ones obtained by the other methods[1].

As we said in the beginning of this section, we consider two models of degradations which correspond to two different satellites: SPOT 5 and a specific mode of SPOT 1. In both cases, the Fourier transform of the impulse response s is almost supported by $\{-\frac{N}{2}+1, ..., \frac{N}{2}\}^2$ (we only give their form inside $\{-\frac{N}{2}+1, ..., \frac{N}{2}\}^2$). Moreover, the noise is approximated by a Gaussian noise[2]. The standard deviation of this Gaussian noise is, in both cases, realistic and gives rise to the same difficulty as the real noise.

- The convolution kernel of the first model is given, for $(k,l) \in \{-\frac{N}{2}+1, ..., \frac{N}{2}\}^2$, by

$$\widehat{s^1}_{k,l} = e^{-2\gamma_k|\frac{k}{N}|-2\gamma_l|\frac{l}{N}|}\left(\frac{sin(2\pi\frac{k}{N})}{2\pi\frac{k}{N}}\right)\left(\frac{sin(2\pi\frac{l}{N})}{2\pi\frac{l}{N}}\right)\left(\frac{sin(\pi\frac{l}{N})}{\pi\frac{l}{N}}\right),$$

  where $\gamma_k = 1.505$, $\gamma_l = 1.412$ and the standard deviation of the noise $\sigma_1 = 2.4$ (see Figure 11.2).

- The convolution kernel of the second model is given, for $(k,l) \in \{-\frac{N}{2}+1, ..., \frac{N}{2}\}^2$, by

$$\widehat{s^2}_{k,l} = e^{-2\gamma_k|\frac{k}{N}|-2\gamma_l|\frac{l}{N}|}\left(\frac{sin(4\pi\frac{k}{N})}{4\pi\frac{k}{N}}\right)\left(\frac{sin(4\pi\frac{l}{N})}{4\pi\frac{l}{N}}\right),$$

  for the same values for γ_k and γ_l. The standard deviation of the noise is $\sigma_2 = 0.5$ (see Figure 11.3).

Remark that the main difference between the two models of degradation is that the Fourier transform of the second convolution kernel s^2 vanishes inside $\{-\frac{N}{2}+1, ..., \frac{N}{2}\}^2$, while the one of s^1 does not. We can therefore expect to obtain better results, in the case of the second degradation model, with the variational method that will interpolate the spectrum of the image where $\widehat{s^2}$ vanishes (in practice the bared zones on Figure 11.3).

The "artificial" images corresponding to the two models of degradation above are respectively called Blurred Image 1 and Blurred Image 2.

[1]Unfortunately, for the restoration of Blurred Image 1 (see the description of the degradation model to follow), we could not reach that goal without loosing all the details of the image. So we have chosen a parameter yielding acceptable result (in spite of the remaining noise).

[2]The real noise is the sum of three noises having different structures

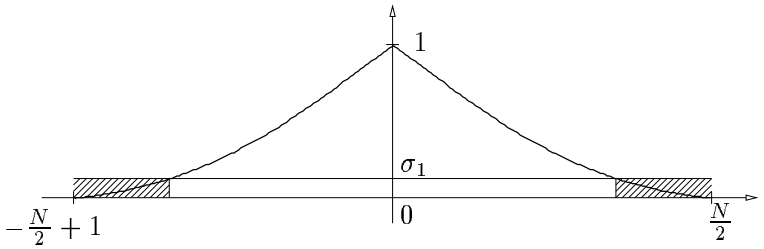

Figure 11.2: Profile of the convolution kernel spectrum $\widehat{s^1}$ (for convenience, σ_1 is not at the real scale).

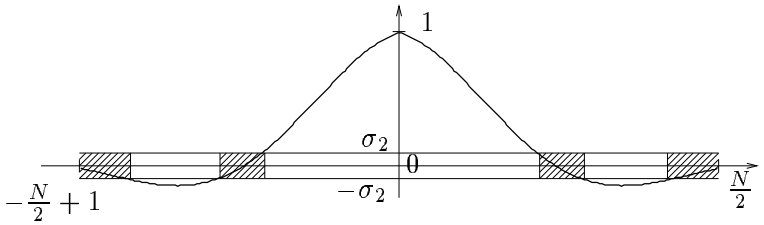

Figure 11.3: Profile of the convolution kernel spectrum $\widehat{s^2}$ (σ_2 is not at the real scale).

11.1.2 Results

The statistics are split into two tables. The first one sums-up the results obtained by the three methods, for Blurred Image 1 (see Table 11.1), and the second one, for Blurred Image 2 (see Table 11.2). However, we have to keep in mind that neither the FCNR nor the variational methods aim at minimizing these errors (the FCNR controls the structure of the noise, and the variational method controls the regularity of the image). Let us indicate also that the parameters of these methods has not been fixed with regard to these statistics but on visual criterion.

Looking at Table 11.1, note that the FCNR and the variational method yield, on the whole, comparable statistics while the results are much worse, on any region, for the Wiener filter. Looking at the different zones in detail, we observe that the FCNR is more efficient than the variational method on Zones 1 and 2 and less on Zones 3 and 4, which confirms the fact that the Total Variation penalizes textures but preserves strong edges (it does not generate Gibbs effects in their vicinity).

If we look now at Table 11.2, the wavelet-packets based algorithm and the Wiener filter yield poor results. The Fourier transform of the convolution kernel used to obtain Blurred Image 2 cancels on "intermediate" frequencies, so that it leaves the framework in which these methods are accurate.

These comments are confirmed when we look at the images. The "ideal" one is represented on Figure 11.1. This is the image we would like to reach while starting from the blurred images of Figure 11.4. Looking at this, we can figure out the complexity of this issue since lots of details seems to be definitely lost, especially for Blurred Image 2.

		Wiener filter	Invertible FCNR	Variational method
Image	l^1	4.44	4	3.66
	l^2	6.54	5.56	5.57
Zone 1	l^1	5.92	4.29	5.56
	l^2	7.3	5.39	6.86
Zone 2	l^1	2.82	1.82	1.87
	l^2	3.46	2.34	2.4
Zone 3	l^1	3.53	3.10	2.77
	l^2	4.51	3.89	3.81
Zone 4	l^1	5.15	4.99	4.47
	l^2	6.66	6.67	6.01

Table 11.1: Statistics for the restorations of Blurred Image 1.

However, thanks to the low noise level, some of these details will be recovered, without creating artifact or noise enhancement.

The restored images are represented on Figures 11.5, 11.6 and 11.7. The Wiener restoration yields noise that we cannot remove without loosing a lot of information, but the results are reasonably sharp. Wavelet-packets based method is very successful with Blurred Image 1, the restored images looking like being free of any noise and with a good sharpness. Moreover, note that the main advantage of the method is that the result (in the case of Blurred Image 1) looks almost like being a natural image. On the other hand, in the case of the Blurred Image 2, the result is still very blurred and present Gibbs effects. At last, the Total Variation based method yields good result in both cases, but it tends to remove the texture of Zone 1, and to create homogeneous zones. It is the sole of the four methods which does not create any Gibbs effect when deblurring the second image. All these remarks are confirmed on the blow-ups of Figures 11.8 and 11.9.

11.2 Image deblurring with oversampling

We are now going to compare the Rudin-Osher-Fatemi variational method when it includes oversampling and oversampled versions (using sinc interpolation or duplications) of the classical Rudin-Osher-Fatemi method (without oversampling).

We display on Figures 11.10 and 11.11 oversampled version (using sinc-interpolation) of the restored image using Rudin-Osher-Fatemi method without oversampling and a Rudin-Osher-Fatemi including oversampling, both in the case Blurred Image 1 (see Section 11.1.1). We see (on the road of Figure 11.10) that the Rudin-Osher-Fatemi method, when it includes oversampling, remove the aliasing (the parasitic oscillations). However, due to

		Wiener filter	Invertible FCNR	Variational method
Image	l^1	5.08	6.72	4.14
	l^2	7.38	9.31	5.8
Zone 1	l^1	5.79	6.08	4.64
	l^2	7.04	7.47	5.87
Zone 2	l^1	2	2.42	2
	l^2	2.56	3.16	2.62
Zone 3	l^1	4.27	7.01	2.92
	l^2	5.6	8.24	4.21
Zone 4	l^1	7.51	7.83	5.65
	l^2	10.21	10.48	7.59

Table 11.2: Statistics for the restorations of Blurred Image 2.

the noise level contained in the blurred image, we see a kind of "low frequency" remaining noise (the huge oscillations in the homogeneous zones) that makes the method badly adapted [3].

We present on Figures 11.12 and 11.13 the same restoration/oversampling methods as previously but in a more realistic case that is the case of the convolution kernel s^1 (see Section 11.1.1) with Gaussian noise of standard deviation 0.5. This clearly shows the ability of the Rudin-Osher-Fatemi method, that includes oversampling, to improve the restoration of edges by removing the initial aliasing.

At last, Figure 11.14 presents an experiment, using the convolution kernel s^1 (see Section 11.1.1) with Gaussian noise of standard deviation 1. We display the blurred image, the restoration using Rudin-Osher-Fatemi method with oversampling and two oversampling (a duplication and a sinc-interpolation) of the results of the Rudin-Osher-Fatemi method without oversampling. We can do, about this experiments, the same conclusion as the one done on the oversampling problem presented in chapter 7. This shows (at least for numerical reasons) that if one want to deconvolve and oversample an image it is better to make both operations at the same time.

[3] Remark that the problem of oversampling such images is quiet unrealistic due to the very low available information

Figure 11.4: Degraded images. Up-Down: Blurred Image 1 and Blurred Image 2.

Figure 11.5: Restoration with a Wiener filter (Up-Down: of Blurred Image 1 and Blurred Image 2).

Figure 11.6: Restoration with the FCNR (Up-Down: of Blurred Image 1 and Blurred Image 2).

Figure 11.7: Restoration with the Rudin-Osher-Fatemi method (Up-Down: of Blurred Image 1 and Blurred Image 2).

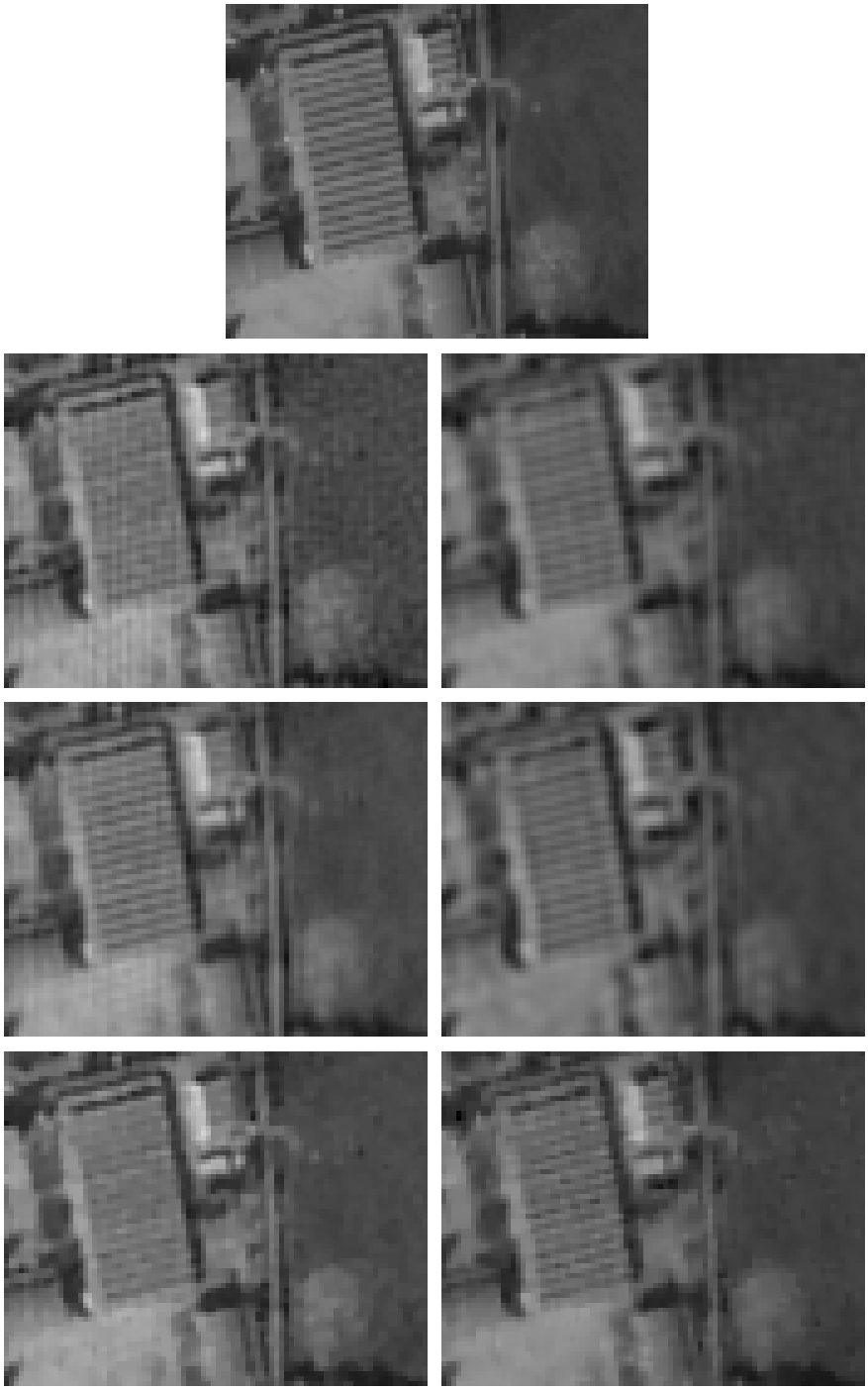

Figure 11.8: Top: Reference Image. Left-Right: restoration of respectively Blurred Images 1 and 2. Up-Down: with a Wiener filter, with the FCNR, with the Rudin-Osher-Fatemi method.

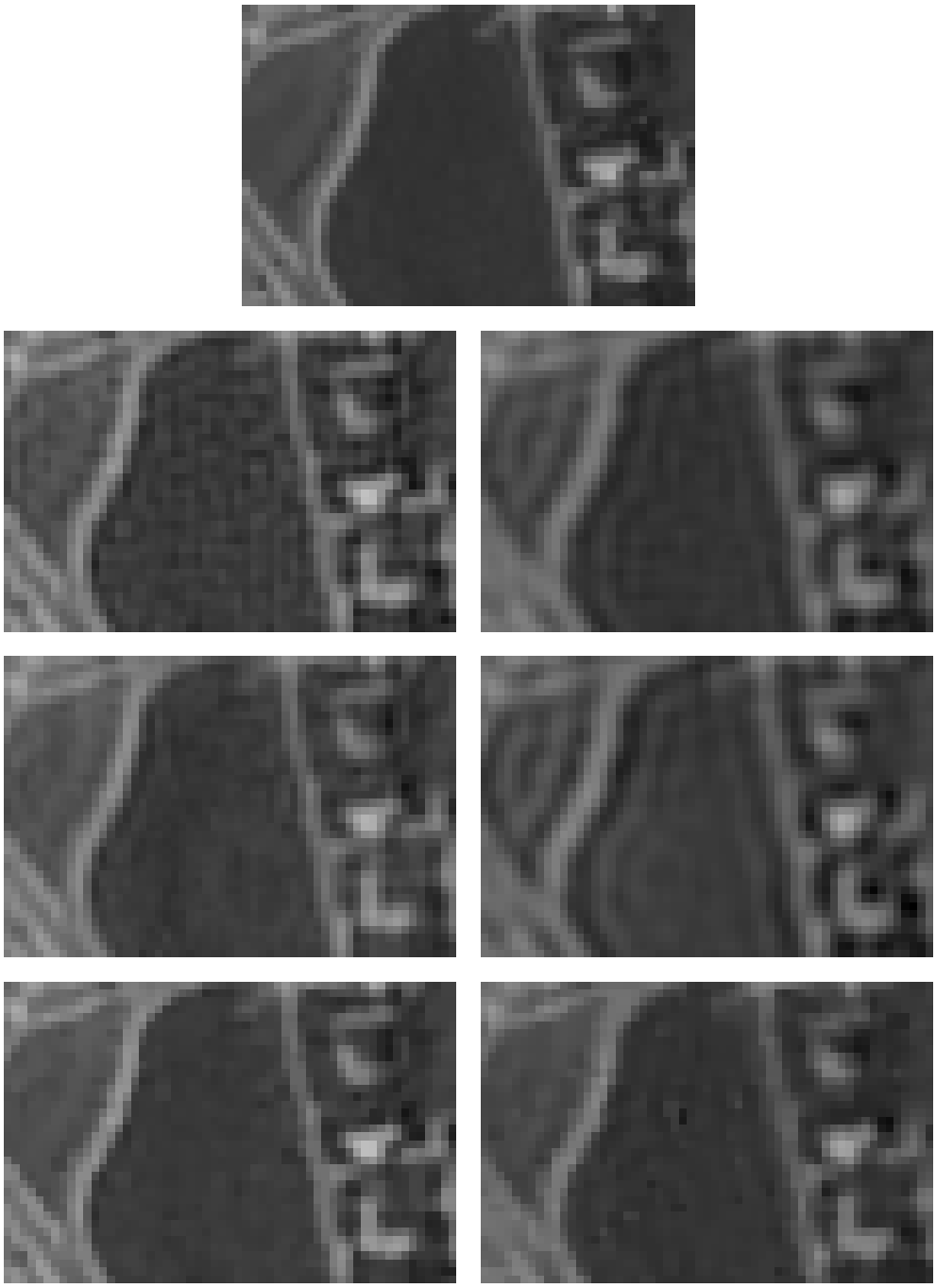

Figure 11.9: Top: Reference Image. Left-Right: restoration of respectively Blurred Images 1 and 2. Up-Down: with a Wiener filter, with the FCNR, with the Rudin-Osher-Fatemi method.

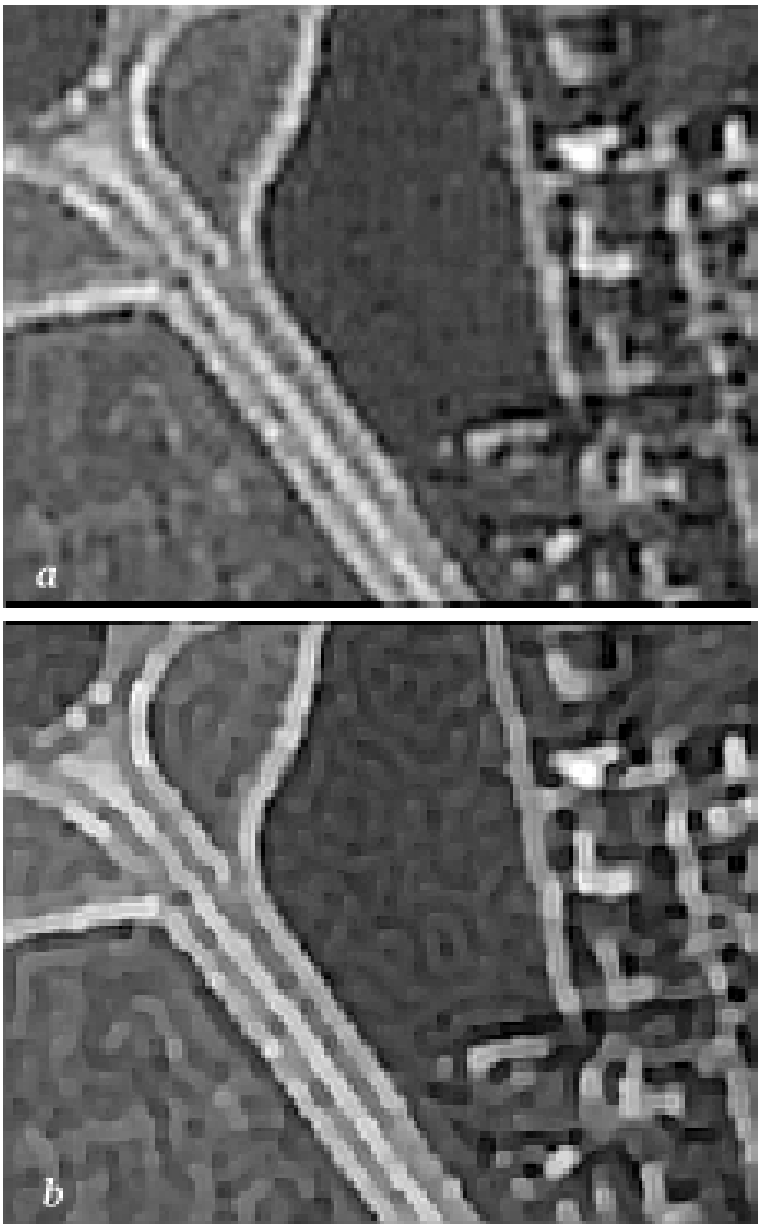

Figure 11.10: Both images have been sharpened.
a: Restoration using Rudin-Osher-Fatemi method on which is applied a sinc interpolation.
b: Restoration using the ability of Rudin-Osher-Fatemi method to oversample images.

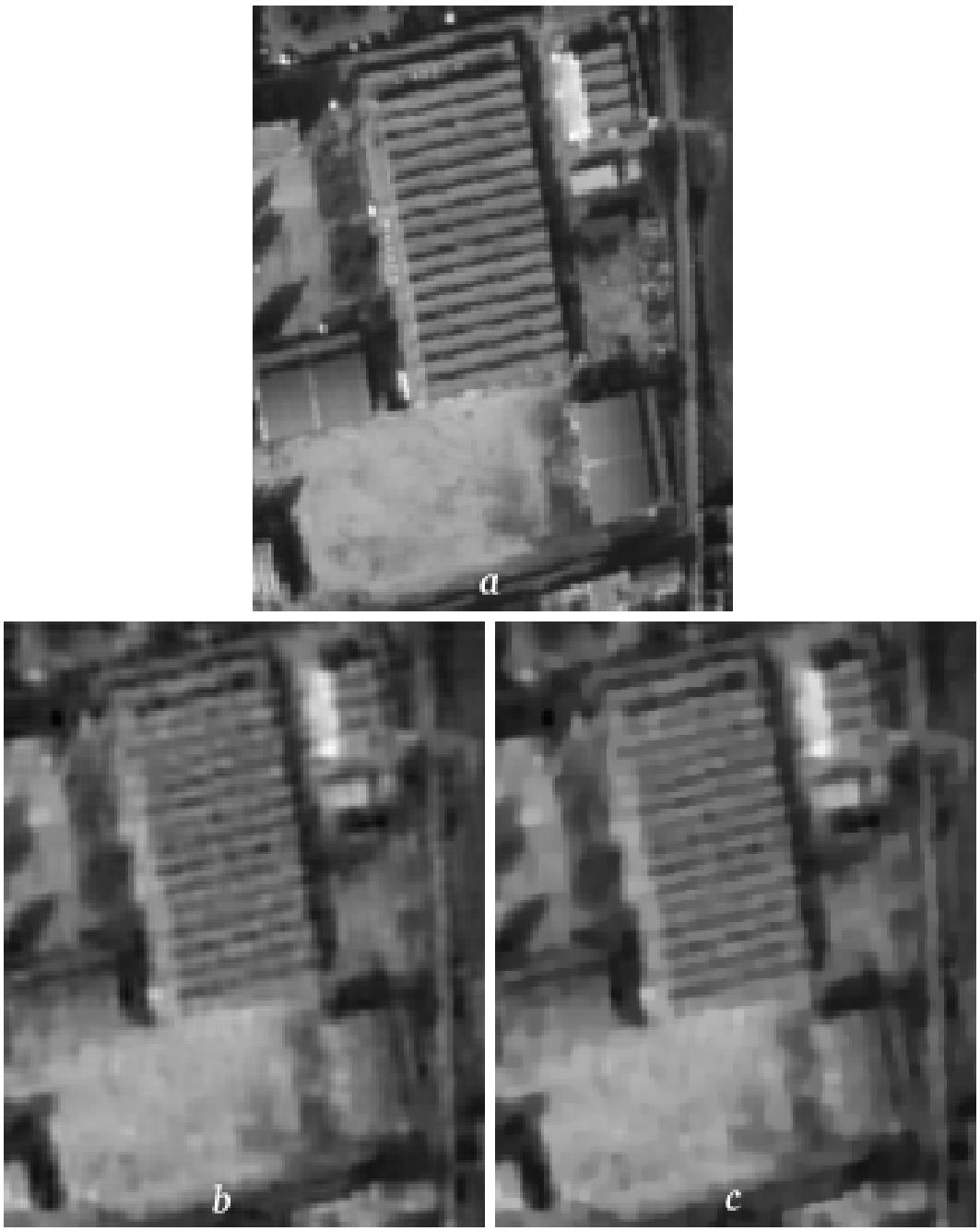

Figure 11.11: a: Reference image (adapted to this sampling grid).
b: Restoration using Rudin-Osher-Fatemi method on which is applied a sinc interpolation.
c: Restoration using the ability of Rudin-Osher-Fatemi method to oversample images.

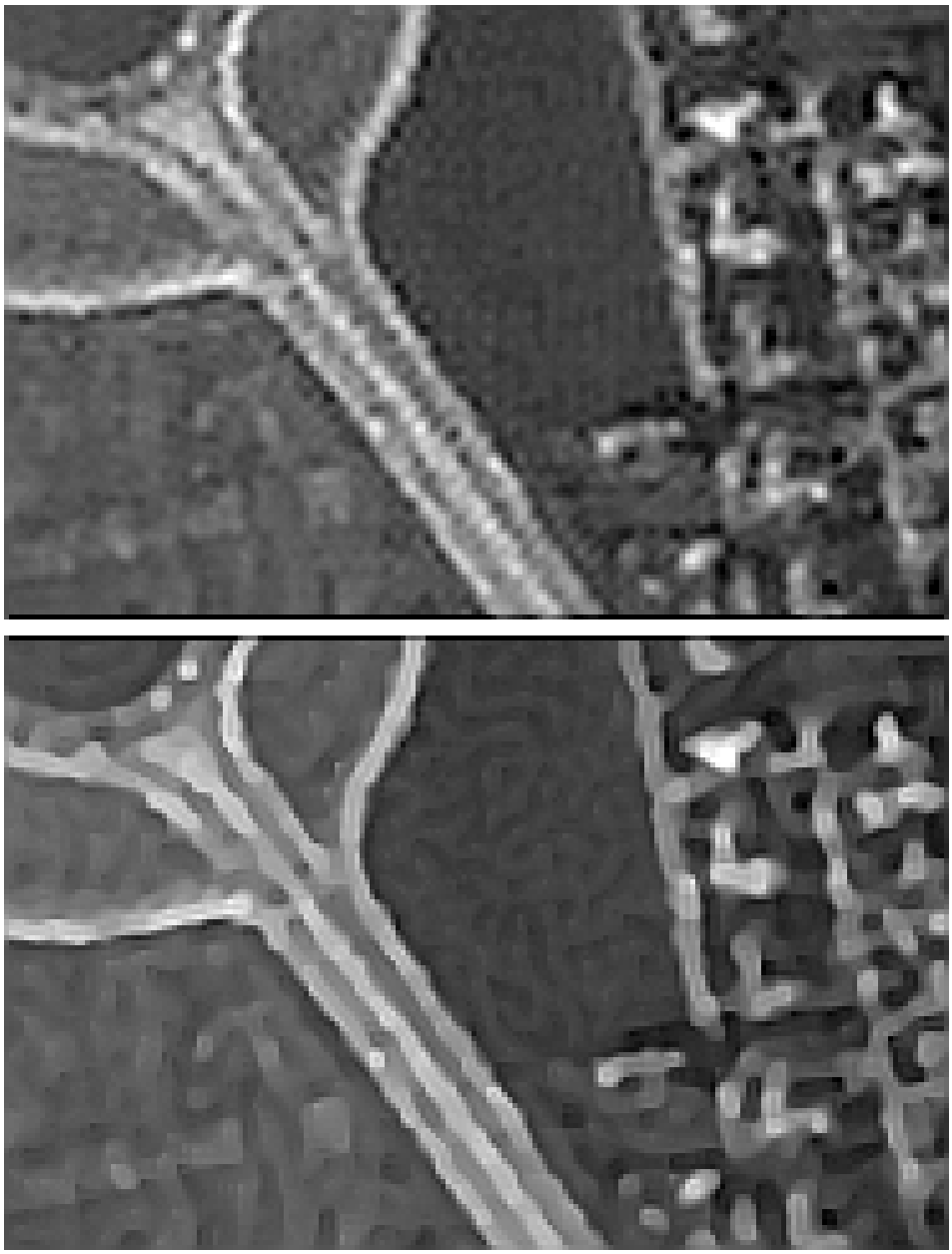

Figure 11.12: Both images have been sharpened.
Up: sinc-interpolation of a restoration using Rudin-Osher-Fatemi method (without image oversampling). Down: a restoration which uses the ability of Rudin-Osher-Fatemi functional to oversample images.

Figure 11.13: Up: sinc-interpolation of a restoration using Rudin-Osher-Fatemi method (without image oversampling). Down: a restoration which uses the ability of Rudin-Osher-Fatemi functional to oversample images.

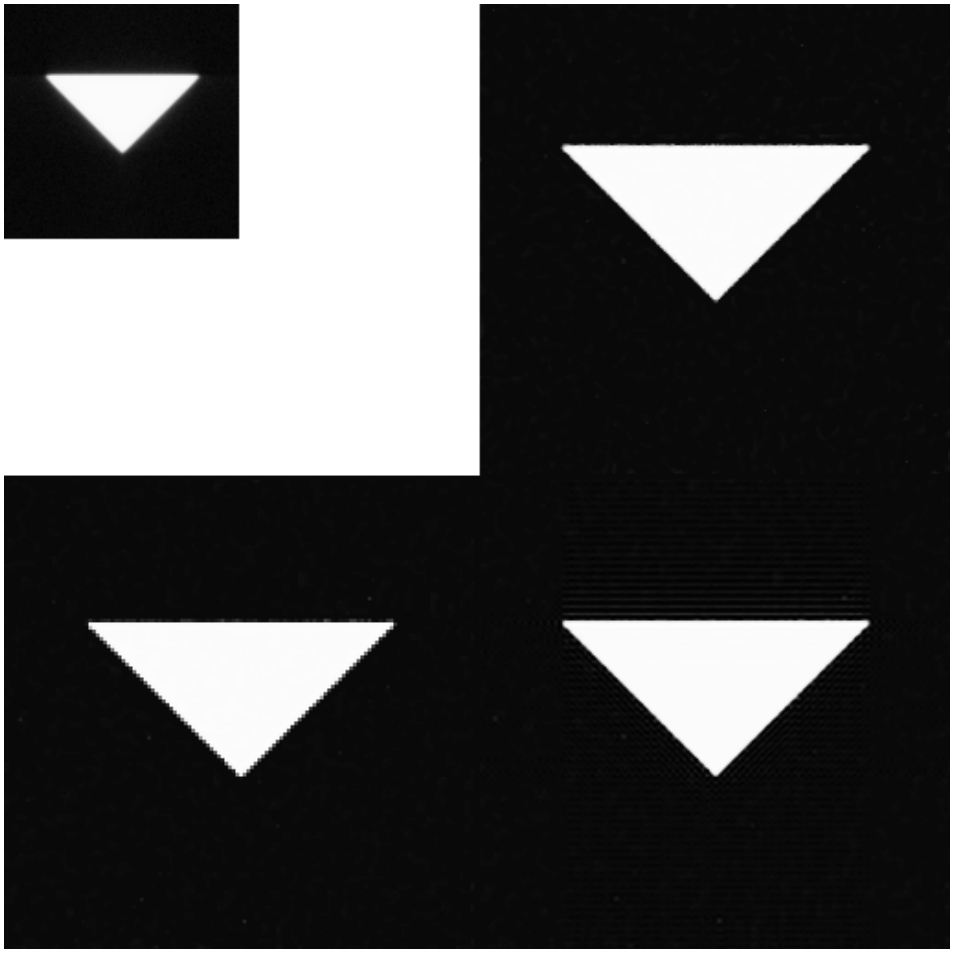

Figure 11.14: Up-Left: the blurred and noisy small image Up-Right: a restoration which uses the ability of Rudin-Osher-Fatemi functional to oversample images. Down-Left: duplication interpolation of a Rudin-Osher-Fatemi restoration (without image oversampling). Down-Right: sinc-interpolation of a Rudin-Osher-Fatemi restoration (without image oversampling).

Appendix A

Fourier transforms

We will distinguish, in the following, two kinds of spectral representations depending on whether the function is defined over the torus of size N, $(N\mathbb{T})^2$ or a finite grid $\{0, ...N-1\}^2$. For commodity, we denote $(N\mathbb{T})^2$ by $(\mathbb{T}_N)^2$.

Definition A.1 (Fourier transforms) *We define*

- *the Fourier series of a function $w \in L^2((\mathbb{T}_N)^2)$, by*

$$\hat{w}_{\frac{k}{N},\frac{l}{N}} = \int_{(\mathbb{T}_N)^2} w(x,y)\, e^{-2i\pi\frac{(kx+ly)}{N}}\,,$$

  for $(k,\, l) \in \mathbb{Z}^2$.

- *the Discrete Fourier Transform (DFT) of $w \in \mathbb{R}^{\mathbb{N}^2}$, for N even, by*

$$\hat{w}_{k,\,l} = \sum_{m,n=0}^{N-1} w_{m,n}\, e^{-2i\pi\frac{km+ln}{N}}\,,$$

  for $(k,\, l) \in \{-\frac{N}{2}+1, ..., \frac{N}{2}\}^2$.

These two transformations are invertible and we have

Proposition A.1 (Inverse Fourier transforms) *The Fourier transforms are invertible. Moreover, the inverse of the*

- *Fourier series is given, for any $w \in L^2((\mathbb{T}_N)^2)$, by*

$$w(x,y) = \frac{1}{N^2} \sum_{(k,\,l)\in\mathbb{Z}^2} \hat{w}_{\frac{k}{N},\frac{l}{N}}\, e^{2i\pi\frac{(kx+ly)}{N}}\,,$$

  for $(x, y) \in (\mathbb{T}_N)^2$.

– *Discrete Fourier Transform is given, for any* $w \in \mathbb{R}^{\mathbb{N}^2}$, *by*

$$w_{m,n} = \frac{1}{N^2} \sum_{k,\, l=-\frac{N}{2}+1}^{\frac{N}{2}} \hat{w}_{k,\, l}\, e^{2i\pi \frac{km+ln}{N}} ,$$

for $(k,\, l) \in \{-\frac{N}{2}+1, ..., \frac{N}{2}\}^2$.

Moreover, we have the Parseval formulas.

Proposition A.2 (Parseval) – *Let* v *and* w *be in* $L^2((\mathbb{T}_N)^2)$, *we have*

$$\int_{(\mathbb{T}_N)^2} w(x,y)\overline{v(x,y)}dxdy = \frac{1}{N^2} \sum_{(k,\, l)\in\mathbb{Z}^2} \hat{w}_{\frac{k}{N},\frac{l}{N}}\, \overline{\hat{v}_{\frac{k}{N},\frac{l}{N}}} ,$$

– *Let* v *and* w *be in* $\mathbb{R}^{\mathbb{N}^2}$, *we have*

$$\sum_{m,n=0}^{N-1} w_{m,n}\overline{v_{m,n}} = \frac{1}{N^2} \sum_{k,\, l=-\frac{N}{2}+1}^{\frac{N}{2}} \hat{w}_{k,\, l}\overline{\hat{v}_{k,\, l}} ,$$

where $\overline{z}$ *denotes the complex conjugate of* $z \in \mathbb{C}$.

Remark that, these formulas, when letting $v = w$, guarantee

$$\|w\|_2 = \frac{1}{N^2} \|\hat{w}\|_2 ,$$

for any w in either $L^2((\mathbb{T}_N)^2)$ or $\mathbb{R}^{\mathbb{N}^2}$.

If we define the convolution operators by

$$v * w(x,y) = \int_{(\mathbb{T}_N)^2} w(x-x', y-y')\, v(x',y')dx'dy'$$

for $(v,w) \in L^2((\mathbb{T}_N)^2)^2$, and

$$(v*w)_{m,n} = \sum_{m',n'=0}^{N-1} w_{m-m',n-n'}\, v_{m',n'}$$

for $(v,w) \in \mathbb{R}^{\mathbb{N}^2}$ (v and w are assumed N-periodic), we have the convolution theorem.

Proposition A.3 (convolution) – *Let* v *and* w *be in* $L^2((\mathbb{T}_N)^2)$, *we have*

$$\widehat{(v*w)}_{\frac{k}{N},\frac{l}{N}} = \hat{w}_{\frac{k}{N},\frac{l}{N}}\, \hat{v}_{\frac{k}{N},\frac{l}{N}} ,$$

for any $(k,\, l) \in \mathbb{Z}^2$.

– *Let* v *and* w *be in* $\mathbb{R}^{\mathbb{N}^2}$, *we have*

$$\widehat{(v * w)}_{k,\,l} = \hat{w}_{k,\,l}\, \hat{v}_{k,\,l}\,,$$

for $(k,\, l) \in \{-\frac{N}{2}+1, ..., \frac{N}{2}\}^2$.

We also have some basic properties, such as

– translation[1]: For any $w \in L^2((\mathbb{T}_N)^2)$, noting $\tau_{(x_0,y_0)}(w)(x,y) = w(x-x_0, y-y_0)$, we have

$$\widehat{\left(\tau_{(x_0,y_0)}(w)\right)}_{\frac{k}{N},\frac{l}{N}} = e^{-2i\pi\,\frac{kx_0+ly_0}{N}}\, \hat{w}_{\frac{k}{N},\frac{l}{N}}\,.$$

– derivatives: For any $p \in \mathbb{N}$, and any $w \in C^p((\mathbb{T}_N)^2)$, and $q \le p$

$$\widehat{\left(\frac{\partial^p w}{\partial x^q \partial y^{p-q}}\right)}_{\frac{k}{N},\frac{l}{N}} = \frac{(2i\pi)^p\, k^q\, l^{p-q}}{N^p}\, \hat{w}_{\frac{k}{N},\frac{l}{N}}\,.$$

Remark that the resemblance between the Fourier transforms and their inverse permits to state some properties similar to the above ones in the case of the concerning convolutions of Fourier transforms, or translations of Fourier transforms (in such a case, the translation is integer-wise).

[1] a similar statement can be done for the Discrete Fourier Transform

Bibliography

[1] R. Acart and C. Vogel. Analysis of bounded variation methods for ill-posed problems. *Inverse problems*, 10:1217–1229, 1994.

[2] J. Allebach and P. W. Wong. Edge-directed interpolation. In *Proceedings of the International Conference on Image Processing*, volume 3, pages 707–710, 1996.

[3] L. Ambrosio, N. Fusco, and D. Pallara. Functions of bounded variation and free discontinuity problems, 1998. Notes de cours du centre Émile Borel.

[4] H.C. Andrews and B.R. Hunt. *Digital signal processing.* Technical Englewood Cliffs, NJ: Prentice-Hall, 1977.

[5] S.M. Berman. Sojournes and extremes os stochastic processes. *Wadsworth, Reading, MA*, 1989.

[6] Bony. Distribution et transformation de fourier. Notes de cours de l'ecole polytechnique.

[7] V. Caselles, J. L. Lisani, J. M. Morel, and G. Sapiro. Shape preserving local histogram modification. *IEEE Transactions on Image Processing*, 8(2), February 1999.

[8] A. Chambolle and P.L. Lions. Restauration de données par minimisation de la variation total et variantes d'ordre supérieur. In *Procedings of GRETSI*, September 1995.

[9] A. Chambolle, R.A. De Vore, N. Lee, and B.J. Lucier. Nonlinear wavelet image processing: Variational problems, compression and noise removal through wavelet shrinkage. Technical report, CEREMADE, 1998. short version in: IEEE Trans. Image Processing, Vol. 7, No. 3, pp. 319-335, 1998.

[10] Antonin Chambolle and Pierre-Louis Lions. Image recovery via total variation minimization and related problems. *Numer. Math. 76, No.2. [ISSN 0029-599X]*, 1997.

[11] T. F. Chan and P. Mulet. On the convergence of the lagged diffusivity fixed method in total variation image restoration. CAM Report 97-46, UCLA Math Department, 1997.

[12] C. K. Chui. *An Introduction to Wavelets.* Academic Press, 1992.

[13] A. Cohen, R. De Vore, P. Petrushev, and H. Xu. Nonlinear approximation and the space bv. Technical Report R98047, universie de Paris 6, 1998. available at http://www.ann.jussieu.fr/.

[14] R.R. Coifman and D.L. Donoho. Translation-invariant de-noising. Technical Report 475, Standford University, May 1995.

[15] R.R. Coifman, Y. Meyer, and M.V. Wickerhauser. Wavelet analysis and signal processing. In *Wavelets and their Applications*, pages 153–178. Jones and Barlett. B. Ruskai et al. eds, 1992.

[16] G. Demoment. Image reconstruction and restoration: Overview of common estimation structures and problems. *IEEE Transactions on acoustics, speech and signal processing*, pages 2024–2036, 1989.

[17] F. Dibos. Restauration d'images par minimisation de fonctionnelle, 1999. Notes de cours du DEA MIA.

[18] D. Donoho and I.M. Johnstone. Minimax estimation via wavelet shrinkage. Technical report, Departement of Stat., Stanford University, 1992.

[19] D.L. Donoho and I.M. Johnstone. Ideal spatial adaptation by wavelet shrinkage. *Biometrika*, 81(3):425–455, 1994.

[20] S. Durand, F. Malgouyres, and B. Rougé. Image de-blurring, spectrum interpolation and application to satellite imaging. Technical report, ENS Cachan, 1999. Submitted at MMAN.

[21] L.C. Evans and R.Gariepy. *Measure Theory and fine properties of functions.* CRC Press Ann Harbor, 1992.

[22] R. Fletcher. *Practical Methods of Optimization. Vol. 2: Constrained Optimization.* Wiley-Interscience Publication, 1981.

[23] F. Guichard and F. Malgouyres. Total variation based interpolation. In *Proceedings of the European Signal Processing Conference*, volume 3, pages 1741–1744, 1998.

[24] A.K. Jain. *Fundamentals of digital image processing.* Prentice Hall, Englewood cliffs, 1989.

[25] T. Kailath. A view of three decades of linear filtering theory. *IEEE transaction on information theory*, IT20(2), March 1974.

[26] J. Kalifa. *Restauration minimax et déconvolution dans un base d'ondelettes miroirs.* PhD thesis, Ecole Polytechnique, 1999.

[27] N. B. Karayiannis and A. N. Venetsnopoulos. Image interpolation based on variational principles. *Signal Processing*, 26(1), January 1992.

[28] H.J. Landau and H.O. Pollak. Prolate spheroidal wave functions, fourier analysis and uncertainity iii: The dimension of the space of essentially time and bandlimited signals. *Bell System Technical Journal*, 41:1295–1336, July 1962.

[29] M. Lindenbaum, M. Fischer, and A. Bruckstein. On gabor's contribution to image enhancement. *PR.*, 27(1):1–8, 1994.

[30] E. Maeland. On the comparison of interpolation methods. *IEEE Transactions on Medical Imaging*, 7(3), September 1988.

[31] F. Malgouyres and F. Guichard. Edge direction preserving image zooming: a mathematical and numerical analysis. subnitted at SINUM, 1999.

[32] S. Mallat. A theory for multiresolution signal decomposition: the wavelet representation. *IEEE Transaction on patern analysis and machine intelligence*, July 1989.

[33] S. Mallat. *A Wavelet Tour of Signal Processing.* Academic Press, 1998.

[34] S. Matej, S. S. Furuie, and G.T. Herman. The relevance of statistically significant differences between reconstruction algorithms. *IEEE Transactions on Image Processing*, 5(3), March 1996.

[35] Y. Meyer. *Ondelettes et opérateurs.* Hermann, 1990.

[36] J.M. Morel and S. Ladjal. Notes sur l'analyse de fourier et la theorie de shannon en traitement d'images. in "Analyse de Fourier et traitement d'images", Journées X-UPS, 1998.

[37] M. Nikolova. Local strong homogeneity of a regularized estimator. To appear in SIAM.

[38] J. P. Oackley and M. J. Cunningham. A function space model for digital image sampling and its application in image reconstruction. *Computer Vision, Graphics, and Image Processing*, 49:171–197, 1990.

[39] S. K. Park and R. A. Schrowengerdt. Image reconstruction by parametric cubic convolution. *Computer Vision, Graphics, and Image Processing*, 23:258–272, 1983.

[40] B. Rougé. Remarks about space-frequency and space-scale to clean and restore noisy images in satellite frameworks. progress in wavelets and applications. In *Proceedings Toulouse conference*, 1993.

[41] B. Rougé. Fixed chosen noise restauration (fcnr). In *IEEE 95 Philadelphia*, 1995.

[42] B. Rougé. Theorie de la chaine image optique et restauration a bruit final fixe, Juillet 1997. Memoire d'Habilitation a Diriger des Recherches, Option Mathématiques Appliquees.

[43] B. Rougé and A. Seghier. Nonlinear spectral extrapolation: new results and application to spatial and medical imaging. In *San Diego Symposium*, July 1995.

[44] L. Rudin, S. Osher, and E. Fatemi. Nonlinear total variation based noise removal algorithms. *Physica D*, 60:259–268, 1992.

[45] Leonid Iakov Rudin. *Images, Numerical Analysis of Singularities and Shock Filters.* PhD thesis, California Institute of Technology, 1987.

[46] C. E. Shannon. Communication in the presence of noise. *Proceedings of the IRE*, 37:10–21, 1949.

[47] S. Thurnhofer and S. K. Mitra. Edge-enhanced image zooming. *Optical Engineering*, 35(7), 1996.

[48] M. Unser, A. Aldroubi, and M. Eden. Enlargement or reduction of digital image with minimum loss of information. *IEEE Transactions on Image Processing*, 4(3), March 1995.

[49] S. J. Wernecke and L.R. d'Addario. Maximum entropy image reconstruction. *IEEE Transactions on computers*, c-26(4), April 1977.

[50] L. Yaroslavsky. Efficient algorithm for discrete sinc interpolation. *Applied Optics*, 36(2), 1997.

[51] K. Yosida. *Functional Analysis.* Springer Verlag, 1965.

RÉSUMÉ: Nous faisons d'abord des rappels sur la théorie de l'échantillonnage et définissons une image digitale par: $u_{m,n} = s * v(m,n)$, pour $(m,n) \in \Omega \cap \mathbb{Z}^2$, un paysage v défini sur $\Omega \subset \mathbb{R}^2$ et un filtre s.

Le problème du suréchantillonnage consiste à chercher un représentant, défini sur Ω, de l'image v, étant donné u et s. Nous avons analysé leur capacité à préserver les fonctions cylindriques (fonctions qui ne varient que dans une direction et modélisent les contours). Nous avons d'abord montré que les suréchantillonnages linéaires, préservant ces fonctions, sont des convolutions de "l'interpolation sinus cardinal". Nous avons ensuite défini des méthodes de suréchantillonnages de type Maximum A Postériori, basées sur la minimisation de la variation totale. Nous avons montré des résultats d'existence, "d'unicité faible" et donné une façon de calculer une solution à ces modèles. Nous avons de plus montré qu'ils peuvent préserver les fonctions cylindriques et permettent ainsi de prolonger les structures du spectre initial. Ces résultats théoriques sont confirmés par des expériences.

Nous nous sommes enfin penchés sur le problème de la déconvolution d'images digitales bruitées (on cherche une image mieux échantillonnée et debruitée $\tilde{s} * v(m,n)$). Nous avons d'abord présenté une méthode de seuillage basée sur l'approximation de la déconvolution par un opérateur diagonal dans une base de paquets d'ondelettes. Cette méthode s'avère mal adaptée aux cas où la transformée de Fourier de s s'annule dans le carré de Nyquist. Nous avons aussi mis en évidence la capacité de la méthode de Rudin-Osher-Fatemi à résoudre ce genre de problèmes. Nous avons montré par ailleurs qu'il est possible en modifiant cette méthode d'enlever "l'aliasing" dans le cas d'images faiblement bruitées.

ABSTRACT: We make first some reminders on sampling theory and define a digital image by: $u_{m,n} = s * v(m,n)$, for $(m,n) \in \Omega \cap \mathbb{Z}^2$, a landscape v, defined over $\Omega \subset \mathbb{R}^2$, and a filter s.

Oversampling consists in searching a function, defined over Ω, representing the landscape v, given u and s. We focus on their ability to preserve cylindric functions (which fluctuate along a single direction and model edges). We first show that linear oversampling, that preserve cylindric functions, are some convolutions of the "sinus cardinal interpolation". Then, we define some Maximum A Posteriori oversampling, based on the minimization of the total variation. We show some existence and "weak uniqueness" statements and give a way to estimate a solution to the model. We then prove that these methods preserve cylindric functions and permit to extend the structures of the initial spectrum. These theoretical results are proven by experiments.

We turn then to the deconvolution of noisy digital images (we expect a noise free and properly sampled image $\tilde{s} * v(m,n)$). We first expose a shrinkage method based on the approximation of the deconvolution by an operator which is diagonal in a wavelet packet basis. This method appears to be inefficient in cases where the Fourier transform of s cancels inside the Nyquist square. We show the ability of Rudin-Osher-Fatemi method to restore properly these kind of problems. We also show that it is possible, by modifying this method, to remove "aliasing" when the initial noise is small.

DISCIPLINE: Mathématiques.

MOTS-CLÉS: Suréchantillonnage, déconvolution, images digitales, variation totale, méthode variationnelle, restoration d'image, extrapolation de spectre, transformée de Fourier.

CMLA, ENS Cachan
61, avenue de président Wilson
94235 Cachan Cedex